TABLE OF CONTENTS

NASA Technical Paper 1221

A Nonlinear Trajectory Command Generator for a Digital Flight-Control System

Luigi S. Cicolani and Stein Weissenberger

NOVEMBER 1978

NASA

NASA Technical Paper 1221

A Nonlinear Trajectory Command Generator for a Digital Flight-Control System

Luigi S. Cicolani and Stein Weissenberger
Ames Research Center
Moffett Field, California

National Aeronautics
and Space Administration

**Scientific and Technical
Information Office**

1978

SYMBOLS

A	acceleration error, referred to path axes
A_N	normal applied specific force, g
A_{ps}	transformation from runway to path axes
A_u	longitudinal applied specific force, g
$\underline{a}, \underline{a^*}, \underline{ac}$	actual, reference, and commanded accelerations, respectively
$\underline{act}$	total feed-forward and feedback acceleration command
$\underline{ad}$	steady acceleration disturbance
$\underline{\tilde{ad}}$	random acceleration disturbance
$a_m^{(i)}, a_M^{(i)}$	minimum, maximum operational values of path axis acceleration components
$\underline{c}$	location of center of circular path
(E_1, E_2, E_3)	position, velocity, and acceleration error relative to the next reference trajectory leg, referred to path axes
$(\underline{e}_1, \underline{e}_2, \underline{e}_3)$	transition dynamics position, velocity, and acceleration states
(en_1, en_2, en_3)	difference between position, velocity, and acceleration of two successive reference trajectory legs, referred to path axes
$(\underline{er}, \underline{ev}, \underline{ea})$	position, velocity, and acceleration command errors
$\underline{e}_{2m}, \underline{e}_{2M}$	minimum and maximum velocity excursion saturation parameters
$\underline{e}_{20m}, \underline{e}_{20M}$	bounds of initial values of components of $\underline{e}_2$
$\underline{e}_{3m}, \underline{e}_{3M}$	acceleration excursion saturation parameters
$\underline{e}_{30m}, \underline{e}_{30M}$	bounds of initial values of components of $\underline{e}_3$
$\dot{e}_{3m}, \dot{e}_{3M}$	acceleration rate saturation parameters
$\underline{F}_a$	aerodynamic force
f, f_c, f_{cT}	applied specific forces of aircraft, of trajectory command, and of total acceleration command, respectively
G	plant dynamics

$\underline{g}$	acceleration of gravity
$g_i(\underline{r},\underline{v},\underline{a},\dot{\underline{a}})$	operational constraint functions
I	unit matrix
ICTD	transition initialization switching parameter
k_1,k_2	linear control law gains
L	locus of possible initial conditions for a transition
m	either reference trajectory leg counter or order of plant dynamics
P	optimal cost function metric of TD linear mode control law
$(\underline{p}_1,\underline{p}_2,\underline{p}_3)$	path axes reference frame
R_c	horizontal plane radius of curvature
$\underline{r},\underline{r}^*,\underline{rc}$	actual, reference, and commanded aircraft position, respectively
$\underline{ro}$	initial position
S	set of parameters defining reference trajectory
s	either arc length or Laplace operation
$(\underline{s}_1,\underline{s}_2,\underline{s}_3)$	runway axis reference frame
T	optimum transition initialization time
t	time
t_o	initial time for a trajectory leg
$\underline{uc}$	vector of aircraft control commands
$\underline{u},u$	transition dynamics control law
VM	maximum cost in region of linear control in TD
V,VN	cost function of linear TD control law
$\underline{v},\underline{v}^*,\underline{vc},\underline{va}$	actual, reference, commanded inertial velocity, and air velocity, respectively
v,v*,vc,va	actual, reference, commanded inertial speeds and airspeed of aircraft, respectively

$\dot{v}, \dot{v}c$	actual, commanded speed rates of aircraft
$\underline{vo}$	initial velocity
(x,y,z)	runway axis Cartesian coordinates
(x_1,x_2,x_3)	canonical states for transition dynamics
$(y_1,y_2,\ldots,y_m)$	canonical states for plant dynamics
$(z_1,z_2,\ldots,z_{m+2})$	system tracking error states
α	aircraft angle of attack
β	aircraft sideslip angle
$\gamma, \gamma^*, \gamma_c$	actual, reference, commanded flight-path angle, respectively
$\underline{\Delta a}$	corrective feedback acceleration command
Δt	time relative to current time
Δt^*	optimum transition initialization time relative to current time
δ_i	axis initialization indicator
ϵ_2, ϵ_3	velocity and acceleration threshold values
ζ	damping ratio
ξ_2, ξ_3	bounded intervals containing initial values of $\underline{e}_2, \underline{e}_3$
ρ	air density
$\sigma(x)$	TD nonlinear mode control law switching function
τ, τ_L, τ_1	characteristic times of linear dynamic elements
ϕ_V	roll angle measured about aircraft velocity vector
ϕ_{VC}	commanded roll angle
$\dot{\phi}_{VC}$	commanded roll rate
ψ_V, ψ_{VC}	actual, commanded heading of the aircraft velocity vector
Ω, Ω_L	transition dynamics linear mode regions

Subscripts, Superscripts, and Special Symbols

$(\underline{\ })$	vector quantity
$(\ )_p$	vector given in path axis Cartesian coordinates
$(\ )_s$	vector given in runway axis Cartesian coordinates
$(\ )^{(i)}$	ith component of a vector, $(\ )$
$\mathrm{d}[(\cdot)]$	the value of $(\ )$ limited by bounds noted in context
$\hat{(\ )}$	estimated value of $(\ )$
$(\ )^T$	vector or matrix transpose

Abbreviations

AWJSRA	Augmentor Wing Jet STOL Research Aircraft
CG	Command Generator
CTOL	Conventional Takeoff and Landing Aircraft
DME	Distance Measuring Equipment
MLS	Microwave Landing System
STOL	Short Field Takeoff and Landing Aircraft
VTOL	Vertical Takeoff and Landing Aircraft
TD	Transition Dynamics
TR	Trajectory Regulator

A NONLINEAR TRAJECTORY COMMAND GENERATOR FOR A DIGITAL FLIGHT-CONTROL SYSTEM

Luigi S. Cicolani and Stein Weissenberger*

Ames Research Center

SUMMARY

A nonlinear Command Generator (CG) is synthesized for a digital autopilot capable of controlling VSTOL aircraft to track complex four-dimensional reference trajectories in an advanced terminal area air traffic control environment. The reference trajectory is assumed to consist of a sequence of straight-line or circular arc "legs" with discontinuities at the leg junction times. The CG generates smooth transitions from one leg to the next while maintaining a variety of operational constraints on maneuvering as dictated by safety, aircraft limitations, and passenger comfort, including bounds on velocities, accelerations, and acceleration rates.

The basic approach regards the discontinuity as an error from the next leg of the reference trajectory which is then relaxed to zero in accordance with a suitable control law. A dual-mode control law is synthesized; it is globally asymptotically stable, has a maximal region of initial conditions using linear control, and uses minimum-time-to-origin control outside the linear region. Selectable control law parameters include the damping and settling time of the linear mode dynamics, saturation limits on velocity and acceleration excursions, and an acceleration rate limit.

Transition maneuvers are generated independently along longitudinal, lateral, and normal flight-path axes, and the complete trajectory command is given by superposition of these transitions with the reference trajectory. Maneuver characteristics, such as duration, overshoot of the reference flight condition, and control activity, are optimized with respect to the time of initiating the transition from one leg to the next, and this optimization is done independently on each axis.

Operational application of the CG was examined in detail in a simulation of a flight-control system with the augmentor wing jet STOL research aircraft; the basic repertoire of single-axis maneuvers and operational constraints are discussed, and the system behavior is tested on a rigorous STOL approach path and as affected by various approximations in the CG synthesis and types of disturbances found in the operational environment. The simulation results indicate that a satisfactory nonlinear system with general maneuvering capabilities was developed which satisfies the basic design objectives while maintaining a practicable degree of simplicity.

---

*National Research Council Postdoctoral Research Associate.

INTRODUCTION

Problem Outline

This report describes a trajectory Command Generator (CG) for an advanced digital flight-control system whose structure was developed in reference 1. This structure provides a logical framework for designing autopilots for a wide range of aircraft, including CTOL, STOL, and VTOL, with capabilities of executing complex four-dimensional (one time and three space coordinates) terminal-area flight paths as directed by an air traffic control and guidance system or as selected by a pilot. Although the CG design is formulated here in the context of the structure of reference 1, its function could be embedded in most automatic flight-control systems independent of internal structure. Further, the structure of the command generator is independent of the aircraft being controlled.

The control structure of reference 1 is outlined in figure 1. The Force Trimmap is the central element of the structure and computes the aircraft control command $\underline{uc}$ necessary to achieve an input commanded acceleration $\underline{act}$. These computations are based on a model of the aerodynamic and engine forces of the aircraft being controlled (cf. ref. 2). The next level of the structure is the Trajectory Regulator (TR), which produces compensatory acceleration commands $\underline{\Delta a}$ on the basis of the error between the commanded and estimated trajectories. The TR is intended to operate on relatively small path errors and hence is designed as a continuous-time linear, constant coefficient compensator, whose bandwidth is large compared to that of the command signals it receives from a higher level of the control structure. The combined Trimmap and TR form an acceleration controller structure that can execute and track commanded trajectories:

$$\left\{\underline{rc}(t), \underline{vc}(t), \underline{ac}(t), \qquad t_o \leq t \leq t_f\right\}$$

where $\underline{rc}$ and $\underline{vc}$ are three-dimensional inertial commanded position and velocity, provided these commands are kinematically consistent, within the aircraft flight envelope limits on velocity and acceleration, and provided that the trajectory errors remain sufficiently small that the total acceleration command $\underline{act}$ and actual velocity also satisfy these limits.

It is the function of the trajectory Command Generator (CG) at the next level of the structure to ensure that these conditions are met. The CG is a feed-forward controller with position and velocity commands passed forward to the regulator and an acceleration command to the Trimmap. If trajectory errors become too large at, say, t_o, the CG can initiate a transition maneuver that begins at the current estimated aircraft state $\hat{\underline{r}}(t_o)$, $\hat{v}(t_o)$ and relaxes the corresponding errors from the reference state to zero in accordance with a control law that bounds the velocity and acceleration excursions of the transition maneuver within specified limits. The synthesis of this control law is a central analytical problem of this paper.

The CG relieves the Trajectory Regulator and maintains acceptable commands in the following principal situations: (1) when very large tracking errors develop due to a period of large wind disturbances and it is desired to return to course; (2) when there has been a switch from one navigation sensor to another with a significant change in the estimated trajectory state and it is desired to reduce the newly sensed error from the reference; or (3) when a discontinuity in the input reference trajectory is imminent and it is desired to maneuver to the new reference trajectory. In this last situation, the CG fills a role intermediate between the acceleration controller and the input reference trajectory. The source of the reference trajectory inputs may be a terminal area air traffic control and four-dimensional guidance system (ref. 3) or a trajectory tracking mode selection panel used by the pilot. These inputs are assumed to be a set of parameters sufficient to define the trajectory on the time interval $[t_o, t_f]$ as a sequence of circular-arc or straight-line segments with constant path acceleration; each segment is defined from its initial position and velocity, the acceleration on the segment, and the corresponding initial time. A complete reference trajectory is then generated from a sequence S of such input parameters

$$S = \left\{ \left(t_{o_i}, \underline{ro}_i, \underline{vo}_i, \dot{v}_i, R_{c_i} \right),\ i = 1,2,\ldots,M;\ t_o = t_{o_1} < t_{o_2} < \ldots < t_M < t_f \right\}$$

where $\dot{v}$ and R_c refer to the speed rate and horizontal plane radius of curvature and are assumed constant on each segment $[t_{o_i}, t_{o_{i+1}}]$. The input trajectory is assumed to be piecewise flyable; that is, each segment or leg corresponds to a steady or slowly varying flight condition within the flight envelope of the aircraft, but discontinuities in position, velocity, and acceleration can occur at each leg-switching time (t_{o_i}). The CG modifies the input trajectory to provide flyable transition maneuvering between successive legs by regarding the discontinuity as an error from the new leg of the input reference, which is then relaxed to zero in accordance with a suitable control law designed to satisfy operational constraints on aircraft maneuvering and provide command trajectories intermediate in bandwidth between the input commands and the trajectory regulator commands. The reference leg-switching times (t_{o_i}) are usually known in advance so that a leg transition maneuver can also be initiated in advance of the reference switching time in order to minimize the required maneuver acceleration activity.

Command Generator Structure and Transition Dynamics

The structure of the CG is shown in figure 2. First, the position, velocity, and acceleration trajectory errors are formed in path axes:

$$\left.\begin{aligned} er_p &= A_{ps}(\hat{r}_s - r_s^*) \\ ev_p &= A_{ps}(\hat{v}_s - v_s^*) \\ ea_p &= A_{ps}(act_s - a_s^*) \end{aligned}\right\} \qquad (1)$$

where (r_s^*, v_s^*, a_s^*) and $(\hat{r}_s, \hat{v}_s)$ represent the reference and estimated trajectory states in a runway axis system with origin at the runway (fig. 3). The acceleration error is defined from act in equations (1) to obtain a desired continuity property in the output, as is noted below. These errors are transformed into the path axes system used by the transition dynamics; the path axes are sketched in figure 3 and are orthogonal with axes along the tangent of the commanded path (longitudinal axis), normal to the tangent in the horizontal plane (lateral axis), and normal to the tangent in the vertical plane (normal axis). The transformation matrix from runway axes to path axes is given by

$$A_{ps} = \begin{bmatrix} \cos\gamma \cos\Psi_v & \cos\gamma \sin\Psi_v & -\sin\gamma \\ -\sin\Psi_v & \cos\Psi_v & 0 \\ \sin\gamma \cos\Psi_v & \sin\Psi_v \sin\gamma & \cos\gamma \end{bmatrix} \tag{2}$$

where Ψ_v and γ specify the heading and flight-path angle of the velocity vector (fig. 3).

The error states (eqs. (1)) provide initial values for the transition dynamics states at those discrete times $\{t_{o_i}\}$ specified by the initialization switching logic

$$\left.\begin{aligned} e_1(t_o) &= er_p(t_o) \\ e_2(t_o) &= ev_p(t_o) \\ e_3(t_o) &= ea_p(t_o) \end{aligned}\right\} \tag{3}$$

The transition dynamics (TD) consists of three autonomous dynamic systems,

$$\dot{\underline{e}}^{(i)} = f^{(i)}(\underline{e}^{(i)}) , \qquad f^{(i)}(\underline{0}) = \underline{0} , \qquad i = 1,2,3 \tag{4}$$

where the ith system governs the relaxation of position, velocity, and acceleration errors along the ith path axis, and the state vector for each system is

$$\underline{e}^{(i)} = \left(e_1^{(i)}, e_2^{(i)}, e_3^{(i)}\right)^T \tag{5}$$

The complete maneuver command is constructed by combining these error relaxation maneuvers defined by the TD for each axis into the position, velocity, and acceleration vectors $\underline{e}_1$, $\underline{e}_2$, $\underline{e}_3$, and then transforming to runway axes and summing with the reference trajectory

$$\left.\begin{aligned} rc_s(t) &= r_s^*(t) + A_{ps}^T e_1(t) \\ vc_s(t) &= v_s^*(t) + A_{ps}^T e_2(t) \\ ac_s(t) &= a_s^*(t) + A_{ps}^T e_3(t) \end{aligned}\right\} \qquad (6)$$

Coriolis accelerations associated with transitions can be neglected, as in equations (6), for the passenger operations considered here. These accelerations depend on the combination of path axis angular velocity (due to $\dot{\psi}_v$ or $\dot{\gamma}$) and transition excursions; however, rotation rates are held to small values in passenger operations, the effect is of short duration, and the size of the effect can be bounded by bounding the size of the initial errors that are to be relaxed by the TD. In summary, the CG structure in figure 2 constructs a maneuver command that begins at t_o and at the then-current position and velocity, and acceleration command

$$\left.\begin{aligned} \underline{rc}(t_o^*) &= \hat{\underline{r}}(t_o) \\ \underline{vc}(t_o^*) &= \hat{\underline{v}}(t_o) \\ \underline{ac}(t_o^*) &= \underline{act}(t_o) \end{aligned}\right\} \qquad (7)$$

and relaxes these states, by means of the TD, to the reference trajectory,

$$\lim_{t\to\infty} \begin{pmatrix} \underline{rc}(t) \\ \underline{vc}(t) \\ \underline{ac}(t) \end{pmatrix} = \begin{pmatrix} \underline{r}^*(t) \\ \underline{v}^*(t) \\ \underline{a}^*(t) \end{pmatrix} \qquad (8)$$

Path axes are used in the TD because aircraft maneuvering can be specified independently for each axis because of the nearly decoupled control that conventional aircraft have over motion along these axes. The path axis components of acceleration are related to kinematic variables of interest in aircraft trajectories by

$$\left.\begin{aligned} a_p^{(1)} &= \dot{v} \\ a_p^{(2)} &= v \cos\gamma \dot{\psi}_v = \frac{v^2}{R_c} \\ a_p^{(3)} &= v\dot{\gamma} \end{aligned}\right\} \qquad (9)$$

so that accelerations along each of the three axes control, respectively, speed, heading, and flight-path angle. Aircraft maneuvering can then be constructed as a superposition of single-axis motions; for example, the input reference trajectory is typically a sequence of legs that may be in static equilibrium ($\underline{a} = \underline{0}$), constant radius turns (constant R_c), or constant speed rate flight (constant $\dot{v}$) or combinations of the latter two. The transition dynamics modify this input trajectory by adding bounded time-varying

accelerations along all three path axes as required for good execution of the reference input path. For passenger operations, only modest accelerations are permitted; typical limits are

$$\left.\begin{aligned} |a_p^{(1)}| &\leq 0.1\ g \\ |a_p^{(2)}| &\leq 0.35\ g \\ |a_p^{(3)}| &\leq 0.125\ g \end{aligned}\right\} \qquad (10)$$

Outline of Development

The main analytical tasks of this work are the synthesis of the transition dynamics (eqs. (4)) and the development of the TD initialization switching logic. The transition dynamics are necessarily nonlinear because the trajectory is required to satisfy flight-operational bounds on velocity, acceleration, and acceleration rate. A dual-mode control is used to synthesize these dynamics, giving a linear system for sufficiently small initial errors and a nonlinear system for larger errors. In addition to satisfying trajectory bounds, the transition dynamics are required to be globally asymptotically stable; that is, errors must relax to zero starting from any initial value. Further, the dynamic system should be parameterized to permit adjustment of maneuver characteristics. Our approach to achieve these objectives uses an idea first reported by Kuznetzov (ref. 4), who defined the region of linear control using as a Lyapunov function the optimal cost function from the linear optimal control problem. The method is adapted to the present problem by a modification due to Willems (ref. 5), which permits a significant and straightforward enlargement of this region of linear control. A similar goal of linear region enlargement was achieved by Zachary et al. (ref. 6) where the approach, while direct, was analytically less simple and less easily applied to a variety of systems than the present method. Additional devices in the synthesis of the control law include Jordan canonical transformations and phase-plane analysis. A general approach to the design of dual-mode controllers is developed in detail in appendix A, modified to impose velocity bounds in appendix B, and applied to the present TD synthesis in the next section.

The simplest initialization switching logic for the TD is to initialize at those times $\{t_{o_i}\}$ at which discontinuities occur in the reference input trajectory; this results in a unique transition for any given pair of successive legs. However, it is possible to optimize the commanded maneuvers regarding control activity and overshoot of the reference flight condition by adjusting the transition initialization times from the reference times. Such optimization is also a necessary property of an operationally acceptable flight system and corresponds to good "piloting technique" in manual flight operation when advance warning of a leg junction is available (e.g., ref. 7). Any leg of the reference can be extrapolated beyond its duration in the reference trajectory so that the initial conditions (eqs. 7)

for the transition to the next leg in the sequence are defined for any time earlier or later than the reference switching times. Consequently, the initialization times can be varied from the $\{t_{oi}\}$ to improve properties of the ensuing transition. General switching criteria and closed-form solutions for the corresponding optimum switching times are derived for the dual-mode TD in the fourth section of this paper. The results are given for arbitrary leg-junction discontinuities and are applied independently on each path axis; that is, the three autonomous dynamic systems of the TD are initialized independently and the results for each axis superposed as in equations (6) to yield an output command with the properties (eqs. (7) and (8)) at each initialization and in steady state. An alternative approach (ref. 8) considers two successive legs extended indefinitely in time, with the first leg defined on $(t \leq t_o)$ and the second on $(t > t_o)$ and then formulates the transition as the solution of a linear optimal tracking problem on $(-\infty < t < \infty)$. While the approach in reference 8 allows systematic trade-off of reference path tracking excursions with control effort, it requires two sets of transition dynamics and, based as it is on linear theory, fails to enforce the various state and control constraints necessary for operational acceptability of the CG.

The application tasks of the report are to derive a Command Generator algorithm for use in an application of the flight control structure of figure 1 to the Ames experimental powered-lift aircraft, the augmentor wing jet STOL research aircraft (AWJSRA), and to evaluate the algorithm in simulation tests. A computer implementation is outlined and parameter values are selected to impose the kinematic constraints of the assumed passenger operational domain and the limits of AWJSRA capabilities. The output commands for the basic repertoire of single-axis maneuvers are examined to determine the effectiveness of the nonlinear TD in imposing the desired constraints and of the TD initialization switching logic in optimizing the maneuvers, and to determine the effect of approximations in the theory and design. Finally, the execution of a STOL approach trajectory is examined with a simulation of the flight control system and the AWJSRA. The results illustrate the general capability of the CG and of the flight control system to generate and execute satisfactory multiaxis maneuver commands. The test examines the effects of such features of the operational environment as off-reference initial conditions due to uncompleted earlier maneuvering, sensor switching events, and both random and steady disturbances. These tests include the principal disturbances to which the operational system will be subject. Future evaluation and development of the CG and system logic with increasingly realistic simulations and with pilot evaluation is planned.

The structure and even many parameter values of the CG element of the flight control system are independent of the specific aircraft for which it is designed. Thus, details of the AWJSRA are suppressed in most of the discussion in this report and the design and test conclusions are largely applicable to a class of aircraft (CTOL and STOL) and to a class of operations (passenger).

TRANSITION DYNAMICS

Figure 4 is a block diagram of the transition dynamics consisting of three decoupled dynamic systems that govern the erro: dynamics along each of the flight-path axes (these dynamics are initialized in accordance with eq. (3)). For a single axis, the system consists of a control law, $u^{(i)}(\underline{e}^{(i)})$, which is the basic acceleration command that defines the maneuver, and a filter, $(\tau_s^{(i)} + 1)^{-1}$, which produces a smooth acceleration, e_3. The resulting position (e_1), velocity (e_2), and the acceleration (e_3) commands from the three axes are combined with the reference trajectory to produce the output commands to the regulator and Trimmap elements of the autopilot.

The control law, $u^{(i)}(e^{(i)})$, developed in this section, is linear for small errors but saturates at limit values for large errors and is also designed to limit velocity excursion, $e_2^{(i)}$. Parameters of the linear mode of the control law are selected to obtain the desired damping and response time, while the saturation limits and switching boundaries of the nonlinear mode are designed to impose operational limits on the acceleration and velocity excursions which can be used for maneuvering in the neighborhood of the reference trajectory state. Because the control $u^{(i)}$ can be discontinuous, a filter is introduced to obtain continuous acceleration commands $e_3^{(i)}$. Further, the filter parameter, $\tau^{(i)}$, is selected to limit maneuver acceleration rates, $\dot{e}_3^{(i)}$, in accordance with the rate limits of aircraft capabilities to vary engine and aerodynamic forces.

The third-order transition dynamics system for each axis seen in figure 4 will be used in the applications work. However, it is potentially useful to add a predictive modeling element that accounts for the predictable control lag effects on maneuver tracking; this expanded structure is outlined in the next section. The remainder of this section considers the control law design for a single axis, and the axis superscript $(\ )^{(i)}$ is dropped from the notation.

Transition Dynamics Design Objectives

The various constraints to be imposed on the TD and the objectives of the control-law synthesis are defined next. First, the state equation for the TD is

$$\left.\begin{aligned} \dot{\underline{e}} &= A\underline{e} + \underline{b}u(\underline{e}) \\ \text{where} \quad A &= \begin{bmatrix} 0 & \tau & 0 \\ 0 & 0 & \tau \\ 0 & 0 & -\tau^{-1} \end{bmatrix}, \quad \underline{b}^T = (0,0,\tau^{-1}) \end{aligned}\right\} \tag{11}$$

These dynamics are initialized to (1) reduce the regulator feedback error to zero, and (2) retain continuity of the total acceleration command to the Trimmap; that is, the components of $\underline{e}$ are initialized as

$$\left.\begin{aligned} e_1(t_o) &= \hat{r}_p(t_o) - r_p^*(t_o) \\ e_2(t_o) &= \hat{v}_p(t_o) - v_p^*(t_o) \\ e_3(t_o) &= [\![\, act_p(t_o^-) \,]\!] - a_p^*(t_o) \end{aligned}\right\} \qquad (12)$$

It can be assumed that both the reference and current states in equations (12) are within the finite operational limits of the aircraft in velocity and acceleration. However, the acceleration command, $\underline{act}\ (t_o)$, might be outside the aircraft capabilities and should be bounded by the operational limits on acceleration (e.g., eqs. (10)) in order to ensure initialization at an admissible acceleration command. The bounded value is indicated by the bracket notation, $[\![\, \cdot \,]\!]$, which is defined as

$$[\![x]\!] \equiv \max\{x_{min}, \min\{x, x_{max}\}\} \qquad (13)$$

where x_{min}, x_{max} are understood to be known extreme values of x. The initial TD states are, therefore, contained in some bounded region denoted as

$$\left.\begin{aligned} e_2(t_o) &\in [-e_{20m}, e_{20M}] \\ e_3(t_o) &\in [-e_{30m}, e_{30M}] \end{aligned}\right\} \qquad (14)$$

The transition dynamics generate the maneuver as an error from the reference state and then the CG command, referred to path axes, is

$$\begin{pmatrix} rc_p \\ vc_p \\ ac_p \end{pmatrix} = \begin{pmatrix} r_p^* \\ v_p^* \\ a_p^* \end{pmatrix} + \begin{pmatrix} e_1 \\ e_2 \\ e_3 \end{pmatrix} \qquad (15)$$

Constraints are imposed on the TD states based on operational considerations. These can be written in the form

$$\left.\begin{aligned} e_2(t) &\in \xi_2 \equiv [-e_{2m}, e_{2M}] \\ e_3(t) &\in \xi_3 \equiv [-e_{3m}, e_{3M}] \\ \dot{e}_3(t) &\in [-\dot{e}_{3m}, \dot{e}_{3M}] \end{aligned}\right\} \qquad (16)$$

These impose bounds on excursions about or overshoot of the reference trajectory; the velocity constraints limit the excursions in speed (or direction or flight-path angle) required to change position longitudinally

(or laterally or in altitude) and also limit any overshoot in maneuvering to a reference speed (or direction or flight-path angle). Similarly, the limits on e_3 bound the acceleration overshoot in maneuvering to a new reference acceleration as, for example, when entering a turn. Lastly, bounds on the acceleration rate, $\dot{e}_3$, are imposed in order to limit the corresponding required aircraft control rates in accordance with the limits of aircraft control rate capabilities.

The bounds ξ_2, ξ_3 in equations (16) are generally interior to the bounds on initial states in equations (14), as illustrated in sketch (a).

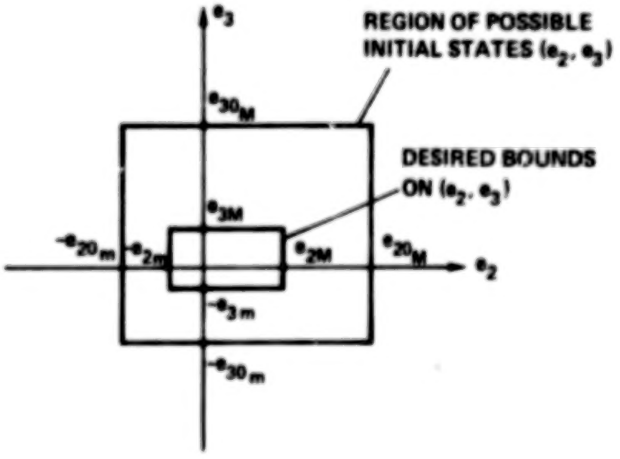

Sketch (a).- Bounds on TD states.

Thus, initial values of (e_2, e_3) can be outside ξ_2 and ξ_3 so that the TD should drive these states into ξ_2 and ξ_3 in such cases. The bounds in equations (16) define the desired ranges of values in which the TD states are to be confined once entered; that is, the TD should have the property

$$\left.\begin{aligned} &\text{If } e_2(t_o) \in \xi_2 \text{ then } e_2(t) \in \xi_2, \quad t > t_o \\ &\text{If } e_3(t_o) \in \xi_3 \text{ then } e_3(t) \in \xi_3, \quad t > t_o \end{aligned}\right\} \tag{17}$$

The desired behavior for e_3 is obtained by bounding the control u as shown next. Solving the state equation for e_3 yields

$$e_3(t) = \left[e_3(t_o) + \frac{1}{\tau}\int_{t_o}^{t} u(\eta)e^{\eta/\tau}\, d\eta\right]e^{-t/\tau} \tag{18}$$

from which it follows that if u is bounded by

$$u(t) \in \xi_3 \tag{19}$$

then $e_3(t)$ satisfies

$$e_3(t) \in \left[-e_{3m} + (e_3(t_o) + e_{3m})e^{-t/\tau}, e_{3M} + (e_3(t_o) - e_{3M})e^{-t/\tau}\right] \quad (20)$$

Generally, if $e_3(t_o)$ is outside the bounds, then it is driven into ξ_3 and, once satisfied, the bounds remain satisfied for all further time.

The rate constraints $\{\dot{e}_{3m}, \dot{e}_{3M}\}$ also limit the acceleration rate of the CG trajectory in equation (15), assuming that the reference command has constant path axis acceleration. Note that aircraft control rates required for the maneuvers are proportional to the commanded acceleration rates; hence the rate limits in equations (16) reflect aircraft limits on the rates at which engine and aerodynamic forces can be varied. The desired rate limits can be imposed by the selection of τ. If u is bounded by equation (19), then it can be shown from equations (11) and (18) that the maneuver rate is bounded by

$$\tau\dot{e}_3(t) \in [-(e_{3m} + e_3(t_o)), (e_{3M} - e_3(t_o))]$$

Rate limits may then be imposed by requiring

$$\tau \geq \max\left\{\frac{e_{30m} + e_{3m}}{\dot{e}_{3m}}, \frac{e_{30M} + e_{3M}}{\dot{e}_{3M}}\right\} \quad (21)$$

Thus far, it has been shown that the structure of the transition dynamics permits maintenance of some of the constraints (eqs. (16)) provided that u and τ are bounded according to equations (19) and (21). It remains to indicate how velocity constraints are imposed and to complete the synthesis of the transition dynamics control law $u(e_1, e_2, e_3)$. There are four important constraints and objectives that u must meet: (1) $u \in \xi_3$, (2) the equilibrium of the resulting dynamic system (eqs. (11)) must be asymptotically stable in the large, and (3) because of the simplicity and smoothness of linear control, the linear control region should be as large as practicable. Furthermore, the time spent under nonlinear control should be minimized and there should be not more than a single transfer from nonlinear to linear control. Finally, (4) velocity excursion constraints must be imposed.

Control Law Synthesis

To accomplish the objectives listed above for the control law design, it is convenient to first transform the state space to Jordan canonical form (cf. ref. 9), changing from the system description of equations (11) to

$$\left.\begin{aligned}\dot{x}_1 &= x_2\\ \dot{x}_2 &= u(x_1, x_2)\end{aligned}\right\} \quad (22a)$$

and

$$\dot{x}_3 = \frac{u - x_3}{\tau} \tag{22b}$$

via the transformation equations

$$\underline{e} = \begin{bmatrix} 1 & -\tau & \tau^2 \\ 0 & 1 & -\tau \\ 0 & 0 & 1 \end{bmatrix} \begin{bmatrix} x_1 \\ x_2 \\ x_3 \end{bmatrix} \tag{23}$$

where the new state variables are (x_1, x_2, x_3). The inverse transformation is

$$\begin{pmatrix} x_1 \\ x_2 \\ x_3 \end{pmatrix} = \begin{bmatrix} 1 & \tau & 0 \\ 0 & 1 & \tau \\ 0 & 0 & 1 \end{bmatrix} \underline{e} \tag{24}$$

Figure 5 is a block diagram of a TD structure employing these transformations. Use of the canonical form greatly simplifies the design since the actual third-order system may now be controlled by a second-order law, $u(x_1, x_2)$, as already indicated by the notation in equations (22a). This benefit is also retained when higher-order transition dynamics are treated. Although the control is now independent of x_3, the characteristic root τ for the x_3 dynamics is selected by the designer and, more importantly, if the control is synthesized so that the (x_1, x_2) subsystem is asymptotically stable, then the entire system is stable since $u \to 0$ implies $x_3 \to 0$.

A control law $u(x_1, x_2)$ satisfying the four objectives listed above is derived in detail in appendices A and B and illustrated in figure 6(a). The state plane (x_1, x_2) is divided into a region of linear control Ω_L, which is compact and contains the origin, and the remainder of the state plane $\bar{\Omega}_L$, on which the control is nonlinear. The linear control law is derived from quadratic optimal control theory and the region Ω_L is computed from Lyapunov stability theory modified to obtain a large linear region with the property that all trajectories started in Ω_L remain in it, that is,

$$\text{If } x(t_o) \in \Omega_L \text{ then } x(t) \in \Omega_L, \quad t > t_o$$

with

$$u(x) \in \xi_3 \text{ for all } x \in \Omega_L$$

where

$$x^T \equiv (x_1, x_2)$$

The nonlinear control is designed for minimum time-to-origin from points in $\bar{\Omega}_L$ within the control constraints. This differs from a minimum time-to-Ω_L control law but the distinction is not significant.

The resulting control law and switching boundaries are summarized as follows: Let $k = (k_1, k_2)^T$ be the gains of the linear control law. The region of linear control is given by the following combination of three regions of the state plane

$$\Omega_L \equiv \{x: x^T P x \leq V_m\} \cap [\{x: -k^T x \in [0, e_{3M}] \text{ and } x_2 \leq e_{2M}\} \cup \{x: -k^T x \in [-e_{3m}, 0] \text{ and } x_2 \geq -e_{2m}\}] \tag{25}$$

The switching parameter for the minimum time-to-origin saturated control is given an

$$\sigma = \begin{cases} e_{3m} x_1 + \frac{1}{2} x_2^2, & x_2 > 0 \\ e_{3M} x_1 - \frac{1}{2} x_2^2, & x_2 < 0 \end{cases} \tag{26}$$

and the control law is

$$u(x) = \begin{cases} -k^T x & x \in \Omega_L \\ -e_{3m} & x \in \bar{\Omega}_L \text{ and } [\{\sigma > 0, x_2 \geq -e_{2m}\} \text{ or } \{\sigma = 0, x_2 > 0\}] \\ 0 & x \in \bar{\Omega}_L \text{ and } [\{\sigma > 0, x_2 < -e_{2m}\} \text{ or } \{\sigma < 0, x_2 > e_{2M}\}] \\ e_{3M} & x \in \bar{\Omega}_L \text{ and } [\{\sigma < 0, x_2 \leq e_{2M}\} \text{ or } \{\sigma = 0, x_2 < 0\}] \end{cases} \tag{27}$$

The boundaries of Ω_L, the nonlinear region control switching lines ($\sigma = 0$, $x_2 = -e_{2m}, e_{2M}$), and the control law $u(x)$ are illustrated in figure 6(a). Some typical transitions that result from this control are shown in figure 6(b). From an initial state in Ω_L (at $\underline{x}_{01}$) the state is driven by the linear control to the origin without leaving Ω_L. Starting in $\bar{\Omega}_L$, the state may be driven at saturated control into Ω_L (from $\underline{x}_{02}$); or into the switching line first (from $\underline{x}_{03}$), where the saturated control switches sign and the state is then driven into Ω_L along the switching line; or into the velocity limit (from $\underline{x}_{04}$) where the control is simply nulled until the switching boundary is encountered; or, finally, the transient may begin in the region of saturated velocity and null control (at x_{05}), in which case the control remains null until the switching boundary is encountered.

For the linear mode, the gains $\underline{k}$ of the control law, as well as the metric P and the parameter V_m used to define Ω_L, can all be given in terms of the parameters of the characteristic roots of the maneuver dynamics, ρ, τ_L (damping ratio and time constant); suitable expressions, derived in appendix A, are

$$
\left.
\begin{aligned}
k_1 &= \frac{1}{(\tau_L \zeta)^2} \\
k_2 &= \frac{2}{\tau_L} \\
P &= \begin{bmatrix} k_1 k_2 & k_1 \\ k_1 & k_2 \end{bmatrix} \\
V_m &= \tau_L \zeta^2 (32\ \zeta^4 - 24\ \zeta^2 + 6) \max\{e_{3m}, e_{3M}\}
\end{aligned}
\right\} \qquad (28)
$$

Thus, desired linear mode maneuver characteristics, such as critical damping, are easily imposed. For aircraft maneuvering, damping in the range, $0.707 \leq \zeta \leq 0.1$, is desired while τ_L, the desired maneuver settling time, is based on passenger comfort restrictions or aircraft response limits on each axis. (The derivation of the linear control law is restricted by the condition, $\rho \geq 0.5$, but this is not a significant restriction here.) In the useful special case of critical damping ($\zeta = 0.707$) the control has some special properties. Assuming equal control bounds ($e_{3m} = e_{3M} = e_{3e}$) it can be shown that the end points of the pieces of the boundary enclosing Ω_L have the simple coordinates shown in figure 6(c). From this, it is apparent that the linear control region expands with τ_L; that is, if slower dynamics are specified then larger initial state errors are relaxed with linear dynamics. In addition, the switching boundaries, $\sigma = 0$, intersect those sides of the boundary of Ω_L on which the linear control saturates so that no discontinuity in $u(t)$ occurs at the switch from nonlinear to linear modes for all those transitions which enter Ω_L along the switching curve.

The velocity excursion limits, $\{-e_{2m}, e_{2M}\}$, are imposed on the canonical velocity x_2 in this control law by the two regions of null control. Noting that $\dot{x}_2$ and u are equal by construction, the control law gives nonincreasing $|x_2|$ whenever x_2 is outside the limits; that is,

$$
\text{If } x_2 \notin \xi_2 \quad \text{then } \frac{d}{dt} |x_2| \leq 0 \qquad (29)
$$

so that during a maneuver the state cannot violate these limits once they are satisfied; that is,

$$
\text{If } x_2(t_o) \in \xi_2 \quad \text{then } x_2(t) \in \xi_2, \quad t > t_o \qquad (30)
$$

The maneuver may initialize at any value of x_2; if $x_2(t_o)$ is within the bounds it remains there, but if not, then either $|x_2|$ is reduced at the maximum possible rate or the state moves with constant velocity, $x_2(t_o)$, to the switching boundary in finite time, and then $|x_2|$ is reduced at the maximum rate and enters ξ_2 at some finite time, $\bar{t}_1$

$$\text{If } x_2(t_o) \notin \xi_2 \quad \text{then } x_2(t) \in \xi_2, \quad t \geq t_1 > t_o \tag{31}$$

Thus, the canonical velocity is directly limited by the velocity bounds.

The corresponding effect of the control law on the actual speed excursions, e_2, can be derived from equations (11) and (23), which yield

$$x_2 - e_2 = \tau \dot{e}_2 \tag{32}$$

from which it follows that e_2 is always moving toward x_2

$$\left.\begin{aligned} &\text{If } e_2 < x_2, \quad \text{then } \dot{e}_2 > 0 \\ &\text{If } e_2 > x_2, \quad \text{then } \dot{e}_2 < 0 \end{aligned}\right\} \tag{33}$$

Then, as a result of equations (30), (31), and (33), the actual speed also satisfies property (eq. (31)), except that the time at which e_2 enters ξ_2 may differ from the time at which x_2 enters.

To summarize, the control law was synthesized to satisfy the four objectives listed at the start of the synthesis and the constraints (eqs. (16)). The synthesis utilized a Jordan canonical transformation (eq. (24)) which reduced the problem to one of stabilizing and controlling a second-order subsystem in (x_1, x_2) (eqs. (22a)). In the resulting control law (eqs. (25)-(27)) the x-plane was divided into regions of linear and nonlinear control, Ω_L, $\bar{\Omega}_L$. In both regions the control u is bounded

$$-e_{3m} \leq u \leq e_{3M}$$

so that on any transition, $e_3(t)$ satisfies the same bounds in accordance with equation (20); the control is such that the velocity excursion constraints on $x_2(t)$ and $e_2(t)$ are satisfied in finite time from any point in the x-plane and, once satisfied they remain satisfied. The linear region Ω_L is compact, contains the origin, is invariant (no trajectory can exit Ω_L), and the linear control provides asymptotic stability for the system from any point in Ω_L, as is shown in appendix A. Finally, for points not in Ω_L, the control provides minimum time to the origin and finite time to Ω_L; thus the equilibrium of the system (eqs. (11) or (22)) is globally asymptotically stable.

Vertical Axis Transition Examples

Results are now given that illustrate the control law and its application to vertical axis maneuvers to execute altitude and flight-path angle changes. The required maneuvering for these cases is almost entirely along the normal path axis; values of the transition dynamics parameters for this axis are taken as

$$e_{3m} = e_{3M} = 0.125 \text{ g}$$

$$e_{2m} = e_{2M} = 4.25 \text{ m/s}$$

$$(\zeta, \tau_L) = (0.73, 2)$$

$$\tau = 2$$

Figure 7(a) shows the transition maneuver generated to execute a step drop of 60 m in the reference altitude for level flight; initial conditions are

$$(e_1(t_o), e_2(t_o), e_3(t_o)) = (-60, 0, 0)$$

The transition is shown as time histories of the output command ($rc_s^{(3)}$, $vc_s^{(3)}$, $ac_s^{(3)}$), the reference command ($r_s^{*(3)}$, $v_s^{*(3)}$, $a_s^{*(3)}$), and the transition acceleration control u. In this example, the error states (e_1, e_2, e_3) are the differences between the reference and output commands shown. As seen in figure 7(a), the aircraft descends to the new reference altitude without overshoot and at a descent rate that saturates at the speed limit, e_{2M}. Thus, the velocity excursion limits for this axis act as the maximum descent and climb rates at which the CG executes altitude changes. The effectiveness of the velocity limiting logic in bounding both x_2 and e_2 is also seen in the state-plane plots of (x_1, x_2) and (e_1, e_2). The control history u(t) consists of a pushover period with saturation at e_{3M}, followed by a null period during which the descent rate is saturated at e_{2M}, and ending with a pullup period that is initially saturated at $-e_{3m}$ and terminates in the linear control regime. Although u(t) is discontinuous, the corresponding filtered acceleration command $e_3(t)$ and the output $ac_s(t)$ are continuous and rate-limited. The character of the entire maneuver is dominated by the nonlinear speed and acceleration saturation features of the control law, a phenomenon necessary to achieve acceptable maneuvering within operational limits even for the present modest altitude step example. A summary view of the CG function in this example is obtained by comparing the output command history (rc_s, vc_s, ac_s) with the input reference commands (r_s^*, v_s^*, a_s^*) in figure 7(a).

The same altitude step example with the addition of a large altitude rate tracking error of 6 m/sec and an acceleration error of 0.125 g (due to TR activity at the initial time) at the maneuver initialization time is shown in figure 7(b). The transition dynamics adapt to this error by initializing in accordance with equation (12) at

$$\underline{e}(t_o) = (-60, -6, 0.125 \text{ g})^T$$

This initialization nulls the apparent tracking errors seen by the trajectory regulator at t_o^+ and maintains continuity of the acceleration command to the Trimmap, act, within the bounds (e_{3Om}, e_{3OM}). The output commands (vc_s, ac_s), are now discontinuous at t_o, and the early part of the maneuver differs in the behavior of (rc_s, vc_s) compared to figure 7(a) in order to relax the initial velocity error.

Figure 8(a) shows a flight-path angle change maneuver; the reference input path changes at t_o from level flight to descent at 4.3 m/sec. The initial conditions for the transition dynamics states for this case are

$$\underline{e}(t_o) = (0,-4.3,0)^T$$

The commanded altitude history lags the reference path and eventually catches it without overshoot. The commanded descent rate necessarily overshoots the reference descent rate temporarily to attain the reference glide path. However, it is possible to eliminate the descent rate overshoot by initializing the transition to a new glide slope in advance of the reference switching time as is commonly done in acquiring the ILS beam for final approach. Criteria and formulas for appropriately advancing the switching time are discussed later in this report. The control u(t) in figure 8(a) corresponds to a pitchover saturated at e_{3M} followed by a pullup to the reference flight-path angle saturated initially at $-e_{3m}$. This pullup and its associated reversals of the acceleration command and aircraft controls can also be eliminated by initiating the pitchover in advance of the reference switching time.

Figure 8(b) compares the pitchover maneuver for five sets of transition dynamics parameter values listed in table 1 for the cases in figure 8(b):

TABLE 1.- PARAMETER VALUES FOR EXAMPLE PITCHOVER MANEUVERS

Case	(ρ,τ_L)	τ, sec	e_{2m},e_{2M}, m/sec	e_{3m},e_{3M}
(1) Reference case	0.73,2	2	4.3	0.125 g
(2) Slower linear dynamics	.73,6	2	4.3	.125 g
(3) Reduced acceleration rate limit	.73,2	6	4.3	.125 g
(4) Reduced speed limit	.73,2	2	1.25	.125 g
(5) Reduced acceleration limit	.72,2	2	4.3	.06 g

Reference case (1) is identical to that in figure 8(a). Case (2) shows the effect of increasing the time constant τ_L of the linear mode dynamics from 2 to 6 sec. This expands the linear region Ω_L considerably (as noted in fig. 6(c)), and the transient now occurs entirely in the linear mode. In the resulting maneuver, peak acceleration and velocity overshoot have decreased, but the maneuver duration has lengthened. Generally, increased τ_L gives a smoother transient by expanding the linear mode region, but at the expense of increased maneuver time.

In case (3), the time constant that limits acceleration rate τ is increased to 6 sec. This expands the initial canonical state and the entire x-plane transition. Peak acceleration rate is markedly reduced as is peak acceleration, but a period of speed saturation appears, along with the largest speed overshoot among the cases shown; the position error state is also increased everywhere, and the maneuver is lengthened. In general, τ is effective in controlling peak acceleration rates and should not be set higher than necessary to achieve this objective.

In case (4), the speed excursion limit is reduced to 1.25 m/sec, and this is seen to be effective in reducing the velocity overshoot, but with a lengthened maneuver.

Acceleration limits are reduced in case (5), effectively reducing the peak acceleration. The entire maneuver is slowed down and position error is increased everywhere due to the lower acceleration limit. These limits should thus be selected solely to control the peak acceleration.

MANEUVER TRACKING PROPERTIES OF THE SYSTEM

In this section the transition dynamics are considered in the context of the complete flight-control system. Maneuver tracking errors are analyzed and the use of predictive modeling of the aircraft response in the transition dynamics in order to prevent the use of feedback for maneuver execution is considered. The initialization rules and control law for the expanded transition dynamics are also given.

The maneuver commands are executed and tracked by the acceleration controller shown in figure 1. Tracking errors develop during all maneuvers due to control response lag, and these errors activate the Trajectory Regulator feedback in the same manner as path errors due to external disturbances. Since the feedback is added to the maneuver acceleration command, sufficiently large tracking errors due to control lags can cause the total acceleration command to the Trimmap to exceed the acceleration limits that were carefully imposed on the trajectory command. We consider here how to modify the transition dynamics design so that, in the absence of external disturbances, the corrective feedback acceleration command during maneuvering is nulled or minimized. One approach, explored in the next section and applied in the AWJSRA system, is to reduce or minimize the acceleration activity (and, hence, control lags) required to transition between any successive pair of trajectory legs. Another approach, explored here, is based on predicting the tracking errors from a model of the aircraft. If such a model is included in the transition dynamics then the position and velocity commands transmitted to the Trajectory Regulator are the predicted aircraft response to the feed-forward maneuver acceleration commands and the feedback commands excited by maneuvering are eliminated to the accuracy of the model. Furthermore, the bounds on excursion velocity and acceleration and on acceleration rates can now be imposed on the predicted aircraft states as well as the commanded states.

The block diagram of figure 9 represents the complete system of figure 1 for a single path axis (the superscript (i) indicating the axis is dropped from the notation throughout this section). Estimation errors and Coriolis accelerations are neglected in the discussion. The element G(s) denotes the transfer function between the commanded and actual accelerations. For conventional aircraft, G(s) principally models the engine, roll, and pitch dynamics, respectively, for the longitudinal, lateral, and normal path axes. The steady-state gain of G(s) is taken as unity. The acceleration disturbance a_d includes the inevitable error in the Trimmap's model of the aircraft forces. This error is assumed constant or slowly varying here and, together with G(s), represents the combined Trimmap and aircraft elements of figure 1 for a single axis. An additional random disturbance noise, $\tilde{a}_d$, represents the effects of wind turbulence. The transition dynamics have been expanded to include an approximate model of the plant dynamics $\hat{G}(s)$ and an estimate of the Trimmap mismatch, $\hat{a}_d$. The dimensions of G and $\hat{G}$ are assumed equal, ignoring possible dimensional mismatch, and denoted as m. In the modified transition dynamics e_3 is the commanded maneuver acceleration while y_1, e_2, e_1 are now the *predicted* acceleration, velocity, and position excursion states of the aircraft. The third-order transition dynamics of the previous section are a special case of figure 5 with

$$m = 0 \ , \quad \hat{G}(s) = I \ , \quad \hat{a}_d = 0$$

Finally, the linear feedback law of the TR is seen in figure 9 and, for generality, it includes acceleration error feedback.

An inspection of figure 9 suggests that the tracking errors z_1, z_2, z_3 can be eliminated in the absence of external disturbances provided all modeling is perfect ($\hat{G} = G$, $\hat{a}_d = a_d$); the transition dynamics are properly initialized to match corresponding aircraft states; the regulator gains, k_1, k_2, k_3 are chosen to stabilize the acceleration controller; and the reference acceleration, a_p^* , is constant. This is actually the case, as is shown next.

Maneuver Tracking

To determine tracking properties, a complete set of state equations for the system of figure 5 is necessary. For the TD these can be given as

$$\left.\begin{aligned}
\dot{e}_1 &= e_2 \\
\dot{e}_2 &= \hat{y}_1 \\
\dot{\hat{y}}_1 &= \hat{y}_2 \\
&\vdots \\
\dot{\hat{y}}_{m-1} &= \hat{y}_m \\
\dot{\hat{y}}_m &= -\sum_{i=1}^{m} \alpha_i \hat{y}_i + \alpha_1 e_3 \\
\dot{e}_3 &= (u - e_3)/\tau
\end{aligned}\right\} \qquad (34)$$

and for the aircraft,

$$\left.\begin{aligned}
\dot{r}_p &= v_p \\
\dot{v}_p &= y_1 + a_d + \tilde{a} \\
\dot{y}_1 &= y_2 \\
&\vdots \\
\dot{y}_{m-1} &= y_m \\
\dot{y}_m &= -\sum_{i=1}^{m} \alpha_i y_i + \alpha_1 (a_p^* + e_3 - \hat{a}_d + k_1 z_1 + k_2 z_2 + k_3 z_3)
\end{aligned}\right\} \quad (35)$$

Here, G(s) and $\hat{G}(s)$ have been given state variable representations in phase-canonical coordinates $\{y_i\}$ and $\{\hat{y}_i\}$, and the model parameters $\{\alpha_i, \hat{\alpha}_i, i = 1, \ldots, m\}$. Tracking errors for the complete system are now defined as:

$$\left.\begin{aligned}
z_1 &= r_p^* + e_1 - r_p \\
z_2 &= v_p^* + e_2 - v_p \\
z_3 &= a_p^* + \hat{y}_1 - y_1 - a_d - \tilde{a}_d \\
z_4 &= \hat{y}_2 - y_2 \\
&\vdots \\
z_{m+2} &= \hat{y}_m - y_m
\end{aligned}\right\} \quad (36)$$

Differentiating equations (36) and using equations (34) and (35) gives the error state equation:

$$\left.\begin{aligned}
\dot{z}_1 &= z_2 \\
\dot{z}_2 &= z_3 \\
\dot{z}_3 &= z_4 + \dot{a}^* - \dot{a}_d \\
\dot{z}_4 &= z_5 \\
&\vdots \\
\dot{z}_{m+2} &= -\alpha_2 z_4 - \ldots - \alpha_m z_{m+2} - \alpha_1 (k_1 z_1 + k_2 z_2 + (k_3 + 1) z_3) \\
&\quad -\alpha_1 (a_d - \hat{a}_d) - \sum_{i=1}^{m} (\hat{\alpha}_i - \alpha_i) \hat{y}_i
\end{aligned}\right\} \quad (37)$$

from which the following tracking properties are obtained.

Assume:

1. Perfect modeling: $\{\hat{\alpha}_i\} = \{\alpha_i\}$, $\hat{a}_d = a_d$

2. Constant disturbance and reference acceleration:

   $\dot{a}_d = \dot{a}^* = 0$, $\tilde{a}_i = 0$

3. k_1, k_2 stabilize equations (37) (the roots of the matrix

$$A = \begin{bmatrix} 0 & & \\ 0 & & \\ \cdot & & \\ \cdot & & I \\ \cdot & & \\ 0 & & \\ \hline -\alpha_1 k_1 & -\alpha_1 k_2 - \alpha_1(1 + k_3) - \alpha_2 \ \ldots \ -\alpha_m \end{bmatrix} \qquad (38)$$

   are all in the left half of the complex plane),

then

1. $\lim_{t \to \infty} \underline{z}(t) = 0$

2. $[\underline{z}(t_o) = 0] \Rightarrow [\underline{z}(t) = 0, \quad t > t_o]$

Under the stated conditions, the errors tend to zero and the aircraft asymptotically approaches the CG trajectory independent of initial conditions and the transition maneuver. Further, by initializing the TD to null the errors, $\underline{z}(t_o)$, ideal tracking with nulled errors at all times is obtained, independent of the trajectory. Under ideal tracking, the feed-forward commands would then excite no regulator activity and operational bounds imposed on the CG trajectory would be satisfied by the actual trajectory of the aircraft as well. The TD initialization rules for this ideal tracking are, using equations (36),

$$\begin{aligned} e_1(t_o) &= r_p(t_o) - r_p^*(t_o^+) \\ e_2(t_o) &= v_p(t_o) - v_p^*(t_o^+) \\ \hat{y}_1(t_o) &= a_p(t_o) - a_p^*(t_o^+) \\ \hat{y}_2(t_o) &= y_2(t_o) \\ &\vdots \\ \hat{y}_m(t_o) &= y_m(t_o) \end{aligned} \qquad (39)$$

This provides initialization rules for all TD states except the acceleration command e_3 which can be initialized for continuity of the total acceleration command to the Trimmap to obtain continuous commands to the aircraft controls:

$$e_3(t_o) = [[\, act(t_o) \,]] + \hat{a}_d - a^*(t_o) \tag{40}$$

Here, the bracket notation $[[\cdot]]$ indicates that the operational bounds on aircraft accelerations are imposed on e_3 and supersede, if necessary, the continuity condition.

A case of practical interest occurs if no estimate of a_d is used ($\hat{a}_d = 0$) and a_d has a nonzero constant value, but otherwise the assumptions of equations (38) hold. Then;

$$\text{If} \quad \dot{a}_d = \dot{a}_p^* = 0 \qquad \text{then} \quad \begin{pmatrix} z_1 \\ z_2 \\ z_3 \end{pmatrix} \xrightarrow[t]{} \begin{pmatrix} a_d/k_1 \\ 0 \\ 0 \end{pmatrix}$$

Here, the trajectory regulator compensates for any constant disturbance or Trimmap model error at the cost of a steady position tracking error. However, the steady-state regulator output is now

$$\Delta a_p \xrightarrow[t]{} -a_d$$

and is itself an estimate of the disturbance.

Control Law Synthesis

In the synthesis of the control law for the expanded transition dynamics (eqs. (34)) the objectives are the same as for the simpler third-order system: to achieve asymptotic stability with good transient properties and to satisfy the constraints (eqs. (16)), repeated here as:

$$e_2 \in [-e_{2m}, e_{2M}]$$

$$e_3 \in [-e_{3m}, e_{3M}]$$

$$\dot{e}_3 \in [-e_{3m}, \dot{e}_{3M}]$$

Fortunately, the same synthesis procedure used in the previous section can be applied to the more complex system (eqs. (34)), as is demonstrated next.

The constraints on acceleration excursion and rate, e_3, $\dot{e}_3$, are again satisfied by bounding the control u as in equation (19) and selecting the filter time constant τ in accordance with equation (21). These results occur because e_3 in equations (34) satisfies the same state equation as does e_3 in equations (11).

For the control law synthesis it is again convenient to decompose the state equations into Jordan canonical form. Transforuing to canonical state variables, we obtain

$$\begin{bmatrix} \dot{x}_1 \\ \dot{x}_2 \\ \dot{x}_3 \\ \cdot \\ \cdot \\ \cdot \\ \dot{x}_{m+2} \\ \dot{x}_{m+3} \end{bmatrix} = \left[\begin{array}{cc|c|c} 0 & 1 & & 0 \\ 0 & 0 & & 0 \\ \hline & & & \\ & 0 & \Lambda & 0 \\ & & & \\ \hline & 0 & & -\tau^{-1} \end{array}\right] \begin{bmatrix} x_1 \\ x_2 \\ x_3 \\ \cdot \\ \cdot \\ x_{m+2} \\ x_{m+3} \end{bmatrix} + \begin{bmatrix} 0 \\ 1 \\ \hline \\ b \\ \\ \hline \tau^{-1} \end{bmatrix} u \qquad (41)$$

where (Λ, b) are of the Jordan form (ref. 9). Since $\hat{G}(s)$ is assumed asymptotically stable the characteristic roots of Λ are all in the left half plane and the unforced dynamics of $(x_3, \ldots, x_{m+2})$ are stable. The structure of equation (41) contains three independent subsystems, each driven by $u(t)$, so that to obtain asymptotic stability of the entire state it suffices to synthesize u for stability of the (x_1, x_2) subsystem $((x_1, x_2, u) \to (0, 0, 0))$. Thus, the control can again be taken as a function of only two states, $u(x_1, x_2)$, with precisely the same result previously given by equations (25)-(27). The corresponding canonical structure of the transition dynamics is shown in figure 10.

The velocity constraints are imposed by the control law on the canonical velocity x_2 which again satisfies these constraints in accordance with equation (31). The commanded maneuver, as distinguished from the predicted maneuver, is given by integrating the acceleration command to the Trimmap; that is, by the states (e_1', e_2') in the auxilliary equations:

$$\left.\begin{aligned} \dot{e}_1' &= e_2' \\ \dot{e}_2' &= e_3 \\ \dot{e}_3 &= \frac{1}{\tau}(u - e_3) \end{aligned}\right\} \qquad (42)$$

The states (e_1, e_2, y_1) in equations (34) are the predicted aircraft response to the command e_3. Since the system (eqs. (42)) is identical to equations (11) it follows that the commanded velocity excursion e_2' satisfies the velocity constraints exactly as did e_2 in the previous section in accordance with equations (30) and (31). The behavior of the predicted velocity e_2 relative to x_2 is governed by the following transfer function (obtained using expressions for $\dot{x}_2, \dot{e}_2$ from eq. (41) and the block diagram of fig. 9)

$$\frac{e_2(s)}{x_2(s)} = \frac{\hat{G}(s)}{\tau s + 1} \qquad (43)$$

During saturation of the canonical velocity, $x_2(t)$ is constant at either $-e_{2m}$ or e_{2M} and then, recalling that $\hat{G}(s)$ has a steady state value of unity, equation (43) yields the desired steady-state saturation of the predicted velocity, that is,

$$\text{If } x_2(t) \text{ is constant} \quad \text{then} \quad \lim_{t \to \infty} e_2(t) = x_2$$

Finally, for reference, the canonical system was derived (using ref. 9) for two useful example cases:

$$\text{(a)} \quad \hat{G}(s) = \frac{1}{\tau_1 s + 1}$$

$$\text{(b)} \quad \hat{G}(s) = \frac{1}{(\tau_1 s + 1)^2}$$

where $\tau_1 \neq \tau$, and $\tau_1, \tau \neq 0$. The results are listed in table 2 (shown on the following page).

TRANSITION INITIALIZATION SWITCHING CRITERIA

Thus far, the transition maneuvering has been constructed on the basis of a single leg of the reference input trajectory. The discontinuities at any leg switch are viewed as initial errors with respect to the new leg, which are to be relaxed by the TD, beginning at each of the reference leg switch times ($t_o^{(m)}$, m = 1, 2, . . ., M). However, maneuver characteristics can often be improved by initiating the transition in advance of the reference leg switch time, and criteria for selecting the switching time are indicated next. The practical value of such advance initialization is already well known in manual flight control for such operations as intercepting the final glide slope just before landing as well as for the more complex maneuvers of reference 8. We seek a generalization of these manual flight tactics, suitable for our automatic flight-control system and applicable to the broader class of input commands considered here.

It is useful to adopt notation which distinguishes the sequence of legs from which the reference trajectory is defined. This sequence is defined by a set of input parameters

$$S = \left\{ \left(t_o^{(m)}, \underline{ro}^{(m)}, \underline{vo}^{(m)}, \dot{v}^{(m)}, rc^{(m)} \right), \quad m = 1, \ldots, M \right\} \tag{44}$$

The elements of S are the states of leg-m at time $t_o^{(m)}$. The trajectory for leg m can be defined at all times and is denoted $(\underline{r}^{(m)}(t), \underline{v}^{(m)}(t), \underline{a}^{(m)}(t))$. The reference trajectory switches from leg m to leg m + 1 at time $t_o^{(m+1)}$ and is thus defined on some flight duration $[t_o^{(1)}, t_F]$ by

TABLE 2.- CANONICAL EQUATIONS FOR PREDICTIVE MODELING CASES

$\hat{G}(s)$	$\frac{1}{\tau_1 s + 1}$ $\quad \tau_1 \neq \tau$ $\tau_1, \tau \neq 0$	$\frac{1}{(\tau_1 s + 1)^2}$ $\quad \tau_1 \neq \tau, \quad \tau_1, \tau \neq 0$
State equations	$\dot{x}_1 = x_2$ $\dot{x}_2 = u$ $\dot{x}_3 = (u - x_3)/\tau_1$ $\dot{x}_4 = (u - x_4)/\tau$	$\dot{x}_1 = x_2$ $\dot{x}_2 = u$ $\dot{x}_3 = (x_4 - x_3)/\tau_1$ $\dot{x}_4 = (u - x_4)/\tau_1$ $\dot{x}_5 = (u - x_5)/\tau$
Transformations	$\begin{pmatrix} x_1 \\ x_2 \\ x_3 \\ x_4 \end{pmatrix} = \begin{bmatrix} 1 & \tau+\tau_1 & \tau\tau_1 & 0 \\ 0 & 1 & \tau_1 & \tau \\ 0 & 0 & 1-r & r \\ 0 & 0 & 0 & 1 \end{bmatrix} \begin{pmatrix} e_1 \\ e_2 \\ e_3 \\ e_4 \end{pmatrix}$ $\begin{pmatrix} e_1 \\ e_2 \\ e_3 \\ e_4 \end{pmatrix} = \begin{bmatrix} 1 & -\tau-\tau_1 & -\tau_1^3/d & \tau^3/d \\ 0 & 1 & \tau_1^2/d & -\tau^2/d \\ 0 & 0 & -\tau_1/d & \tau/d \\ 0 & 0 & 0 & 1 \end{bmatrix} \begin{pmatrix} x_1 \\ x_2 \\ x_3 \\ x_4 \end{pmatrix}$ $r \equiv \tau/\tau_1$ $d \equiv \tau - \tau_1$	$\begin{pmatrix} x_1 \\ x_2 \\ x_3 \\ x_4 \\ x_5 \end{pmatrix} = \begin{bmatrix} 1 & -\tau-2\tau_1 & 2\tau_1(2\tau_1-\tau) & -\tau_1^2(4\tau_1+\tau) & (\tau\tau_1^3+\tau^3\tau_1+7\tau_1^2\tau^2-2\tau_1^4-\tau^4) \\ 0 & 1 & 2\tau_1 & \tau_1^2 & \tau_1(\tau_1^2-\tau^2-2\tau_1\tau)/d^2 \\ 0 & 0 & 1 & \tau & 0 \\ 0 & 0 & -d/\tau_1 & -d & r \\ 0 & 0 & 0 & 0 & 1 \end{bmatrix} \begin{pmatrix} e_1 \\ e_2 \\ e_3 \\ e_4 \\ e_5 \end{pmatrix}$ $\begin{pmatrix} e_1 \\ e_2 \\ e_3 \\ e_4 \\ e_5 \end{pmatrix} = \begin{bmatrix} 1 & \tau+2\tau_1 & -\tau_1^3/d & \tau_1^3(2\tau_1-3\tau)/d^2 & \tau^4/d^2 \\ 0 & 1 & \tau_1^2/d & \tau_1^2(2\tau-\tau_1)d^2 & \tau^3/d^2 \\ 0 & 0 & -\tau_1/d & -\tau\tau_1/d^2 & \tau^2/d^2 \\ 0 & 0 & 1/d & \tau_1/d^2 & -\tau/d^2 \\ 0 & 0 & 0 & 0 & 1 \end{bmatrix} \begin{pmatrix} x_1 \\ x_2 \\ x_3 \\ x_4 \\ \dot{x}_5 \end{pmatrix}$

$$\left\{\begin{pmatrix}\underline{r}^*(t)\\ \underline{v}^*(t)\\ \underline{a}^*(t)\end{pmatrix},\ t \in [t_o^{(i)}, t_F]\right\} = \left\{\left\{\begin{pmatrix}\underline{r}^{(m)}(t)\\ \underline{v}^{(m)}(t)\\ \underline{a}^{(m)}(t)\end{pmatrix},\ t \in [t_o^{(m)}, t_o^{(m+1)}]\right\},\ m = 1, \ldots, M\right\} \tag{45}$$

where $t_o^{(M+1)} \equiv t_F$.

The leg-switching problem is illustrated in figure 11 for the pitchover example; the altitude histories for two successive legs of the reference trajectory are shown, with the reference switch time $t_o^{(m+1)}$ corresponding to the time of equal altitude for the two legs; the two legs are visualized as extending indefinitely far backward and forward in time. The relative error between the current trajectory and the next leg is defined at all times by

$$\left\{[\hat{\underline{r}}(t) - \underline{r}^{(m+1)}(t),\ \hat{\underline{v}}(t) - \underline{v}^{(m+1)}(t),\ \hat{a}(t) - a^{(m+1)}(t)];\ -\infty < t < \infty\right\} \tag{46}$$

Thus a set of error states is defined from which the transition can be initiated, and the initialization time can be selected from this set to obtain the most favorable initial state for the subsequent transient. The possibility that the extension of leg-switching times to all t will bring the switch into conflict with other legs of the reference can be neglected here since in practice the parameters of S are selected such that the $\{t_o^{(m)}\}$ are close to the optimum switching times compared to the leg durations. Figure 11 shows three transitions generated by the TD previously defined, assuming perfect tracking and estimation at the time of initialization. Trajectory (a), which initializes at $t_o^{(m+1)}$, requires significant position excursion from the reference and, more significantly, a flight-path angle overshoot to rendezvous with the reference trajectory and maximum initial jerk. In contrast, trajectory (b), initiated at time T prior to t_o, reduces the tracking excursions, eliminates the velocity overshoot, and reduces the implied acceleration excursions and acceleration rates for the maneuver, compared to (a). Finally, trajectory (c) is initiated too early and the TD attempts to climb to the backward extrapolation of the next leg. As in case (a), this requires maximum initial jerk followed by a control reversal and also the flight-path angle excursion exceeds the initial error that was to be relaxed. Thus, the initialization time generally has a significant effect on the characteristics of the ensuing transition synthesized by the CG. Criteria for the selection of this time are developed next.

Initialization Time Criteria

In this section, criteria are established to optimize leg-switch transitions with respect to the possible initial error states for the TD defined in equation (46). At any time t these states are defined by

$$\left.\begin{aligned} E_1(t) &= A_{ps}(t)(\hat{r}_s(t) - r_s^{(m+1)}(t) \\ E_2(t) &= A_{ps}(t)(\hat{v}_s(t) - v_s^{(m+1)}(t) \\ A(t) &= A_{ps}(t)(\hat{a}_s(t) - a_s^{(m+1)}(t) \\ E_3(t) &= A_{ps}(t)(act_s(t) - a_s^{(m+1)}(t) \end{aligned}\right\} \qquad (47a)$$

where A_{ps} is the transformation to path axes from runway axes (eq. (2)). Then, for a single path axis, the corresponding initial values of the canonical TD states are, from equation (24)

$$\left.\begin{aligned} x_1^{(i)}(t) &= E_1^{(i)}(t) + \tau^{(i)} E_2^{(i)}(t) \\ x_2^{(i)}(t) &= E_2^{(i)}(t) + \tau^{(i)} E_3^{(i)}(t) \end{aligned}\right\} \quad i = 1, 2, 3 \qquad (47b)$$

The natural acceleration error A, in equations (47a), governs the local evolution of the states E_1, E_2, and is distinguished from the constructed acceleration state, E_3, used to initialize the TD. For simplicity, the formula for the canonical states x_1, x_2 above assumes the third-order transition dynamics although the criteria established here are valid for the higher order TD of the previous section.

The criteria for selecting a best initialization time T for a single path axis depend on characteristics of the ensuing transition maneuver and differ for the nonlinear and linear modes. For the nonlinear mode transitions, the control u(x(t)) may undergo a discontinuous change with a sign reversal during the transition. The resulting commanded acceleration rate magnitude or jerk $|\dot{e}_3^{(i)}|$ of the transition and the corresponding aircraft control rates (i.e., engine thrust, roll-angle, and pitch-angle command rates) are a local maximum at such a discontinuity. In addition, control sign reversals imply the possibility of velocity reversals and unnecessarily large velocity and acceleration excursions. Thus, the smoothness of the nonlinear mode transient strongly depends on whether there is a control sign reversal during the transient and, consequently, a good criterion for initialization time selection is simply to prevent such reversals; that is, select T so that

$$\sigma[x(t)] = 0 \quad \text{and} \quad x(t) \in \tilde{\Omega}_L \qquad (48)$$

where σ is given by equation (26) and x(t) is given from equations (47). This criterion ignores the character of the final linear mode portion of the transient since maneuver characteristics of interest are dominated by the nonlinear portion. Further, the locus of possible initial states x(t) defined in equations (47) may not intersect the switching curve, but this occurs only in cases such that the nominal transition is independent of the initialization time.

The effects of this choice of initialization time are illustrated in figure 12(a) for the pitchover maneuver. Maneuvers initialized at 0, 4, and 10 sec prior to the reference leg switch time are compared, assuming no errors in tracking the reference path at initialization. Reference time initialization (a) shows control sign reversal in $u(t)$ and $e_3(t)$ and velocity overshoot. Case (b), which initializes 4 sec earlier and for which there is no control sign reversal, is an obvious improvement over (a); the velocity excursion for the maneuver does not exceed the discontinuity on the reference path, and the period at saturated control, maneuver duration, and peak acceleration rates are all considerably reduced. Finally, (c) begins too early and introduces control sign and velocity reversals early in the transient where it attempts to climb to the backward extrapolation of the next leg. These three transitions are further compared in the x-plane in figure 12(b). The switching curves and boundaries separating regions of linear and nonlinear transitions are shown as dashed lines, and the locus of possible initial conditions for the transition, defined from equation (46), is given by the line L. Only nonlinear transitions can occur in this example because L never enters Ω_L. The reference time initialization (at a) shows x_2 overshooting zero until the switching curve, $\sigma = 0$, is reached; a control sign reversal and reduction of the canonical speed follows. For the earliest initialization (c), the speed $|x_2|$ increases until the switching boundary is encountered, followed by control reversal and speed reduction. In both cases, the speed excursion on the transient, $(x_2)_{max} - (x_2)_{min}$, greatly exceeds the initial speed discontinuity to be relaxed. Finally, (b), which initializes when L encounters the switching curve, enters the linear region without control sign or speed reversals and also requires the least maneuver time, time at saturated control, and speed excursion among these cases. Thus, the transition in this example is optimized (in the above sense) by initializing at the control switching curve.

For transitions initialized in the linear region, the initialization time can be selected to eliminate or minimize the magnitude of initial jerk to obtain the (locally) smoothest maneuver. Some consequences of this choice in the pitchover example are seen in figure 12(c). Here the locus L of possible initial conditions crosses the linear mode region. The zero-initial-jerk transition begins at (d) and uses the lowest velocity and position excursions and peak acceleration command compared to earlier initialization (at e) or later initialization (at a, c, or the reference leg switching time, b) and all nonlinear transitions are poorer in these measures than some linear transitions that can be initialized from L. Consequently, minimum initial jerk is the criterion used to initialize linear transitions; that is, the linear-mode jerk associated with initializing at t is given from equations (47) as

$$J_o(t) = \frac{\left|-x^T(t)k^{(i)} - E_3^{(i)}(t)\right|}{\tau}$$

and then T is selected such that

$$J_o(t) \text{ is minimized and } x(T) \in \Omega_L \tag{49}$$

An alternative linear-mode initialization criterion, studied in reference 8, would minimize the cost function of the linear optimal control with respect to the set of possible initial conditions. Criteria have been stated for the initialization time for both linear and nonlinear modes of the TD. By applying these criteria, transitions are smoothed, eliminating either initial acceleration rate or unnecessary control sign reversals. Such choices of initialization time also approximately minimize the extremes of acceleration and velocity excursions as well as, roughly, the overall acceleration activity and maneuver duration required, compared to other initialization times. The criteria given here lead to closed-form results for the initialization time which can be incorporated in the CG structure of figure 2 as the initialization switching algorithm; these are derived next.

The above criteria (eqs. (48) and (49)) apply independently on each path axis and, in general, distinct optimum switching times ($T^{(i)}$, i = 1, 2, 3) are obtained. The details of synthesizing the 3-axis command during the period between initializing the transition on one axis and on all three axes are given last in this section.

Linear Mode Transition Initialization Time

Throughout the derivation of the initialization time formulas, only a single axis is considered and the axis superscript is dropped from the notation. Third-order transition dynamics are assumed ($\hat{G}(s) = 1$) and the formulas are derived for the time-to-go, ΔT, to the optimum initialization time for the convenience of on-line use of these results in the CG. If t is the current time, then optimum initialization time T is

$$T = t + \Delta T \tag{50}$$

For linear transitions, ΔT is calculated to minimize the jerk that occurs immediately following initialization; that is, to minimize over all Δt, the quantity

$$J_0(t + \Delta t) = \frac{\left|-k^T x(t + \Delta t) - E_3(t + \Delta t)\right|}{\tau} \tag{51}$$

To evaluate the dependence of terms in equation (51) on Δt, let $(E_1(t), E_2(t), E_3(t), A(t))$ be the current error from the next leg and let the future behavior of this error state be predicted assuming constant relative acceleration, $L(t)$:

$$\begin{pmatrix} E_1(t + \Delta t) \\ E_2(t + \Delta t) \\ A(t + \Delta t) \end{pmatrix} = \begin{bmatrix} 1 & \Delta t & \Delta t^2/2 \\ 0 & 1 & \Delta t \\ 0 & 0 & 1 \end{bmatrix} \begin{pmatrix} E_1(t) \\ E_2(t) \\ A(t) \end{pmatrix} \tag{52}$$

and constant relative acceleration command, $E_3(t + \Delta t) = E_3(t)$. This assumption is valid nominally (no disturbances, perfect tracking) and locally valid otherwise.

The evolution of the corresponding canonical coordinates and initial TD acceleration and control are given from equation (52) using

$$\left.\begin{aligned} x_1(t + \Delta t) &= E_1(t + \Delta t) + \tau E_2(t + \Delta t) \\ x_2(t + \Delta t) &= E_2(t + \Delta t) + \tau E_3(t) \\ e_3(t + \Delta t) &= E_3(t) \\ u(t + \Delta t) &= -k_1 x_1(t + \Delta t) - k_2 x_2(t + \Delta t) \end{aligned}\right\} \tag{53}$$

The time-to-go, ΔT, which nulls initial jerk, is obtained by substituting equations (52) and (53) in (51) and solving

$$0 = k_1 E_1(t) + (k_2 + \tau k_1) E_2(t) + (\tau k_2 + 1) E_3(t) + \frac{[k_1 E_2(t) + (k_2 + \tau k_1) A(t)]\Delta t + k_1 A(t) \Delta t^2}{2} \tag{54}$$

In the remaining derivation the variable t is dropped from $E_1(t)$, $E_2(t)$, etc. when denoting conditions at the current time. The solution of equation (54) yields the following cases:

$$\Delta T = \begin{cases} \text{undefined} & \text{If } A, E_2 = 0 \\ -a & \text{If } A = 0, \ E_2 \neq 0 \\ -b + \sqrt{\max(0, b^2 - c)} & \text{If } A \neq 0 \end{cases} \tag{55}$$

where

$$a = \frac{\left(E_1 + \left(\tau + \frac{k_2}{k_1}\right) E_2 + \frac{\tau k_2 + 1}{k_1} E_3\right)}{E_2}$$

$$b = \frac{E_2}{A} + \tau + \frac{k_2}{k_1}$$

$$c = 2 \frac{\left(E_1 + \left(\tau + \frac{k_2}{k_1}\right) E_2 + \frac{\tau k_2 + 1}{k_1} E_3\right)}{A}$$

Three cases are distinguished in equation (55). In the first case (E_2, $A = 0$) only a position step discontinuity occurs between the current state and the next leg as, for example, when a step change in altitude or lateral or longitudinal position occurs at the reference leg switch and there is perfect tracking. In this case, the initial conditions for the TD are fixed and independent of the initialization time; the initialization time is selected, therefore, on some basis other than minimum initial jerk.

In the second case ($E_2 \neq 0$, $A = 0$) a velocity and, possibly, a position discontinuity, occurs but no acceleration change as, for example, where a discontinuity in speed or flight-path angle or direction occurs at the reference leg switching time and there is perfect tracking (e.g., fig. 12(c)). If, in addition, the reference legs are position-continuous at $t_o(E_1(t_o) = 0)$, as is often the case, then equation (55) gives the optimum initialization time as

$$T = t_o - \left(\tau + \frac{k_2}{k_1}\right) \tag{56}$$

This value is always earlier than ("leads") the reference time and is independent of $E_2(t_o)$. This lead can be incorporated in the reference trajectory itself by specifying a position discontinuity at t_o such that T and t_o are identical; from equation (55) the required discontinuity is

$$E_1(t_o) = -E_2(t_o)\left(\tau + \frac{k_2}{k_1}\right)$$

In the last case in equation (55) an acceleration discontinuity occurs on the reference trajectory at t_o as, for example, when one of the legs is a turn or executes a constant acceleration speed change. Here, the quadratic equation (54) has two solutions which are either real or complex. They are complex if there is no time Δt at which the control, $u(t + \Delta t)$ given by equations (53) can null the jerk. In this case, jerk is minimized by initializing at $t = -b$ and consequently this is taken as the optimum initialization time.

If two real solutions occur, initial jerk is nulled at both times, but it can be shown that the acceleration magnitude $|e_3|$ increases following initialization at the earlier time and decreases following the later initialization. Thus, the earlier solution produces a transition on which the acceleration excursion $e_{3max} - e_{3min}$ necessarily exceeds the initial acceleration discontinuity E_3 between the two legs; consequently the later initialization has been selected in equation (55).

Frequently, reference trajectories with an acceleration discontinutiy have continuous position and velocity at the reference leg switch time ($E_1(t_o)$, $E_2(t_o) = 0$) and then equation (55) gives:

$$T = t_o - \left(\tau + \frac{k_2}{k_1}\right)\left(1 - \sqrt{\max\left\{0, 1 - \frac{2k_1(\tau k_2 + 1)}{(\tau k_1 + k_2)^2}\right\}}\right) \tag{57}$$

Thus, the optimum time leads the reference leg switch time by an amount that is independent of the magnitude of $E_3(t_o)$.

For on-line use of equation (55) it should be noted that if ΔT is negative, then the optimum initialization time has been passed and the initial jerk is an increasing function of time; consequently, jerk is minimized by initializing the transition immediately, and equation (50) is modified to

$$T = t + \max\{0, \Delta T\} \tag{58a}$$

Further, the formulation in equation (55) is computationally sensitive at the boundaries between the three cases to the small nonzero values of E_2 or A which occur as a result of tracking errors and disturbances. If (A, E_2) are zero on the reference trajectory, then small tracking errors have a large effect on ΔT but the resulting transition maneuver remains insensitive to the initialization time. If the reference trajectory is a velocity-step case then the optimum time is not sensitive to small nonzero values of A, but the formulation in equation (55) becomes ill-conditioned. Two devices are used in the applications work of this paper to avoid these two difficulties. First, the leg initialization time is limited to a short period, $(t_o - T_1, t_o + T_2)$, in the neighborhood of the reference switch time so that equation (50) is further modified to

$$T = \max\left\{\left[t_o - T_1, \quad \min\left\{t + \max\{0, \Delta T\}, \quad t_o + T_2\right\}\right]\right\} \tag{58b}$$

Secondly, the three cases in equation (55) are distinguished on the basis of approximate nulling of (A, E_2) rather than exact nulling by the use of threshold values, ϵ_2, ϵ_3. The conditions for each case are therefore:

$$\left.\begin{array}{lll} \text{Case 1} & \text{If} & |A| < \epsilon_3, \quad |E_2| < \epsilon_2 \\ \text{Case 2} & \text{If} & |A| < \epsilon_3, \quad |E_2| \geq \epsilon_2 \\ \text{Case 3} & \text{If} & |A| > \epsilon_3 \end{array}\right\} \tag{59}$$

Nonlinear Mode Transition Initialization Time

For nonlinear transitions, initialization is taken at the intersection of the locus of possible initial states with the control switching boundary in accordance with the criterion given in equation (48). This prevents control sign reversals at saturated levels. The intersection occurs at ΔT such that $\sigma[x(t + \Delta T)]$ is nulled, where, as defined earlier,

$$\sigma(x) = \begin{cases} e_{3m} x_1 + \frac{1}{2} x_2^2 & x_2 > 0 \\ e_{3M} x_1 - \frac{1}{2} x_2^2 & x_2 < 0 \end{cases} \tag{60}$$

Different functions define $\sigma(x)$ depending on whether the state $x(t)$ is above or below the x_1-axis and these are distinguished in the notation as

$\sigma^{(+)}$, $\sigma^{(-)}$. Equations (52) and (53) are substituted in equation (60) to evaluate the variation of σ along the locus:

$$\sigma^{(+)}(x(t+\Delta t)) = \left(e_{3m}x_1 + \frac{1}{2}x_2^2\right) + [E_2(e_{3m} + A) + \tau A(e_{3m} + E_3)]\Delta t + A(e_{3m} + A)\frac{\Delta t^2}{2} \tag{61a}$$

$$\sigma^{(-)}(x(t+\Delta t)) = \left(e_{3M}x_1 - \frac{1}{2}x_2^2\right) + [E_2(e_{3M} - A) + \tau A(e_{3M} - E_3)]\Delta t + A(e_{3M} - A)\frac{\Delta t^2}{2} \tag{61b}$$

The appropriate initialization time is selected from those times which null σ in equations (61) and this selection results in the following cases:

$$\Delta T = \begin{cases} \text{undefined} & \text{If } A, E_2 = 0 \\ -a_1 & \text{If } E_2 \neq 0, \ A = 0 \\ -b_1 + \sqrt{\max\{0, b_1^2 - c_1\}} & \text{If } A \neq 0 \end{cases} \tag{62}$$

where

$$a_1 = \frac{u_o x_1 + 0.5|x_2|x_2}{u_o E_2} = \frac{\sigma}{u_o E_2}$$

$$u_o = \begin{cases} e_{3m} & x_2 > 0 \\ e_{3M} & x_2 < 0 \end{cases}$$

$$b_1 = \frac{E_2}{A} + \tau\frac{u + \theta E_3}{u_1 + |A|} = \frac{x_2}{A} + \tau\frac{A - E_3}{A}\frac{u_1}{u_1 + |A|}$$

$$c_1 = \frac{2u_1 x_1 + \theta x_2}{A(u_1 + |A|)}$$

$$\theta = \text{sign } (A)$$

$$u_1 = \begin{cases} e_{3m} & A > 0 \\ e_{3M} & A < 0 \end{cases}$$

Three cases occur in equation (62). First, if there is only a position discontinuity between the current state and the next leg (A, $E_2 = 0$) the

initial conditions for the TD are fixed and independent of the initialization time, and no optimum time is defined.

Secondly, if there is a velocity discontinuity but no acceleration change ($E_2 \neq 0$, $A = 0$) then the locus of initial conditions is parallel to the x_1-axis and equations (61) yield a single time at which the locus intersects the switching boundary (fig. 12(b)). If the reference trajectory has continuous position at the reference leg-switching time and tracking errors are ignored, then the optimum initialization time always leads the reference switching time as given by

$$T = t_o - \left(\tau + \frac{1}{2}\frac{|E_2(t_o)|}{u_o}\right) \tag{63}$$

The required lead depends on the size of the velocity discontinuity $|E_2|$. A velocity change can be specified in the reference trajectory simply as a velocity step at some time t_o, or, if very large lead time is required in equation (63), as a constant acceleration leg of duration E_2/A beginning at t_o. In either case the transition dynamics fill in the remaining details of the maneuver. The lead time in equation (63) can also be incorporated in the reference trajectory by specifying a position discontinuity at t_o such that T and t_o coincide, as given by

$$E_1(t_o) = -E_2\left(\tau + \frac{1}{2}\frac{|E_2|}{u_o}\right)$$

Finally, in the case of acceleration steps ($A \neq 0$) the locus of possible initial transition dynamics states is a parabola with axis of symmetry parallel to the x_1-axis (see sketch (b)) and, from equations (52) and (53), can be given in the form

$$A = \frac{1}{2}\frac{(x_2(t + \Delta t) - x_{2v})^2}{x_1(t + \Delta t) - x_{1v}}$$

with the time and location of the vertex given by

$$\Delta t_v = -\frac{x_2}{A} - \tau\frac{A - E_3}{A}$$

$$(x_{1v}, x_{2v}) = \left(x_1 - \frac{A}{2}\left(\tau + \frac{E_2}{A}\right)^2 , -\tau(A - E_3)\right)$$

For positive (negative) values of A, the locus is traversed with increasing (decreasing) velocity; the x_1-axis crossing occurs at time

$$\Delta t_x = -\frac{x_2}{A}$$

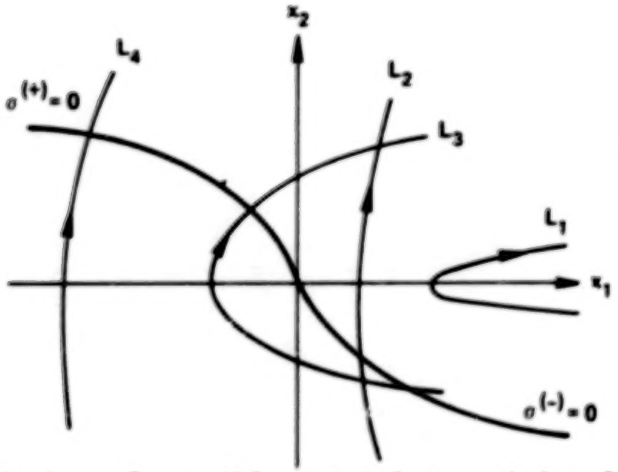

Sketch (b).- Evolution of possible initial transition dynamics states; $A > 0$.

and x_1 reaches a minimum (maximum) at the vertex. In perfect tracking, the vertex falls on the x_1-axis. It is also noted that the switching curve ($\sigma(x) = 0$) consists of two half-parabolas with vertexes at the origin and accelerations, e_{3m} and e_{3M}.

The roots of equations (61) provide various possibilities for 0, 1, or 2 points at which $\sigma(x)$ is nulled, as is illustrated in sketch (b) by the loci L_1, L_2, L_3, L_4 and their intersections with the two branches of the control switching curve. If A is positive, a single solution is selected in equation (62) to minimize $|\sigma^{(+)}|$. Thus, if equation (61a) has two real roots (as for L_3, L_4 in sketch (b)) the later one is selected and thus nulls $\sigma^{(+)}$. If equation (61a) has complex roots (as for L_1, L_2) then the real part of the root is selected ($\Delta t = -b_1$); this minimizes $|\sigma^{(+)}|$ and corresponds to a point on the locus between the x_1- axis crossing and the vertex.

These choices are based on the following rationale. If the locus intersects both branches (L_3), transitions initialized on either branch prevent reversals in u, but those initialized on the lower branch have increasing $|e_3|$ initially so that the acceleration excursion for the transition, $e_{3max} - e_{3min}$, necessarily exceeds the original discontinuity that was to be relaxed, E_3. Transitions initialized on the upper branch decrease $|e_3|$ at the maximum rate initially. If the locus intersects only the lower branch (L_2), transitions initialized on the lower branch have slowly decreasing $|e_3|$ initially and the location and timing of the intersection is sensitive to tracking errors. In this and all cases for which no intersection of the upper branch occurs, initialization is taken at minimum $|\sigma^{(+)}|$. This produces a reversal in u during transition, but the duration of transition, the time spent at saturated control, and the excursions in x_1, x_2 for the transition are all approximately minimized, and the initialization time is relatively insensitive to tracking errors.

For negative values of A, an analogous rationale occurs by reversing the roles of the upper and lower branches of the switching curve, and the corresponding choice of roots of equation (61b) is contained in equation (62).

If the reference trajectory has continuous position and velocity at the leg switch time ($E_1(t_o) = E_2(t_o) = 0$) and tracking errors are neglected, equation (62) gives

$$T = t_o - \tau\left[1 - \sqrt{\frac{u_1}{u_1 + |A|}}\right] \tag{64}$$

Here, T always leads the reference leg switch time but by an amount less than τ.

The same remarks noted for on-line use of the linear case results again apply to on-line use of equation (62); the transition is initialized as soon as the optimum time is passed (eq. (58a)), but the timing adjustment from the reference time is limited to a short period containing t_o, as in equation (58b). Further, it is useful to distinguish the cases in equation (62) on the basis of approximate nulling of A or E_2 as in equations (59).

Synthesis of Three Axis Transition

The preceding results define the initialization time for the transition along a single path axis. These apply straightforwardly in cases when the discontinuities on the reference trajectory are along only one path axis, as in the pitchover example. For maneuvers with discontinuities along two or three axes (e.g., simultaneous turn-entry, pitchover, and speed-change) to be relaxed by the transition, the initialization time optimization criteria apply to each axis independently and result in different optimum times for each axis. In this case, the TD can be initialized independently for each axis but the reference trajectory must also be switched to the next leg for that axis. The method of constructing this modified reference trajectory during the period between initializing one axis and all three axes is given next; the process consists of axis by axis superposition of the relative trajectory between the two successive legs.

First, special formulas are given for extrapolating the next leg (leg m + 1) backward in time from the leg-junction at $t_o^{(m+1)}$. The discontinuity between the two legs at the reference switching time is given by

$$\left.\begin{aligned} en_1^{(m+1)} &\equiv A_{ps}\left(t_o^{(m+1)}\right)\left(r_s^{(m+1)}\left(t_o^{(m+1)}\right) - r_s^{(m)}\left(t_o^{(m+1)}\right)\right) \\ en_2^{(m+1)} &\equiv A_{ps}\left(t_o^{(m+1)}\right)\left(v_s^{(m+1)}\left(t_o^{(m+1)}\right) - v_s^{(m)}\left(t_o^{(m+1)}\right)\right) \\ en_3^{(m+1)} &\equiv A_{ps}\left(t_o^{(m+1)}\right)\left(a_s^{(m+1)}\left(t_o^{(m+1)}\right) - a_s^{(m)}\left(t_o^{(m+1)}\right)\right) \end{aligned}\right\} \tag{65}$$

as referred to path axes of leg m calculated from $\underline{v}^{(m)}(t_o^{(m+1)})$. We define the difference between the two legs for $t \leq t_o$ by assuming constant relative

acceleration in path axes en_3, and using equations (65) as the difference at $t_o^{(m+1)}$; that is

$$\left.\begin{aligned} en_3(t) &= en_3^{(m+1)} \\ en_2(t) &= en_2^{(m+1)} + en_3^{(m+1)}\left(t - t_o^{(m+1)}\right) \\ en_1(t) &= en_1^{(m+1)} + en_2^{(m+1)}\left(t - t_o^{(m+1)}\right) + \frac{1}{2}\, en_3^{(m+1)}\left(t - t_o^{(m+1)}\right)^2 \end{aligned}\right\} \qquad (66)$$

and the extrapolation of leg m + 1 backward in time from $t_o^{(m+1)}$ is constructed from the superposition of leg m and the relative trajectory

$$\begin{pmatrix} r_s^{(m+1)}(t) \\ v_s^{(m+1)}(t) \\ a_s^{(m+1)}(t) \end{pmatrix} = \begin{pmatrix} r_s^{(m)}(t) \\ v_s^{(m)}(t) \\ a_s^{(m)}(t) \end{pmatrix} + \begin{pmatrix} A_{ps}^T(t)en_1(t) \\ A_{ps}^T(t)en_2(t) \\ A_{ps}^T(t)en_3(t) \end{pmatrix} \qquad t \leq t_o^{(m+1)} \qquad (67)$$

Equations (66) restrict the relative trajectory in path axes to one of constant relative acceleration during the period prior to $t_o^{(m+1)}$; if both legs are straight lines with constant inertial acceleration, then the result in equation (67) is identical to extrapolating leg m + 1 from its input parameters. If either leg is a circular arc this is not the case, but the constant relative acceleration extrapolation is the appropriate one for use with the anticipation time formulas previously derived.

The TD can be initialized at any time $t \leq t_o^{(m+1)}$ on the basis of errors from the extrapolated next leg given, using equations (47) and (67), as

$$\begin{pmatrix} E_1(t) \\ E_2(t) \\ E_3(t) \\ A(t) \end{pmatrix} = \begin{pmatrix} A_{ps}(t)\left(\hat{r}_s(t) - r_s^{(m)}(t)\right) \\ A_{ps}(t)\left(\hat{v}_s(t) - v_s^{(m)}(t)\right) \\ [[\, A_{ps}(t)act_s(t)\,]] - A_{ps}(t)a_s^{(m)}(t) \\ A_{ps}(t)\left(\hat{a}_s(t) - a_s^{(m)}(t)\right) \end{pmatrix} - \begin{pmatrix} en_1(t) \\ en_2(t) \\ en_3(t) \\ en_3(t) \end{pmatrix} \qquad (68)$$

The first term in equation (68) is the difference between the estimated state and the state on leg m of the reference trajectory and is nonzero due either to tracking errors or to transitions which were initiated earlier but have not yet been completed.

Finally, if axis i is initialized at time $T^{(i)}$, the initial conditions for its transition dynamics are

$$e_j^{(i)}(0^+) = E_j^{(i)}(T^{(i)}) \qquad j = 1,2,3 \tag{69}$$

and the reference path is switched to the next leg for axis i by means of the superposition

$$\left.\begin{aligned} r_s^*(t) &= r_s^{(m)}(t) + A_{PS}^T(t)D(t)en_1(t) \\ v_s^*(t) &= v_s^{(m)}(t) + A_{ps}^T(t)D(t)en_2(t) \\ a_s^*(t) &= a_s^{(m)}(t) + A_{ps}^T(t)D(t)en_3(t) \end{aligned}\right\} \tag{70}$$

where

$$D \equiv [\sim\delta_i\_]$$

$$\delta_i \equiv \begin{cases} 0 & t < T^{(i)} \\ 1 & t > T^{(i)} \end{cases}$$

This reference trajectory coincides with the prior leg for times earlier than initialization of the first axis and with the next leg for times later than initialization of the third axis.

A COMMAND GENERATOR ALGORITHM

A Command Generator (CG) has been designed from the preceding theoretical analysis for use in an application of the control system structure of figure 1 to Ames' experimental powered-lift aircraft, the augmentor wing jet STOL research aircraft (AWJSRA). This design is defined next with flow charts and equations for the basic structure of the algorithm (fig. 13) and its principal elements; the reference trajectory generator (eqs. (73) and (75)), the transition initialization algorithm (fig. 14), and the transition dynamics (fig. 15). A number of specializing choices occur in this application, and the rationale for these choices is noted in the discussion. The selection of parameter values is discussed in the next section. This algorithm has been subjected to and is the result of the simulation tests described in the following two sections. It is noted that the CG design structure, many parameter values, and the conclusions drawn from the simulation tests are independent of the specific aircraft being controlled within the class of CTOL and STOL aircraft, and for passenger operations; therefore, details of the AWJSRA are omitted in most of the discussion.

Input Parameters and Reference Trajectory Generator

Figure 13 shows a flow chart of the CG logic executed each computation cycle in flight. The first element generates the reference trajectory for the current time and leg. The reference trajectory is assumed defined initially by a set of parameters which are the initial conditions for a set of M legs of the trajectory:

$$S = \{[t_o^{(m)}, ro_s^{(m)}, vo_s^{(m)}, \dot{v}^{(m)}, R_c^{(m-1)}], \quad m = 1, 2, \ldots, M\} \qquad (71)$$

These are the initial position and velocity in runway coordinates and the speed rate and horizontal plane radius of curvature for the leg. A number of properties are satisfied by these parameters and are assumed in the CG design. The set of initial leg times $\{t_o^{(m)}\}$ is ordered and strictly increasing and the reference path is intended to sequence through these legs switching from leg m - 1 to leg m at $t_o^{(m)}$. The leg durations, $(t_o^{(m+1)} - t_o^{(m)})$ are normally longer than the transition settling time implied by the leg-junction discontinuities, $(ro_s^{(m+1)} - r_s^{(m)}(t_o^{(m+1)}))$, etc., and the leg switching times are normally close to the optimum transition initialization times implied by the leg-junction discontinuities. These last two properties are not necessary conditions for the functioning of the CG logic of figure 13, but are expected properties of the class of operational inputs which have motivated the transition dynamics concept and which underly the effectiveness of the transition dynamics initialization algorithm. It is also assumed that leg-junction discontinuities are limited in magnitude to avoid significant inconsistencies in the transition kinematics due to neglected Coriolis accelerations. Finally, the reference trajectory is assumed to satisfy operational constraints on the trajectory derived from passenger comfort considerations and the limits of aircraft capabilities.

An analysis of the sources and definition of the reference trajectory is beyond our scope, but it can be generated by an ATC-4D guidance system, such as that described in reference 3. At the start of an approach to an airport, such a guidance system can define a reference path beginning at the current location of the aircraft and passing through a sequence of way-point positions $(ro_s^{(m)})$ corresponding to the established approach routes of the airport; times and velocities at each way-point $(to^{(m)}, vo_s^{(m)})$ and corresponding acceleration parameters $(\dot{v}^{(m)}, R_c^{(m)-1})$ for each leg satisfy operational constraints for steady and nearly-steady flight conditions.

The reference trajectory is generated from the input parameters listed in equation (71). These parameters specify each leg as either a straight line with constant inertial acceleration or a helical path with constant radius of curvature. This set accommodates the restricted domain of passenger aircraft reference trajectories and of related guidance systems such as those of reference 3. For straight legs ($R_c^{-1} = 0$), the acceleration vector is constant and aligned with the flight direction so that the reference trajectory is generated by the equations

$$
\left.
\begin{aligned}
a_s^{(m)}(t) &= \dot{v}^{(m)} \frac{vo_s^{(m)}}{|vo_s^{(m)}|} \\
v_s^{(m)}(t) &= vo_s^{(m)} + a_s^{(m)}(t - t_o^{(m)}) \\
r_s^{(m)}(t) &= ro_s^{(m)} + vo_s^{(m)}(t - t_o^{(m)}) + \frac{1}{2} a_s^{(m)}(t - t_o^{(m)})^2
\end{aligned}
\right\} \qquad (72)
$$

To generate helical paths ($R_c^{-1} \neq 0$), the trajectory coordinates are separated into vertical axis and horizontal plane coordinates. The vertical axis components (denoted z here) are governed by constant acceleration:

$$
\left.
\begin{aligned}
\ddot{z}^{(m)} &= \frac{\dot{\Phi}^{(m)} \underline{vo}^{(m)} \cdot \underline{s}_3}{|vo_s^{(m)}|} \\
\dot{z}^{(m)} &= \underline{vo}^{(m)} \cdot \underline{s}_3 + \ddot{z}^{(m)}(t - t_o^{(m)}) \\
z^{(m)} &= \underline{ro}^{(m)} \cdot \underline{s}_3 + (\underline{vo}^{(m)} \cdot \underline{s}_3)(t - t_o^{(m)}) + \frac{1}{2} \ddot{z}^{(m)}(t - t_o^{(m)})^2
\end{aligned}
\right\} \qquad (73)
$$

where $\{\underline{s}_1, \underline{s}_2, \underline{s}_3\}$ are the runway axes. The horizontal plane coordinates are governed by a constant radius turn, where R_c is positive (negative) for right-hand (left-hand) turns. It is convenient to define the unit tangent and radial vectors in the horizontal plane ($\underline{u}$, $\underline{m}$), the center of the circle, $\underline{c}$, and the arc length from the initial position, s, in sketch (c). The horizontal plane coordinates, (denoted x, y here) are given in terms of these quantities by

$$
\left.
\begin{aligned}
\begin{pmatrix} x^{(m)} \\ y^{(m)} \end{pmatrix} &= c_s + R_c m_s^{(t)} \\
\begin{pmatrix} \dot{x}^{(m)} \\ \dot{y}^{(m)} \end{pmatrix} &= \dot{s}(t) u_s(t) \\
\begin{pmatrix} \ddot{x}^{(m)} \\ \ddot{y}^{(m)} \end{pmatrix} &= \ddot{s} u_s(t) - \frac{\dot{s}^2(t)}{R_c} m_s(t)
\end{aligned}
\right\} \qquad (74)
$$

The required quantities in equations (74) are calculated from the input parameters of equation (71) as follows:

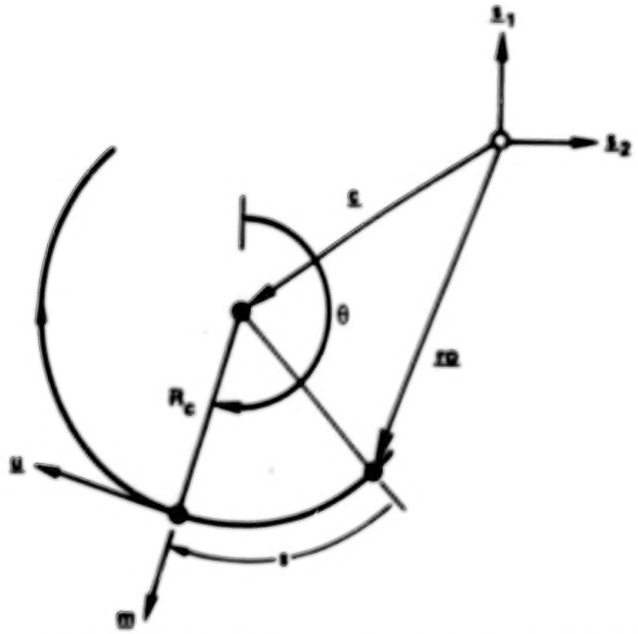

Sketch (c).- Horizontal plane coordinates for helical legs.

$$
\left.
\begin{aligned}
\dot{s}_o &= \left[\underline{vo}^{(m)} \cdot \underline{s}_1{}^2 + \underline{vo}^{(m)} \cdot \underline{s}_2{}^2\right]^{1/2} \\
\ddot{s} &= \frac{\dot{v}^{(m)} \dot{s}_o}{|vo_s^{(m)}|} \\
\dot{s}(t) &= \dot{s}_o + \ddot{s}(t - t_o^{(m)}) \\
s(t) &= \dot{s}_o(t - t_o^{(m)}) + \tfrac{1}{2}\ddot{s}(t - t_o^{(m)})^2 \\
\theta_o &= \tan^{-1} \frac{\underline{ro}^{(m)} \cdot \underline{s}_1}{ro^{(m)} \cdot \underline{s}_2} \\
\theta(t) &= \theta_o + \frac{s(t)}{R_c} \\
m_s(t) &= \begin{pmatrix} \cos\theta \\ \sin\theta \end{pmatrix} \\
u_s(t) &= \begin{pmatrix} -\sin\theta \\ \cos\theta \end{pmatrix} \\
c_s(t) &= \begin{pmatrix} \underline{ro}^{(m)} \cdot \underline{s}_1 \\ \underline{ro}^{(m)} \cdot \underline{s}_2 \end{pmatrix} + R_c m_s(t_o^{(m)})
\end{aligned}
\right\} \qquad (75)
$$

Transition Initialization Algorithm

The transition initialization algorithm in figure 13 is awakened and executed during a restricted period neighboring the reference leg-junction time, $t_o^{(m+1)}$; within this period the algorithm optimizes the time of initiating the transition to the next leg and does so independently on each path axis.

The timing adjustment period should be confined to the duration of the two legs being sequenced, but can be further confined in the present application to a short period, ΔT, on the order of 10 sec, in advance of $t_o^{(m+1)}$. This choice is based on the simplifying practice adopted here and elsewhere (refs. 3 and 8), of specifying reference trajectories with only single-state discontinuities at the leg junction (for each axis, only one of $\{E_1^{(i)}, E_2^{(i)}, E_3^{(i)}\}$ is nonzero at $t_o^{(m+1)}$). The optimum initialization time for this class of reference trajectory discontinuities always precedes or "leads" $t_o^{(m+1)}$ by small amounts, as noted in equations (56), (57), (63), and (64), so that the restricted adjustment period accommodates this class and provides a margin for adaptation to off-reference conditions. The restriction on the choice of leg-junction discontinuities due to the above practice is not operationally significant and, in any case, the algorithm activates the transition at the best time in $(t_o^{(m+1)} - \Delta T, t_o^{(m+1)})$ regardless of the discontinuities encountered.

The transition initialization algorithm is shown in detail in figure 14 and uses equations discussed in the preceding section. The algorithm, when awakened, predicts the optimum time to initiate the transition to leg $m + 1$ on each axis, and whenever these times are reached the TD initialization indicator (ICTD) is turned on and will subsequently cause the TD to initialize. The internal indicator $\delta(i)$ is also set for use in modifying the reference trajectory for this axis during the remainder of the adjustment period. If an axis is found to be ambiguous ($|E_2|$, $|E_3|$ are below their threshold values so that the transition is negligibly dependent on its initialization time), then another indicator, $s(i)$, is used to postpone initialization until the algorithm turns itself off. Termination occurs if all three axes have been switched or are ambiguous ($\Sigma(\delta(i) + s(i)) = 3$), or if the adjustment period has ended ($t = t_o^{(m+1)}$), and consists of incrementing the leg counter m and turning off the internal indicators. A minor detail is the omission in equation (68) of the estimated acceleration tracking errors in evaluating the acceleration A, that governs the predicted locus of possible TD initial states. The omitted signal is dominated by random wind turbulence and is not usefully accommodated.

Transition Dynamics

The last element required for the CG is the transition dynamics, which is shown in detail in figure 15 and uses equations previously discussed in the first two sections. Third-order transition dynamics with no modeling of plant dynamics are used; this choice was found adequate for the modest maneuver acceleration rates permitted in the passenger operations postulated for this application. The effects of this choice on system performance will be noted

in the simulation results. Initialization of the TD is controlled by the flag ICTD, which can be turned on either by the initialization algorithm described above or externally as a result of position sensor switching and associated large changes in sensor bias and in $\hat{r}_s$. The numerous input parameters of the TD

$$\left\{\left(\rho^{(i)}, \tau_L^{(i)}, \tau^{(i)}, e_{2m}^{(i)}, e_{2M}^{(i)}, e_{3m}^{(i)}, e_{3M}^{(i)}, a_m^{(i)}, a_M^{(i)}\right),\ i = 1,2,3\right\}$$

remain to be selected for each axis on the basis of operational considerations. Their selection is discussed in the next section along with illustrative transition examples for the basic single-state, single-axis leg-junction discontinuities.

The saturation parameters ($e_{2m}^{(i)}$, . . ., $a_M^{(i)}$) are denoted in figure 15 simply as functions of the reference state to be calculated at the beginning of each leg, and appropriate equations are derived in the next section for the present design problem. This reflects the general nature of the operational constraints to be imposed in practice; they are limits on functions of the trajectory states from which corresponding saturation limits on the transition states can be calculated in terms of the reference flight condition.

OPERATIONAL CONSTRAINTS, PARAMETER VALUES, AND BASIC TRANSITIONS

The selection of parameter values for the AWSJRA application is discussed next in the light of kinematic details of the simplest and operationally most significant class of maneuvers; that is, transitions for single-axis, single-state leg-junction discontinuities. The TD saturation limits are used to enforce operational constraints on both steady state and transient values of various kinematic variables. These constraints may be generally applicable, such as those based on passenger comfort (ref. 8), or derived for the specific aircraft from safety margin considerations and aircraft performance capabilities (refs. 2 and 10). The list of constraints enforced below is considered preliminary. Considerable latitude for its expansion and elaboration is provided in the CG structure, however, in which the TD saturation limits can be calculated as functions of the reference flight condition and can be given different values for positive and negative excursions.

Lateral Axis Parameters

Lateral axis TD parameter values were selected as

$$
\left.
\begin{aligned}
e_{2m}^{(2)} = e_{2M}^{(2)} = e_{2e}^{(2)} &= 0.25\, v^*(t_o^{(m)}) \\
e_{3m}^{(2)} = e_{3M}^{(2)} = e_{3e}^{(2)} &= 0.2\ g \\
a_m^{(2)} = a_M^{(2)} &= 0.57\ g \\
\tau^{(2)} &= 3\ \text{sec} \\
\left(\rho^{(2)}, \tau_L^{(2)}\right) &= (0.707, 4)
\end{aligned}
\right\} \qquad (76)
$$

For convenience, the notation e_{2e}, e_{3e} is used to denote both minimum and maximum excursion limits when these are equal. In addition, parameters of the reference trajectory are indicated by the superscript $(\ )^*$. The velocity excursion limit, $e_{2e}^{(2)}$, is given as a fraction of the reference aircraft speed at the initial time for the leg, $v^*(t_o^{(m)})$, in order to limit the direction excursions, $(\psi_{VC} - \psi_V^*)$, used during transitions. These quantities are related by

$$
v^* \tan|\psi_{VC} - \psi_V^*| = |e_2^{(2)}| \leq e_{2e}^{(2)} \qquad (77)
$$

and the selected fraction limits direction excursions below 14° at all speeds. During a sidestep, the aircraft departs no more than 14° from the reference flight direction and during a direction step the overshoot, if any, of the new direction, is limited to 14°.

The lateral acceleration excursion limit $e_{3e}^{(2)}$ is selected primarily to limit roll angle and heading rate commands appropriately. These quantities are related by

$$
\underline{a} \cdot \underline{p}_2 = v \cos\gamma\, \dot{\psi}_V = (g \cos\gamma - \underline{a} \cdot \underline{p}_3)\tan\phi_V \qquad (78)
$$

Desired operational limits on roll angle commands are 20° in steady state and 30° transiently (ref. 8). Explicit heading rate limits are not precisely known, but 3.5°/sec is a typical maximum steady-state value for passenger operations. In the present context, equation (78) can be written in terms of reference and transition accelerations:

$$
\underline{a}^* \cdot \underline{p}_2 + e_3^{(2)} = v_c \cos\gamma_c\, \dot{\psi}_{VC} = (g \cos\gamma_c - e_3^{(3)})\tan\phi_{VC} \qquad (79)
$$

and γ_c can be assumed a small angle while $|e_3^{(3)}|$ is limited to 0.125 g, as noted later in this section. Maximum roll angle and heading rate commands are then obtained as

$$
\left.
\begin{aligned}
|\phi_{VC}|_{max} &\doteq \tan^{-1}\left[\frac{\tan\phi_V^* + (e_{3e}^{(2)}/g)}{1 - e_{3e}^{(3)}/g}\right] \\
|\dot{\psi}_{VC}|_{max} &\doteq |\dot{\psi}_V^*| + \frac{e_{3e}^{(2)}}{v_c}
\end{aligned}
\right\} \qquad (80)
$$

During sidestep and direction step transitions ($\underline{a}^* \cdot \underline{P}_2$, $\dot{\phi}^*_V$, $\phi^*_V = 0$), the selected value of $e^{(2)}_{3e}$ limits roll commands to 13° and heading rates are below 3.5°/sec for speeds above 65 knots. For acceleration steps it can be assumed that the reference trajectory satisfies steady-state limits, ϕ^*_{ve}, $\dot{\gamma}^*_{ve}$ (taken as 20° and 3.5°/sec here) or, equivalently, the reference acceleration satisfies:

$$|\underline{a}^* \cdot \underline{P}_2| < \min \left\{ v^* \dot{\gamma}^*_{ve} \cos \gamma^*, \; g \cos \gamma^* \tan \phi^*_{ve} \right\} \tag{81}$$

Then, using the selected value of $e^{(2)}_{3e}$ limits transient roll angle commands below 33° in the worst case and maximum transient heading rate commands are below 6.6°/sec for speeds above 65 knots. Ordinarily, however, the TD initial time optimization effectively eliminates or minimizes overshoot of the steady-state roll angle and heading rate during acceleration steps and the margin for transient excursions is used by the TD only to adapt to off-reference initial conditions.

The parameters $a^{(2)}_m$, $a^{(2)}_M$ limit the initial absolute acceleration command. Its selected value limits the initial roll command to 30°, approximately, in accordance with equation (78) and the desired transient roll command limits.

The filter time constant $\tau^{(2)}$ is selected primarily to limit roll rate commands within the desired operational limit for passenger operations, 10°/sec (ref. 8). Transitional jerk is given from equations (11) by

$$|\dot{e}^{(2)}_3| = \frac{|u^{(2)} - e^{(2)}_3|}{\tau^{(2)}}$$

and, from the derivative of equation (79), the extreme roll rate command is given by

$$|\dot{\phi}_{v_c}|_{max} \doteq \frac{|\dot{e}^{(2)}_3|_{max}}{g \cdot e^{(3)}_{3e}} \tag{82}$$

For position and direction step transitions, the maximum jerk and worst-case roll rate command occur at saturated control reversals:

$$|\dot{e}^{(2)}_3| < \frac{2e^{(2)}_{2e}}{\tau^{(2)}} = 0.13 \text{ g/sec}$$

or

$$|\dot{\phi}_{v_c}|_{max} \doteq 9°/\text{sec}$$

For turn entry or exit with good tracking, the maximum possible jerk and roll rate command occur initially in the transition

$$|\dot{e}_3^{(2)}| < \frac{1}{\tau^{(2)}} (g \tan \phi_{ve}^* + e_{3e}^{(2)}) = 0.19 \text{ g/sec}$$

or

$$|\dot{\phi}_{VC}|_{max} \tilde{=} 12°/\text{sec}$$

Finally, in the worst-case initial conditions (maximum turn from saturated opposite roll and simultaneous unfavorable normal axis maneuver commands) the jerk and roll rate are

$$|\dot{e}_3^{(2)}| < \frac{1}{\tau^{(2)}} (g \tan 30° + g \tan \phi_{ve}^* + e_{3e}^{(2)}) = 0.38 \text{ g/sec}$$

$$|\dot{\phi}_{VC}|_{max} \tilde{=} 22°/\text{sec}$$

These estimates are, however, pessimistic because the TD initialization time optimization results in initial conditions for which the initial control, e_3, reduces the initial jerk, and initial rates are below 5°/sec for turn entry and exit, and below 16°/sec in the worst case.

The time constant $\tau_L^{(2)}$ scales the size of the linear mode region of the state plane Ω_L, as discussed previously. In the present work, τ_L is selected on each axis to be slower than the characteristic times of the plant dynamics in the simulation. This linear region is shown in figure 16 for the lateral axis. Sidestep transitions are initiated on the x_1-axis; sidestep distances greater than 16 m require nonlinear transitions, such as those initiated at x_{01} or x_{02} and usually use maximum excursion roll angle commands and can encounter saturated control reversals (from x_{01}) with corresponding roll rate extremes under 10°/sec. Direction steps in excess of $\tan^{-1}[\tau_L e_{3e}^{(2)}/v^*]$ require nonlinear transitions; the state follows loci, such as L_1 or L_2 in figure 16, until the switching boundary is encountered at which point the transition is initiated in accordance with the optimum initialization time algorithm and usually uses maximum excursion roll angle to turn to the new direction. Optimum initialization of direction steps up to $\tan^{-1}[(\Delta T - \tau)e_{3e}^{(2)}/v^*]$ is accommodated by the advance period, ΔT, as determined from (63). Finally, for the given parameter values, all acceleration step transitions are initiated in the linear region; the state follows a locus, such as L_3 in figure 16, until it enters Ω_L, after which the transition is initiated at the point of minimum initial jerk; this occurs at the boundary of Ω_L in the common case that the acceleration step exceeds $e_{3e}^{(2)}$. These acceleration step transitions require very little roll command overshoot and roll rates are well below 5°/sec as a result of the initialization optimization. The lateral axis single-state reference trajectory discontinuities — position, velocity and acceleration steps — correspond, respectively, in flight operations to sidesteps to a parallel path, step changes in direction of straight flight paths, and entry to or exit from steady turns or reversals of turns. Lateral axis transitions result in rotations, $\dot{\gamma}_v$, of the path axes and related longitudinal axis cross-coupling activity in some of the basic transitions to be discussed next.

Sidestep Transitions

Some kinematic variables from a typical sidestep to a parallel path at a distance of 250 m are shown in figure 17(a). As seen in the x-y trajectory plot, the TD generates a turn away from the reference direction, followed by a straight path to the parallel path and a return to the reference direction. Time histories of Ψ_{vc}, Φ_{vc}, $\dot{\Phi}_{vc}$ demonstrate the effectiveness of the TD in limiting these variables during the transition in accordance with the selected bounds.

The sidestep distance for which the present TD can generate acceptable transitions is limited by several effects of neglected longitudinal axis cross coupling and Coriolis accelerations. First, a reduction in speed is commanded as a result of the combined lateral velocity excursion and path axis rotation, Ψ_V, during the maneuver (see vc in fig. 17(a)). However, it is necessary to increase speed during the sidestep in order to maintain position along the reference trajectory, but no longitudinal axis transition is generated to provide the proper speed variations since the initial conditions for the longitudinal axis transition are zero. These effects must then be compensated by the control system feedback; that is, position errors and corresponding corrective feedback acceleration commands ($\Delta\underline{a} \cdot \underline{p}_1$) develop in order to increase speed (v) as required. This effect is proportional to the direction change and is limited by the TD bound on e_2.

Secondly, the TD excursion trajectory (Δrc_s, Δvc_s, Δac_s) is kinematically incompatible longitudinally since the neglected Coriolis terms are nonzero and principally in the longitudinal direction in this case. A significant longitudinal position discrepancy develops at the rate $\dot{\Psi}_v e_1^{(2)}$ which is greatest during the initial turn from the reference direction and dominates the feedback signal $\Delta\underline{a} \cdot \underline{p}_1$ during this period; the discrepancy is proportional to sidestep distance so that the aircraft longitudinal acceleration capability is saturated by the feedback at sufficiently large sidestep distances. However, satisfactory sidesteps to very large distances can be obtained alternatively by incorporating in the reference trajectory the straight-line segment joining the two parallel paths; this reduces the transitions generated by the TD to direction steps with much reduced Coriolis effects. In any case, the use of feedback to accomplish trajectory commands is undesirable.

Direction-Step Transitions

The TD generates a turn to the new reference direction in this case, with initialization time selected according to equations (56) or (63). Kinematic variables of interest from a typical direction change of 30° during level flight at 100 knots are shown in figure 17(b). Three cases are shown; they correspond to initialization at (1) the reference leg switch time, (2) the optimum initialization time, and (3) an intermediate time. The effectiveness of the initialization time optimization in reducing or eliminating excursions from the reference path, overshoot of the reference direction, roll command activity and reversals, roll rate peaks and activity, and maneuver

duration are apparent as well as the effectiveness of the TD in bounding peak values of roll rate, roll angle, and direction overshoot in accordance with the selected parameter values and for all cases shown. The algorithm allows initialization up to 10 sec in advance of the reference leg switch time, and this period allows for optimum initialization of direction steps up to $\tan^{-1}(20/v^*)$. The 30°-step example uses most of this advance period. Larger direction changes can be accommodated with larger advance periods, but these transitions are better accomplished in the present application by including a constant radius turn in the reference input trajectory.

A longitudinal axis transition is also generated for the direction step and has initial conditions corresponding to the apparent longitudinal velocity step at the leg-junction:

$$\left(E_1^{(1)}(t_o), E_2^{(1)}(t_o), E_3^{(1)}(t_o)\right) = (0, v^*(1 - \cos \Delta\Psi_V), 0)$$

The discontinuity size increases with $|\Delta\Psi_V|$ and is of significant size at 30°. This transition is shown in figure 17(c) for the present example and significant acceleration and velocity activity is commanded. Since the trajectory velocity command results from the combined lateral and longitudinal transitions,

$$vc_s = v_s^* + A_{ps}^{-1} e_2$$

the speed command variation, vc, (shown in fig. 17(c)) depends on the transition velocity coordinates of both axes. In principle, a direction step can be accomplished with no speed variation or corresponding longitudinal axis activity. In the present design the speed variation results from neglected Coriolis terms, whose effects are seen in the inconsistency of the variations of the actual and commanded speeds.

Lateral Acceleration-Step Transitions

Lateral axis acceleration steps occur at any change in the turn radius of the reference flight path, such as at entry to a steady turn from a straight flight path or at exit from a turn. Figure 18 shows results from entry to a level turn at 100 knots, with radius such that the maximum bank angle allowed for trajectory commands (20°) is required. The TD initial conditions correspond to the leg-junction trajectory discontinuity

$$\left(E_1^{(2)}(t_o), E_2^{(2)}(t_o), E_3^{(2)}(t_o)\right) = (0, 0, 0.36\ g)$$

The TD generates a brief transition which essentially smoothes out the roll step command of the reference path in accordance with the roll rate limits and adjusts the transition initialization time to avoid roll or direction overshoot in tracking the reference path (see fig. 18(a)). In this example, the transition acceleration command $e_3^{(2)}$ initializes outside the bounds

on control (±0.2 g), but is relaxed to zero monotonically with very little overshoot of zero.

Further details of this transition are shown in the x-plane plot (fig. 18(b)). The locus, L, of possible initial conditions for the turn entry, and transitions are shown, beginning from three points corresponding to (1) the reference leg junction time, t_o, (2) the optimum time (t_o - 2), and (3) an earlier time (t_o - 6). The optimum transition begins where L enters Ω_L and is entirely in the linear mode; the initial jerk is minimized at this point but is necessarily nonzero because $E_3^{(2)}$ is outside the bounds $e_{3e}^{(2)}$. The locus L has the property in this example that neither initialization criteria ((48), (49)) can be satisfied; that is, if t_L^*, t_{NL}^* are the optimum linear and nonlinear mode initialization times then

$$x(t_L^*) \notin \Omega_L \quad \text{and} \quad x(t_{NL}^*) \notin \bar{\Omega}_L$$

For such cases the on-line initialization algorithm selects the earliest time that one of the following conditions is satisfied

1. $t \geq t_L^*$ and $x(t) \in \Omega_L$
2. $t \geq t_{NL}^*$ and $x(t) \in \bar{\Omega}_L$
3. $t \geq t_o$

In this instance, (1) is satisfied at entry to Ω_L and a minimum initial-jerk transition is generated with very little roll angle overshoot. The advance time required for optimum linear mode initialization of acceleration steps is independent of the size of the steps (see eq. (57)) and, for the lateral axis, is within the 10-sec advance period used in the algorithm.

The effects of initialization time on the control (u), on roll angle (ϕ_{VC}, $\dot{\phi}_{VC}$), and on the position tracking excursion ($e_1^{(2)}$) are also shown in figure 18(b). The transition initiated at the reference time is nonlinear; maximum negative control is used in an effort to "catch up" with the step roll change of the reference trajectory and corresponding roll rate command exceeds the desired 10°/sec limit. The roll command also overshoots the reference roll angle to the excursion limit and into the margin reserved for transient activity.

In contrast, the optimum time initialization reduces roll rates well below the desired limits and virtually eliminates the roll overshoot; and, in comparison with other transitions in figure 18(b), it requires the least duration control activity, roll overshoot and activity, and path excursions from the reference.

Finally, it is noted that no longitudinal axis activity is generated during these acceleration steps either from the TD or from feedback due to neglected cross coupling.

Longitudinal Axis Transitions

For the longitudinal axis, the single state reference trajectory discontinuities correspond respectively to position steps forward or backward along the flight path, step changes in airspeed, and speed rate steps. Their transitions are qualitatively the same as the corresponding position, velocity, and acceleration step transitions for the other axes and need be reviewed only briefly. Path axis rotations and related cross-coupling effects are absent. The following parameter values were selected for the AWJSRA:

$$\left.\begin{aligned} e_{2m}^{(1)} &= e_{2M}^{(1)} = e_{2e}^{(1)} = 0.065\ v^*(t_o) \\ e_{3m}^{(1)} &= e_{3M}^{(1)} = e_{3e}^{(1)} = 0.06\ g \\ a_m^{(1)} &= -g \sin\gamma - 0.15\ g \\ a_M^{(1)} &= -g \sin\gamma + 0.15\ g \\ \tau^{(1)} &= 2\ \text{sec} \\ (\rho^{(1)}, \tau_L^{(1)}) &= (0.707, 6\ \text{sec}) \end{aligned}\right\} \qquad (83)$$

These values reflect the limits of aircraft capabilities rather than passenger comfort restrictions. The velocity bound limits speed excursions used, for example, during position adjustments. This bound was selected as a fraction of the reference speed; it satisfies the small speed reduction margin available at minimum operating speeds and, at higher speeds, it bounds the implied aircraft control activity.

The acceleration limits $e_{3e}^{(1)}$, $a_m^{(1)}$, $a_M^{(1)}$ are selected in relation to the aircraft capability to generate longitudinal forces. These are the static engine and aerodynamic forces and they balance aircraft weight, as well as supply the trajectory acceleration, $\underline{ac}$; that is,

$$\underline{f_c} = \underline{ac} - \underline{g}$$

where $\underline{f_c}$ is the required applied acceleration for the trajectory and is to be supplied by the aircraft engine and aerodynamic forces. The longitudinal component, $\underline{f_c} \cdot \underline{p_1}$, is denoted A_u and is given (in g's) by

$$A_{u_c} = \frac{\sin\gamma_c + \dot{v}c}{g} \qquad (84)$$

Let (A_{u_m}, A_{u_M}) denote the aircraft limits on longitudinal specific force capability. These are determined from a variety of operational constraints on aircraft control usage and margin requirements and, in general, vary with the reference flight conditions (ref. 2). For passenger aircraft generally these

limits are modest and for the AWJSRA they are about ±0.15 g or less. It can be assumed that the reference flight conditions (γ^*, $\dot{v}^*$) provide a margin for transient longitudinal forces, on the order of 0.06 g, and this value is selected as the longitudinal acceleration excursion limit $e_{3e}^{(1)}$. However, it should be noted from equation (84) that this margin is shared by both normal and longitudinal axis variables, γ, $\dot{v}$. Ordinarily, in velocity or acceleration steps, the initialization time is optimized to prevent overshoot of the reference values of either γ^*, $\dot{v}^*$, and the transient margin is used only in some cases of off-reference initial conditions. The initial longitudinal acceleration command is limited by $a_m^{(1)}$, $a_M^{(1)}$ in equations (83) to reflect the approximate limits on the longitudinal specific force.

The rate-limiting time constant $\tau^{(1)}$ is well above the time constant for the aircraft response to longitudinal acceleration commands, which are variously provided in the case of the AWJSRA by the engine, nozzle, and angle of attack variations depending on configuration.

The region of linear control and switching boundaries for the longitudinal axis TD is shown in figure 19(a). Position steps in excess of 11 m require nonlinear transitions and maximum accelerations. The velocity bound is usually encountered; this bound increases with speed and intersects Ω_L at speeds below 109 knots. Speed steps in excess of 7 knots also require nonlinear transitions.

Some results from a backward position step of 80 m during level flight at 100 knots are shown in figures 19(a) and (b). The position error $e_1^{(1)}$ is relaxed from its initial value to zero monotonically by the TD with very little overshoot; the speed command vc is reduced to the value permitted by the excursion limit, where it is held until the position error is reduced sufficiently, and then returns to the reference speed with very little overshoot. The acceleration commands illustrate the effectiveness of the acceleration and acceleration rate limits of the nonlinear transition dynamics.

A 20-knot speed-step transition during level flight is shown in figures 19(a) and (c). These results indicate the effectiveness of the TD initialization algorithm in eliminating saturated control reversal and corresponding overshoot of the new reference speed. It can be calculated that the 10-sec advance period provided in the present design allows optimum initialization of speed steps up to 19 knots. Larger speed changes are better accomplished by including a constant acceleration segment in the reference trajectory. In addition, the 10-sec advance period also accommodates all acceleration steps.

Normal Axis

Transitions corresponding to altitude and flight-path angle steps for the normal axis were discussed in a previous section. Transition dynamics parameter values selected for the AWJSRA are

$$
\left.
\begin{aligned}
e_{2e}^{(3)} &= \min\{v^*(t_o)\sin \Delta\gamma_{max}, 6\} = \min\{0.052\ v^*(t_o), 6\} \\
e_{3e}^{(3)} &= 0.125\ g \\
a_m^{(3)} &= a_M^{(3)} = 0.2\ g \\
\tau^{(3)} &= 2\ \text{sec} \\
(\rho^{(3)}, \tau_L^{(3)}) &= (0.707, 2)
\end{aligned}
\right\} \qquad (85)
$$

The velocity bound is designed to limit flight path angle excursion amplitudes relative to the reference value to 3° and to limit altitude rate excursions to 6 m/sec. These are appropriate passenger operation limits on flight path angle and altitude rate during altitude step transitions. Further, it is assumed that values of γ^*, $\dot{v}^*$ on the reference path are restricted to provide a margin for such flight-path angle excursions within the limits of aircraft longitudinal specific force capabilities, in accordance with equation (84).

The acceleration limit is a passenger comfort constraint (ref. 8) and is well below the minimum aircraft lift margin capability of 0.4 g to 0.7 g required for safety at all reference flight conditions.

The region of linear control Ω_L is the smallest for any of the three axes and is such that nonlinear transitions with saturated control are used for altitude steps above 2.5 m and altitude rate steps above 2.5 m/sec.

The 10-sec advance period allows optimum transition initialization of all flight-path angle steps within the AWJSRA capabilities so that it is unnecessary to consider the use of any constant normal acceleration leg in the reference input trajectory.

Finally, it is noted that a discussion of the important landing flare maneuver is omitted from this paper. The reference trajectory command is specially tailored in this case so that the transient trajectory response of the aircraft satisfies more detailed requirements than for the transitions so far discussed and more than are necessary elsewhere on terminal area flight paths.

Remarks

A task of this section has been to define the desired operational constraints on trajectory commands and relate them to the excursion limits of the TD. For this purpose, various kinematic variables of concern (v, A_u, $\dot{\Psi}_V$, Φ_V, $\dot{\Phi}_V$, γ, $\underline{a} \cdot \underline{p}_3$) and constraints on their steady-state and transient values were introduced. These are constraints on functions of the CG command and can be generalization to a list of the form

$$\{g_i(\underline{rc},\underline{vc},\underline{ac},\dot{\underline{ac}}) \geq 0 , \quad i = 1,2,\ldots, N\}$$

which reflect operational practices.

The input reference trajectory is assumed to satisfy the constraints on steady-state kinematics

$$\{g_i(\underline{r}^*,\underline{v}^*,\underline{a}^*,\underline{0}) = 0 , \quad i = 1,2,\ldots, N\}$$

The constraints can also be given in terms of the reference trajectory and transition states

$$\{g_i(r^*,v^*,a^*;\ e_1,e_2,e_3,\dot{e}_3) \geq 0 , \quad i = 1,\ldots, N\}$$

from which boundaries on the excursion states and corresponding saturation parameter values can be defined as functions of the reference flight condition.

The TD parameters were demonstrated to be effective in general in imposing the desired linear mode transient characteristics and the desired bounds on commanded velocity and acceleration excursions about the reference flight condition. Further, the transition initialization time algorithm was demonstrated to be effective in approximately minimizing control activity and overshoot of the reference acceleration, velocity, and position during the transition. These characteristics are considered necessary conditions for an operationally acceptable trajectory command generator; they are features of good piloting technique which the present design attempts to generalize for use by an automatic flight-control system coupled to an Air Traffic Control/4-D Guidance system having a broad reference trajectory command set at its disposal.

The use of the CG as part of the flight-control system of figure 1 and the system behavior during the execution of an approach trajectory and in the presence of off-nominal events and disturbances is examined in the next section.

SIMULATION TEST RESULTS ON A STOL APPROACH TRAJECTORY

Tests have been carried out using a simulation of the system shown in figure 1, including the AWJSRA plant and corresponding acceleration controller as well as the Command Generator. Details of the plant and its acceleration controller are found in references 2 and 11 but can be omitted from the present discussion since the structure of the Command Generator is independent of these details. The aircraft dynamics are simulated in a simplified form as described in reference 12; that is, the dynamics and the control logic are partitioned into translational and rotational degrees of freedom and the rotational degrees are replaced with a simple second-order model of attitude response to attitude commands while the translational degrees of freedom are accurately represented. In addition, the estimation subsystem of figure 1 is not simulated; the input signal to the control logic, ($\hat{r}_s$, $\hat{v}_s$, $\hat{a}_s$) omits

estimation errors due to random measurement noise but simulates the significant discontinuities in estimated position that can occur during an approach as a result of switching from sensors with large unknown measurement biases (e.g., TACAN-DME, barometric altimeter) to more accurate sensors (e.g., microwave landing system). This simulation is well suited to testing the operation of the CG and the trajectory control subsystem in response to various reference trajectory commands, and to the Trimmap model errors, sensor switching events, and external disturbances expected in operational use.

The reference approach path used for the test is shown in figure 20; it is constructed as a sequence of simple legs, and the corresponding parameters for input to the CG are included in figure 20. This path includes some anticipated features of possible STOL arrival trajectories; compared to CTOL operations higher altitude is maintained until close to the runway and then descents are steep and confined to limited airspace and with speed reduction to the lower STOL landing speeds during descending legs. The test includes leg switches requiring multiple axis maneuvering, sensor switch events requiring unanticipated initialization of the CG from off-reference conditions, and both steady and random disturbance inputs (e.g., Trimmap model errors, wind turbulence) requiring adaptation of the transition maneuver commands to tracking errors.

Time histories from the simulation results are shown in figures 21 and 22. Figure 21 covers the first half of the approach and illustrates the capability of the Command Generator to generate acceptable four-dimensional maneuver commands, both to execute the known reference approach path and in response to unanticipated initializations of the CG to relieve the feedback of saturation level tracking errors. Figure 22 covers the second half of the path and illustrates the behavior of the CG and the system in the presence of both random and steady acceleration disturbances. The variables in both figures are grouped into those describing the TD and CG acceleration command (e_1, e_2, e_3, ac_p in figs. 21(a) and 22(a)), command and response histories of velocity coordinates ((V, γ, Ψ_V) in figs. 21(b) and 22(b)), the tracking errors and corrective feedback acceleration ($\underline{\delta r}_p$, $\underline{\delta v}_p$, $\underline{\Delta a}_p$ in figs. 21(c) and 22(c)), and the applied specific force commands and response ((A_u, A_N, Φ_V) in figs. 21(d) and 22(d)). The variables (A_u, A_N, Φ_V) are the applied specific force supplied by the engine and aerodynamic forces of the aircraft in order to fly the commanded trajectory and support the aircraft weight; that is,

$$\underline{f}_c = \underline{ac} - \underline{g} \tag{86}$$

In cylindrical coordinates and in g units, the specific force along and normal to the path (A_u and A_N, respectively) and the orientation of the normal force from the vertical plane (Φ_V), are given in terms of the trajectory and path axis acceleration components by

$$
\left.
\begin{aligned}
A_u &\equiv \frac{\underline{f} \cdot \underline{p}_1}{g} = \sin\gamma + \frac{\underline{a} \cdot \underline{p}_1}{g} \\
A_N &\equiv \sqrt{\left(\frac{\underline{f} \cdot \underline{p}_2}{g}\right)^2 + \left(\frac{\underline{f} \cdot \underline{p}_3}{g}\right)^2} = \sqrt{\left(\frac{\underline{a} \cdot \underline{p}_2}{g}\right)^2 + \left(\frac{\cos\gamma - \underline{a} \cdot \underline{p}_3}{g}\right)^2} \\
\phi_V &\equiv \tan^{-1}\left(\frac{\underline{a} \cdot \underline{p}_2}{g\cos\gamma - \underline{a} \cdot \underline{p}_3}\right)
\end{aligned}
\right\} \quad (87)
$$

here, $\{\underline{p}_1, \underline{p}_2, \underline{p}_3\}$ are the unit vectors defining the path axes reference frame. These force coordinates are convenient measures of the implied aircraft control activity; the controls are fixed or slowly varying if the applied force is constant and otherwise their commanded rates are proportional to the commanded specific force rates. For CTOL aircraft, (A_u, A_N, ϕ_V) are controlled nearly independently with throttle, elevator, and ailerons, respectively. For STOL aircraft, such as the AWJSRA, which may have powered-lift, variable-configuration and control redundancy, there can be significant cross-coupling of the specific force components among the control variables. These details need not be considered in the present discussion since no model of the plant dynamics was included in the CG design ($\hat{G} = I$) and (A_u, A_N, ϕ_V) can therefore be taken as the measure of the control activity required by the trajectory commands. It is noted that static equilibrium flight conditions ($\underline{a} = \underline{o}$) and steady turns correspond to fixed values of the applied force components. Further, each leg of a reference trajectory in this work corresponds to a fixed or very nearly fixed value of (A_u, A_N, ϕ_V); the complete approach path can therefore be viewed as a sequence of such fixed operating points with the transition dynamics supplying the transient specific force commands required to pass from one operating point to the next.

Basic Maneuvering Behavior

The initial 80 sec of the test illustrate the multiaxis maneuvering capability of the system in the absence of external disturbances and without tracking errors at the time of transition initialization. The reference path switches from level flight to a descending turn at $t = 11.6$ and exits from this leg into a level, straight, decelerating leg at $t = 45$.

The TD functions by adding its transition states (e_1, e_2, e_3) to the reference states; the initialization of this transition is timed independently on each path axis to optimize the maneuver kinematics, and then the three-axis maneuver is the superposition of these single-axis transitions. This functioning is illustrated in figure 21(a); the transition is initiated at slightly different times for each axis in advance of the reference leg-junction times, $t_0^{(2)}$, $t_0^{(3)}$ and the components of the acceleration command, ac_p, are seen to superpose the turn entry and exit on the lateral axis with the pitchover and pull-up on the normal axis and a small deceleration step on the longitudinal axis. Further, the desired characteristics regarding minimal overshoot of the

reference conditions are seen on all three axes in the behavior of e_1, e_2, $ac_p^{(1)}$, $ac_p^{(2)}$ in figure 21(a) and (v_c, γ_c, $\bar{\gamma}_c$) in figure 21(b). Thus, the CG output command retains the desired kinematic features under superposition.

Tracking performance is given by the tracking errors and corrective feedback acceleration shown in figure 21(c). Here, these signals measure the success of the CG design structure and parameter values in providing suitable feed-forward commands for the given plant-acceleration controller system. Ideally, it is desired that these errors be zero in the absence of any other disturbance than the CG command since nonzero values imply that constraints enforced on the CG command are not necessarily satisfied by the aircraft output and that the trajectory regulator is required to use some of its margin to execute the reference path. The errors seen in figure 21(c) are nonzero temporarily during transitions and are due to control lags excited by nonzero acceleration command rates. These rates and, hence, the errors are limited through the TD parameter, τ. These errors can also be nulled approximately if a sufficiently accurate model of the plant dynamics is included in the TD, as discussed in the section on maneuver tracking properties. The present CG design omits a plant model, but the observed tracking errors and feedback acceleration are acceptably small in magnitude and occur only transiently.

Control activity is measured by variation in the applied specific force components (A_u, A_N, Φ_v) defined by equations (85) and shown in figure 21(d) for the CG command ($\underline{f}_c$), the total acceleration command to the Trimmap ($\underline{f}_{ct}$), and the aircraft response ($\underline{f}$). During a transition, aircraft controls differ from their steady-state values for the leg in proportion to the difference of the specific force from its steady-state value so that it is desired that the transitional specific force commands reach steady-state values without unnecessary overshoot, reversal, or activity. However, the command time histories of the specific force components can be more complex than those of the path axis acceleration components and flight-path angle from which they are composed, especially for multiple-axis maneuvering. Referring to $\underline{f}_c$ in figure 21(d), the components Φ_{v_c}, A_{u_c} show little overshoot of steady-state values and this parallels, respectively, the behavior of $ac_p^{(2)}$, γ_c from the CG. However, A_{N_c}, which is a function of both lateral and normal accelerations, drops transiently at first for the pitchover and then rises to its steady-state value for the turn without overshoot, and performs the mirror image maneuver at the turn exit. Thus, the required control activity is potentially very complex in the case of multiple axis maneuvers but the present design economizes this activity as a result of the transition initialization algorithm which economizes the acceleration command activity from which $\underline{f}_c$ is composed. The total specific force command, f_{ct}, shows modestly degraded behavior in figure 21(d) compared to the CG command as a result of tracking errors, with higher amplitude excursions from steady state and some overshoot, but the specific force response of the aircraft retains the desired features. The magnitude of the specific forces required for the maneuvers in figure 21(d), remains within ±0.2 g of the static equilibrium level flight values, and this range is typical of the modest maneuvering domain of passenger operations generally.

Response to Sensor Switching Events

During the time period, [80, 120], the use of the CG to relax large trajectory errors, which would otherwise saturate the feedback control, and the ability of the TD logic to adapt its transition maneuvers to off-reference initial conditions is tested. The test consists of a reference trajectory turn entry (at t = 96) surrounded by sensor switch events; a switch in x-y sensor at 85 sec shifts the estimated position laterally 150 m and at 105 sec an altitude sensor switch shifts the estimated altitude 20 m. At these sensor switches, the CG is signaled automatically to initiate a transition back to the reference trajectory.

The following sequence of events occurs. First, at the x-y sensor switch the TD initiates an appropriate transition back to the reference trajectory, which in this example is a typical sidestep maneuver (fig. 21(a)). Tracking errors develop (fig. 21(c)), principally in the longitudinal direction. Secondly, the turn entry of the reference trajectory is initiated in mid side step (at 94 sec) from states that are considerably off the reference trajectory, both in lateral states, due to the uncompleted sidestep transition, and in longitudinal states, due to the tracking errors. The TD adapts both the initialization timing and its initial conditions in all three dimensions to these off-reference conditions (fig. 21(a)); further, the TR is relieved by the CG initialization as seen by the discontinuous nulling of all error and feedback signals (fig. 21(c)) at this and all transition initializations from off-reference states. During the turn entry, longitudinal tracking errors again increase. Thirdly, at the altitude sensor switch (t = 105) the TD is again initialized from off-reference states and an altitude step maneuver is superposed with the turn entry and with the longitudinal tracking error relaxation.

Tracking errors during this period are principally longitudinal and due to kinematic cross-coupling neglected in the TD and aroused by lateral axis transitions as noted in the previous section. The tracking errors also include the effect of unmodeled plant dynamics; that is, transient nonzero tracking errors develop in response to the CG command and result in use of the TR to execute the commanded trajectory. These effects of this design approximation occur only transiently and are of acceptable magnitude in the present application.

The largest transition acceleration commands during this period are in the lateral direction. The lateral acceleration and corresponding roll commands (figs. 21(a) and (d)) are seen to overshoot their steady-state values for the turn; this overshoot does not occur for the reference initial conditions but cannot be prevented for the unfavorable initial conditions of this test, even by the adaptive initialization timing logic. However, the acceleration overshoot is limited by the TD excursion limit for the lateral axis (0.2 g) and the roll angle command is correspondingly below its 30° limit for transient use.

The longitudinal specific force variations (fig. 21(d)) are dominated by off-reference events during this period of the test, first by the longitudinal

tracking errors and later by the γ-variation of the altitude step. The normal specific force reflects the combined lateral and longitudinal axis activity; the sidestep, turn entry, and the superposition of the altitude step on the steady turn can all be detected in its variations. These specific forces are complex compared to those of the first test period when off-reference events were absent and imply correspondingly complex use of the aircraft controls, but the acceleration commands remain within acceptable limits. In this test, $\underline{f}_c$, (corresponding to the CG commands) is piecewise continuous with discontinuities at the transition initializations due to off-reference conditions. The total command, $\underline{f}_{cT}$, which defines the control commands, is everywhere continuous as a result of the TD initialization rules.

Wind Turbulence Effects

The simulation test includes a period of heavy wind turbulence, $(135 < t < 195)$, during which the reference path switches from a decelerating level turn to a steep glide slope (at $t = 161$) and then to a steeper decelerating turn (at $t = 194$).

Low altitude wind turbulence is a random vector, $\underline{wt}$, assumed generated independently along three axes from processes that are stationary for the flight duration and Gaussian with variances that depend on altitude and direction (ref. 13), but are of the same order of magnitude in all directions. Wind turbulence is converted instantly into aerodynamic force variations that provide the random acceleration disturbances of the system denoted $\tilde{a}_d$ in the system diagram, figure 9. The aerodynamic lift, drag, and side forces and their dependence on the air velocity vector can be given as

$$\underline{F}_a = \frac{1}{2}\rho va^2[-C_D(\alpha)\underline{i}_s + C_Y(\beta)\underline{j}_s - C_L(\alpha)\underline{k}_s]$$

where $(\underline{i}_s, \underline{j}_s, \underline{k}_s)$ are the usual aircraft stability axes, ρ is the air density, (C_D, C_Y, C_L) are the drag, side force and lift coefficients, and (va, α, β) are the body axes spherical coordinates of the aircraft velocity with respect to the air mass (ref. 13). Denoting the body axis frame as $(\underline{i}_b, \underline{j}_b, \underline{k}_b)$ then (va, α, β) are defined as

$$(va, \alpha, \beta) \equiv \left(|\underline{va}|\ ,\ \tan^{-1}\left(\frac{\underline{va}\cdot\underline{k}_b}{\underline{va}\cdot\underline{i}_b}\right),\ \sin^{-1}\left(\frac{\underline{va}\cdot\underline{j}_b}{va}\right)\right)$$

and the variation in aerodynamic force due to wind turbulence is

$$\delta\underline{F}_a = 2\left(\frac{\underline{wt}\cdot\underline{i}_s}{va}\right)\underline{F}_a + \frac{\partial\underline{F}_a}{\partial\alpha}\left(\frac{\underline{wt}\cdot\underline{k}_b}{va}\right) + \frac{\partial\underline{F}_a}{\partial\beta}\left(\frac{\underline{wt}\cdot\underline{j}_b}{va}\right)$$

The first two terms are aligned nearly along $\underline{k}_s$ since aircraft usually have large values of C_L/C_D, of the order of 10, while the third term is along $\underline{j}_b$; thus, the plant maps the wind turbulence field into acceleration disturbances that are principally normal to the path, as is illustrated by the disturbance

time history, ($\underline{a}$-$\underline{ac}$), in the present test (fig. 22(c)). The test case disturbances have large bandwidth and peaks of 0.1 g in the normal direction. These result in modest tracking errors and feedback commands, Δa, having similar orientation but the lower bandwidth of the acceleration controller subsystem.

The transitions generated by the CG (fig. 22(a)) are little affected by the turbulence, even though their initial timing and states are adjusted to relieve the TR, because on the longitudinal and lateral axes only small disturbances and tracking errors occur while on the normal axis the tracking errors are small compared to the discontinuities of the reference trajectory pitchovers. The resulting time histories of the trajectory variables ($\underline{ac}$, vc, γ_c, Ψ_c) during this period show the desired maneuver command behavior with little or no overshoot in lateral acceleration or direction during turn exit or entry, or in normal acceleration or flight-path angle during pitchovers, or in vc during speed rate changes. It is also apparent in figure 22(c) that initializations of the CG relieve the tracking errors due to turbulence only momentarily, because this disturbance field is persistent in time and the corresponding tracking error statistics are promptly reestablished.

The differing character of the specific forces, $\underline{f_c}$, $\underline{f_{cT}}$, $\underline{f}$, in the presence of turbulence is seen in figure 22(d), especially in the normal acceleration component. The CG command, $\underline{f_c}$, reflects the low frequencies of the TD and the constant steady-state values of the reference trajectory legs, and is unaffected by turbulence except for discontinuities at TD initializations. The total command, $\underline{f_{cT}}$, superposes the TR feedback on $\underline{f_c}$ and its excursions parallel $\underline{\Delta a}$ in amplitude and frequency. Finally, the actual force $\underline{f}$ differs from $\underline{f_{cT}}$ by the combined effects of plant dynamics and random acceleration disturbance.

Acceleration Disturbance Effects

The final test illustrates the effects of acceleration disturbances that are constant or slowly varying compared to the characteristic times of the TD, and were denoted as a_d in figure 9. These disturbances result from any uncompensated mismatch between the actual aircraft forces and the algebraic model of aircraft forces used in the Trimmap element of the control system. These disturbances can result from large errors in estimating the various independent parameters of the force model, such as aerodynamic force coefficients, engine thrust model, mean wind, and aircraft weight.

The effects of such errors is tested in the simulation results by the addition of constant drag and lift disturbances of 0.05 g beginning in mid-helical turn (at $t = 250$). These are significant errors compared to the longitudinal acceleration capabilities of the passenger aircraft (usually under ± 0.2 g) and compared to the desired accuracy for the force model. The resulting steady-state behavior of the acceleration controller subsystem is seen in figure 22 during the period prior to the glide slope capture;

the disturbance is exactly cancelled by a steady feedback acceleration command (fig. 22(c)):

$$\underline{\Delta a} = -\underline{ad}$$

but this equilibrium requires a corresponding position standoff error on the longitudinal and normal axes in the amounts:

$$\delta r^{(i)} = \frac{ad^{(i)}}{k_1^{(i)}} \qquad i = 1,3$$

where $\{k_1^{(i)}\}$ are the position error feedback gains. An apparent lateral velocity standoff also occurs in the amount, $v\delta r^{(i)}/R_c$, which reflects the steady-state position of the aircraft on the commanded turn but ahead of the commanded position by the longitudinal standoff distance, and which is nonzero only during turns.

The above errors are present at the time of glide slope capture (t = 288), so that in the transition commands (fig. 22(a)) the basic turn exit and speed rate correction maneuvers required by the reference trajectory are modified to relax the longitudinal and normal position and acceleration feedback offsets of the TR. However, the acceleration controller feedback promptly restores the steady-state offsets, as seen in figure 22(c), by means of a transient which roughly cancels that portion of the feed-forward command intended to relieve the TR. The possibility of mutual cancellation or reinforcement by the two transients is apparent. This process of relieving and restoring the TR offsets due to model errors is repeated at each initialization of the TD.

Further details of the disturbance effects are seen in the specific forces (fig. 22(d)). The acceleration commands of the CG (A_{u_c}, A_{N_c}) exhibit 0.05 g discontinuities at each initialization of the TD, followed by activity generated mostly to relax the TR offsets. The total command, which governs the actual control activity, is better behaved, and shows both continuity and less activity as a result of the mutual cancellation of feedback and TD transients. The plant output also maintains these favorable properties and settles in steady state to the CG acceleration command as desired.

In these tests the steady disturbance was compensated by the feedback control; the resulting offsets of δr and Δa interact with the adaptive initialization of the transition dynamics to produce ineffective transition commands from the CG on the longitudinal and normal axes as noted above. These can be removed, along with the offsets in $\underline{\delta r}$, $\underline{\Delta a}$, by providing compensation for $\underline{ad}$ in the Trimmap element of the control system, as noted in reference 2. Any residual uncompensated disturbance would, however, result in the interaction between CG and the tracking system at leg initialization times noted above and, if of a significant size, further disturbance estimation and compensation in the Command Generator would be useful.

DISCUSSION AND CONCLUSIONS

This report has described the development of a trajectory Command Generator for a class of advanced digital flight-control systems (ref. 1; fig. 1) with capabilities of executing complex four-dimensional terminal area flight paths as directed by an air traffic control and guidance system (ref. 3) or selected by a pilot. The design methodology was presented, including the objectives, structure, and a detailed synthesis procedure for the CG. The CG described here was further examined in an autopilot of the type defined in reference 1 applied to the AWJSRA aircraft and subjected to simulation testing. Factors studied include the nature of the basic operational repertoire of maneuvers and operational constraints, and the system behavior in response to four-dimensional maneuver commands and as affected by various CG design approximations and disturbances found in the operational environment. These simulation results indicate that a satisfactory nonlinear system was developed which satisfies the basic design objectives while maintaining a practicable degree of simplicity. Further, since the CG structure and many of the operational constraints are independent of the aircraft, the simulation results are representative of STOL and CTOL aircraft and of passenger operations generally.

The CG design problem in the context of the system of figure 1 is to generate suitable feed-forward trajectory commands to a trajectory tracking subsystem in order to execute an input reference trajectory. The class of input reference trajectories assumed for the problem is typical of passenger operations, including those of advanced terminal area ATC systems. These are sequences of four-dimensional segments that can be straight lines with constant inertial acceleration or circular arcs with constant radius each of which satisfies operational constraints on steady-state flight. The task of the CG is to provide maneuvers that transition the aircraft from one steady flight condition to the next and satisfy the design objectives for such maneuvers. The input sequence also possesses certain approximate properties in practice which influence the design; that is, the duration of each segment is usually longer than the time required to transfer from the previous segment and the transfer between successive segments can usually be made optimally in the vicinity of the segment junction times. The design criteria relating to the output are that the aircraft trajectory satisfies operational constraints on steady-state and transient kinematics, $\{g_i(\underline{r}, \underline{v}, \underline{a}, \dot{\underline{a}}) = 0,\ i = 1, \ldots, N\}$, and that transition maneuvering be optimized to reduce or minimize acceleration activity and overshoot of the steady-state flight conditions; these are considered necessary conditions for operational acceptability of the system. While these operational constraints are to be satisfied by the actual aircraft trajectory it suffices to enforce them on the feed-forward trajectory commands of the CG provided acceptable tracking errors are obtained from the given aircraft and trajectory tracking system over the desired operational domain of the system.

The CG function is carried out in the proposed design using two principal elements: the transition dynamics (TD) and its initialization algorithm. The trajectory discontinuities between successive legs are viewed as initial errors from the new segment which the TD is to relax to zero in accordance

with the desired operational constraints. A TD was synthesized to generate these transitions independently on each of the aircraft path axes and a dual-mode control law was synthesized for each axis which is globally asymptotically stable with (1) selectable damping and characteristic time of the linear mode transients and a maximal region of initial conditions using linear control; (2) a nonlinear mode with selectable parameters to limit velocity and acceleration excursions about the reference flight condition; and (3) a selectable limit on the maneuver acceleration rates in order to enforce bandwidth restrictions on the maneuver commands. System behavior with this TD was examined in the third section of this paper. Initial conditions for the transition were derived to null initial tracking errors and maintain continuity of the acceleration command to the plant. Further, it was found that perfect tracking was obtained if disturbances were constant and exact models of the plant dynamics and disturbances were incorporated in the TD. The TD structure and control law synthesis were extended to include these models, $\hat{G}(s)$, $\hat{a_d}$. The potential value of minimizing tracking errors is that (1) the use of the trajectory regulator to execute the feed-forward commands is minimized so that its control margin is reserved for the regulation of random unpredictable disturbances; (2) the kinematic constraints are more accurately imposed on the plant output; and (3) the bandwidth of the TD commands for which acceptable system behavior can be obtained is increased. The applications work of this report omitted such models (equivalently, the design assumes $\hat{G}(s) = 1$, $\hat{a_d} = 0$) but satisfactory results can be expected with this design provided (1) the plant dynamics are of sufficiently higher frequency than the transition dynamics and (2) the steady disturbances are sufficiently small. The transition initialization switching logic (established in the fourth section) provides optimization of the transition maneuver. The proposed optimization criteria were to minimize initial jerk for transitions initiated in the linear mode, and to prevent saturated control reversal and corresponding peak jerk in the nonlinear mode. In addition to reducing the local acceleration activity specified by the criteria, transitions are obtained with approximately minimum duration and overshoot of the reference flight conditions as was shown in extensive examples.

The scope of aircraft operations to which this design is applicable is bounded in several ways. First, the problem formulation assumes a class of input reference trajectories typical of passenger operations. The properties of this class are reflected in the CG design both in the concept of transition dynamics and in the use of segment initialization time criteria. However, the flight-control structure of reference 1 is applicable to more general aircraft operations and a larger class of inputs is generated by such operations than can be accommodated by the present CG design. Secondly, the generation of independent transitions in path axes neglects Coriolis accelerations which cross-couple the excursion states during transitions with significant path axis angular velocity. This approximation is not expected to remain adequate for operations outside the modest maneuver domain and angular velocities of the passenger operations postulated in this study. Thirdly, the path axes frame is undefined at special points in the domain of helicopter and VTOL operations (hover and vertical flight) and an alternative choice of axes in which to generate transitions is appropriate for these classes of aircraft.

An algorithm for simulation test and study was presented; it has a simple structure and utilizes equations directly from the text. The class of input reference trajectories and its properties were examined in detail and equations for an appropriate continuous-time reference trajectory generator were given. The period over which the TD could be initiated by the switching algorithm was limited to about 10 sec in advance of the reference leg-junction times based on properties of the input set. Further, it was noted that the desired values of parameters constraining the transition excursions were functions of the reference flight condition and the algorithm provides for their evaluation at the beginning of each leg. Use of a detailed model of plant dynamics, $\hat{G}(s)$, in the TD was not included in the present simulation study in view of lower bandwidth of the trajectory commands compared to plant dynamics.

Parameter values for the TD were established for the present study on the basis of operational constraints on trajectory kinematics. In general, these constraints are an essential part of the design problem associated with the operations for which the design is to be acceptable, especially during approach and landing when the aircraft operates near the boundaries of its performance capabilities. These constraints require a CG structure that recognizes the nonlinearity of the problem and provides for their systematic enforcement. In the CG design problem, some constraints are applicable to the class of operations (passenger comfort constraints) and some are derived for the specific aircraft from safety margin constraints and aircraft performance limits. The appropriate saturation parameters for the TD can then be derived from these constraints as functions of the reference flight condition. The basic repertoire of single-axis maneuvers was also examined to illustrate the significant kinematic variables in passenger operations and to demonstrate the general effectiveness of the TD saturation parameters in limiting excursions and of the TD initialization switching logic in optimizing these variables. The effects of Coriolis accelerations neglected in synthesizing the transitions was also examined; these result in kinematic incompatibility of the trajectory commands and are significant only transiently as longitudinal tracking errors during lateral axis transitions. These errors are proportional to initial values of the lateral TD states, but can be limited when large sidestep distances or large direction steps are to be executed by elaborating the input reference trajectory.

Finally, behavior of the CG and the flight-control system was tested on a STOL approach test trajectory and in response to the principal disturbances present in operations. These tests indicate a number of conclusions.

First, for the postulated class of input trajectories the CG can synthesize satisfactory four-dimensional, multiple-axis transitions from the single-axis transitions. The optimal timing and excursion saturation limits imposed independently on each axis remain effective in the multiple-axis command in minimizing overshoot and limiting excursions and rates of the kinematic variables of interest and of the corresponding aircraft control activity given by the specific force commands.

Secondly, the transition dynamics adapt successfully to off-reference initial conditions of significant magnitude due either to unanticipated initializations as a result, for example, of sensor switch events, or of uncompleted earlier transitions. In the latter case, the optimal timing logic also adapts to the off-reference condition. The bounded set of initial TD conditions over which the system functions acceptably and for which these two conclusions are operationally valid cannot be established in the present simulation. However, the simulation test path from which these conclusions are drawn contains a rigorous set of example maneuvers of greater complexity than is expected operationally.

Third, unmodeled or inaccurately modeled plant dynamics in the TD introduce tracking errors during all transitions and involve the regulator in executing the reference trajectory. Similar effects occur from unmodeled Coriolis accelerations as noted earlier. The effect on performance of these simplifying approximations were found acceptable in the simulation tests but of sufficient magnitude that further development of the theory and its application is of interest in both cases.

Fourth, the CG adapts the initial conditions for transitions to any steady-state or time-varying tracking errors of the acceleration controller subsystem. If these tracking errors are due to persistent steady disturbances (e.g., uncompensated Trimmap model errors) or to random disturbances with persistent statistics (e.g., wind turbulence) then the trajectory tracking subsystem necessarily restores the same steady-state error or its statistics that prevailed before the transition. Thus, ineffective transient activity is added to the transition commands by this adaptation. The effect is proportional to the magnitude of the tracking errors and is acceptable for sufficiently small disturbances. The effects of wind turbulence were found to be small while steady disturbances can be compensated within the trajectory tracking system. Persistent large disturbances which saturate such compensation cannot be effectively relieved by the CG and some other remedy, such as revising the reference flight condition, is indicated. However, the ineffective transient command activity due to uncompensated steady disturbances can be minimized by inclusion of disturbance estimation and compensation in the Command Generator. This problem is also of interest for further study.

Continued simulation study of the proposed CG algorithm is planned using increasingly realistic simulations of the flight-control system and aircraft, and including the estimation and attitude control subsystems.

Ames Research Center
National Aeronautics and Space Administration
Moffett Field, California 94035, May 2, 1978

APPENDIX A

DERIVATION OF DUAL-MODE CONTROL LOGIC

General Solution for the Region of Linear Control

Consider the system

$$\dot{x} = Ax + Bu \tag{A1}$$

where x is an n-vector, u an m-vector, and A; B are constant matrices of appropriate dimensions. Then the control law u that minimizes the performance measure

$$V = \int_0^\infty (x^T Q x + u^T R u) dt \tag{A2}$$

is given by reference 14

$$u = -K^T x \tag{A3}$$

where

$$K = PBR^{-1} \tag{A4}$$

and P is the positive definite, symmetric solution of the Riccati equation

$$PA + A^T P - PBR^{-1}B^T P + Q = 0 \tag{A5}$$

and it is assumed that $R > 0$ and $(A, Q^{\frac{1}{2}})$ is completely observable. For this control law, the optimal cost function is

$$V = x^T P x \tag{A6}$$

which is a Lyapunov function for (A1) and (A3) with the time derivative

$$\dot{V} = -x^T Q x - x^T PBR^{-1}B^T P x \tag{A7}$$

Suppose now that the control law $u(x)$ is subject to saturation in the following way:

$$-u_{m_i} \leq u_i(x) \leq u_{M_i} \tag{A8}$$

where the subscript (i) refers to the ith component of a vector. We can therefore permit the control to be given by

$$u_i(x) = -k_i^T x \tag{A9}$$

for those x satisfying

$$-u_{m_i} \leq -k_i^T x \leq u_{M_i} \tag{A10}$$

Here, k_i refers to the ith column of K. Let us now further restrict u by finding a region $\Omega \subseteq \mathcal{R}^n$ so that if

$$x(t_o) \in \Omega \tag{A11}$$

then

$$x(t) \in \Omega \quad \text{and} \quad u = -K^T x \ , \quad t \geq t_o$$

that is, Ω is a region of asymptotic stability as well as a region in which the control is entirely linear; Ω *is an invariant region of asymptotically stable linear control.*

A simple and convenient way of finding one such region, Ω_o is offered by the function V(x) in (A6). Let X_i be the two lines defined by

$$x^T k_i = u_{m_i}, u_{M_i} \tag{A12}$$

and then compute

$$V_M = \min_{1 \leq i \leq m} \left\{ \min_{\underline{x} \in X_i} [V(\underline{x})] \right\} \tag{A13}$$

which is found to be (cf. the case $m = 1$ in refs. 15 and 16)

$$V_M = \min_{1 \leq i \leq m} \left\{ (k_i^T P^{-1} k_i)^{-1} u_{o_i} \right\} \tag{A14}$$

where

$$u_{o_i} = \min\{u_{m_i}, u_{M_i}\}$$

Then:

$$\Omega_o = \left\{ \underline{x} : \underline{x}^T P \underline{x} \leq V_M \right\} \tag{A15}$$

Now, a dual-mode control scheme may be constructed based on Ω_o: inside Ω_o use the law (A3) and outside Ω_o use a nonlinear, saturating control law. Such a controller will have the property that (ignoring disturbances), once the linear region is entered, the control remains linear. Kuznetsov (ref. 4) was apparently first to use such a method (for $m = 1$) to construct dual-mode controllers. He essentially used a surface like that in (A15) to define the boundary between control regions and explored various possible constructions of the nonlinear controller. The next section presents the details of a particular dual-mode controller for the transition dynamics of this paper. An invariant linear region larger than Ω_o is derived and the control law for the nonlinear mode is given.

Dual-Mode Control Law for $m = 1$, $n = 2$

The invariant linear region Ω_o obtained in (A13) is generally only a subset of the largest such region. Since we put a premium on linear control, it would be desirable to be able to enlarge this region. For the case of interest here ($m = 1$), Ω_o can be extended by various methods, including direct numerical calculation of the largest such region as was done, for example, in reference 6. We adapt the work of Willems (ref. 5) to this purpose because of the convenience of the required calculations.[1]

Consider then the case $m = 1$. Using Willems' results, it can be shown that the region Ω:

$$\Omega \equiv \left\{ x : -u_M \leq k^T x \leq u_m \; ; \; x^T P x \leq V'_M \right\} \tag{A16}$$

is an invariant region of asymptotic stability for the linearly controlled system, where

$$\left.\begin{aligned} V'_M &\equiv V_{M_o} u_o^2 \\ V_{M_o} &\equiv k^T \tilde{A} P^{-1} \tilde{A}^T k [k^T P^{-1} k k^T A P^{-1} A^T k - (k^T A P^{-1} k)^2]^{-1} \\ \tilde{A} &\equiv A - B k^T \end{aligned}\right\} \tag{A17}$$

$$V'_M > V_M \tag{A18}$$

and the equality in (A18) holds only in special cases.

A simple control law for $x \notin \Omega$, which satisfies the saturation constraint (A8), is the usual time-optimal control (i.e., the control that would minimize the time to the origin in the absence of the linear control mode in the region Ω). This control provides the switching logic shown in figure 6(a) excluding the modifications for velocity limiting. This control also has the virtue of approximately minimizing the time spent outside Ω. The minimum time control to the region Ω may also be found; it is generally different from the minimum time control to the origin, although the increased complexity does not justify its use in our application.

---

[1] Our basic method of constructing a dual-mode control is not essentially tied to a quadratic optimal law; any asymptotically stable linear control law could be used, with any one of an available set of quadratic Lyapunov functions used to define the region. The approach here is felt to be somewhat more motivated, however, since it gives rise to a region that has significance in terms of a measure of control performance.

Specific Control Law for Equation (22) Without Velocity Limiting

Considerable simplification is achieved in the implementation of the dual-mode control law when applied to the system described by equations (22a), that is, the system

$$\left.\begin{aligned} \dot{x}_1 &= x \\ \dot{x}_2 &= u \end{aligned}\right\} \qquad (22a)$$

Without loss of generality, we take $R = 1$. It can also be shown that Q_{12} does not affect the locations of the characteristic roots λ_1, λ_2 of the controlled system in this case; hence for simplicity we take $Q_{12} = 0$. Then, expressing all results in terms of the easily understood parameters (ζ, τ_L) instead of the less intuitively appealing parameters Q_{11}, Q_{22}, we obtain

$$\left.\begin{aligned} k_1 &= (\zeta\tau_L)^{-2} \\ k_2 &= 2\tau_L^{-1} \end{aligned}\right\} \qquad (A19)$$

where the characteristic roots are now

$$\lambda_1, \lambda_2 = \left(-1 \pm j\sqrt{|\zeta^{-2} - 1|}\right) \tau_L^{-1}$$

and

$$\left.\begin{aligned} P_{12} &= (\zeta\tau_L)^{-2} \\ P_{22} &= 2\tau_L^{-1} \\ P_{11} &= P_{12}P_{22} \end{aligned}\right\} \qquad (A20)$$

and, after some calculation,

$$V_{M_o} = \tau_L\zeta^2(32\zeta^4 - 24\zeta^2 + 6) \qquad (A21)$$

These results all require that[2]

$$\zeta > \frac{1}{2}$$

---

[2]Although it is unlikely to be desired, characteristic roots with $\zeta < 1/2$ could be obtained by procedures different from the optimal quadratic synthesis above.

The minimum-time control for equation (22a) and for $x \notin \Omega$ is now given by

$$u = \begin{cases} -u_m & \sigma > 0 \quad \text{or} \quad (\sigma = 0, \quad x_2 > 0) \\ u_M & \sigma < 0 \quad \text{or} \quad (\sigma = 0, \quad x_2 < 0) \end{cases} \tag{A22}$$

where

$$\sigma \equiv \begin{cases} u_m x_1 + \frac{1}{2} x_2^2 & x_2 > 0 \\ u_M x_1 - \frac{1}{2} x_2^2 & x_2 < 0 \end{cases} \tag{A23}$$

APPENDIX B

VELOCITY-LIMITING MODIFICATION OF CONTROL ALGORITHM

Appendix A described a dual-mode control algorithm that maintains prescribed saturation limits on the scalar control u in the form

$$u = \begin{cases} -k^T x & \text{for} \quad x \in \Omega \\ (A22) & \text{for} \quad x \in \bar{\Omega} \end{cases} \tag{B1}$$

where Ω is defined by equation (A16). Here the law is modified (for $n = 2$) to maintain, in a certain sense, bounds on the velocity

$$-x_{2m} \leq x_2 \leq x_{2M} \tag{B2}$$

The modifications are developed next by considering different types of initial conditions.

In the case that $x(0)$ is in $\bar{\Omega}$ and $x_2(0)$ satisfies equation (B2), a review of phase plane trajectories and the basic control algorithm equation (A22) shows that a trajectory either enters Ω or else encounters a limit of equation (B2), say, $x_2 = x_{2M}$ (see fig. 23). If equation (B1) is modified so that $u = 0$ at this point, x_2 will remain constant at the limit value, and this control should be held until the first opportunity to decrease x_2 by reinstating the basic algorithm (eq. (B1)). This can occur at either of two events; first, if the switching curve $\sigma = 0$ is encountered before the boundary of Ω (trajectory i_a in fig. 23), then the control simply switches to $u = -u_m$ at the switching curve in accordance with equation (A22). Secondly, if the boundary of Ω is encountered before the curve $\sigma = 0$, then the control remains null but switches to the linear control law of the region Ω as given by equation (B1) when $\underline{k}^T\underline{x} = 0$ (see fig. 24). We need only demonstrate that the modified linear region Ω_L as shown in figure 24 (region Ω with the "bite" 0_1-0_2-0_3 taken out of it) as an invariant one, that is, that trajectories cannot cross the new boundary-line segments 0_1-0_2 and 0_2-0_3 from interior points of Ω_L. This is enforced for 0_1-0_2, a locus of constant x_2, by the nulled control of the modified law along this segment. For segment 0_2-0_3, observe that x_1 is strictly increasing:

$$x_1 < 0, \quad \dot{x}_1 = x_2 > 0$$

and the trajectory is locally parallel to the x_1 axis:

$$\frac{dx_2}{dx_1} = \frac{-k^T x}{x_2} = 0$$

so that a trajectory necessarily evolves into the interior of Ω_L from any point on 0_2-0_3. Since the linear control becomes negative at interior points of Ω_L adjacent to 0_2-0_3, the velocity subsequently decreases. To conclude this case, note that similar arguments apply to maintaining the limit $-x_{2m}$ in the fourth quadrant of the phase plane.

For initial conditions with $x(0)$ in $\bar{\Omega}$ but $x_2(0)$ does not satisfy equation (B2), there are two subcases to consider; first, if

$$\left.\begin{array}{l} x_2(0) < -x_{2m} \quad \text{and} \quad \sigma < 0 \\ \text{or} \\ x_2(0) > x_{2M} \quad \text{and} \quad \sigma > 0 \end{array}\right\} \tag{B3}$$

the control law (eq. (B1)) need not be modified since it already drives the velocity toward the permitted range (eq. (B2)) as rapidly as possible. The second subcase occurs with

$$\left.\begin{array}{l} x_2(0) < -x_{2m} \quad \text{and} \quad \sigma > 0 \\ \text{or} \\ x_2(0) > x_{2M} \quad \text{and} \quad \sigma < 0 \end{array}\right\} \tag{B4}$$

Here we can consider modifying the control to reduce x_2 at the maximum rate as for the first subcase, but the possibility of "chatter"-like phenomena whenever the velocity limit line (where $u = 0$) is encountered must be accounted for. Alternatively, we select $u = 0$ for the entire region given by equations (B4); the resulting free trajectory must exit this region in finite time.

Finally, the remaining possible initial conditions, $x(0) \in \Omega$ either begin in the "bite" removed from the linear region, in which case the control is again nulled as it is on the region defined by equations (B4), or it begins in Ω_L, where the linear control law of equation (B1) remains in force.

In summary, equation (B1) is simply modified to give null control on the following regions:

$$u(x) = 0$$

for

$$x \in \Omega \quad \text{and} \quad \{(-k^T x < 0, x_2 < -x_{2m}) \text{ or } (-k^T x > 0, x_2 > x_{2M})\} \tag{B5}$$

or

$$x \in \bar{\Omega}_L \quad \text{and} \quad \{(\sigma > 0, x_2 < x_{2m}) \text{ or } (\sigma < 0, x_2 > x_{2M})\}$$

REFERENCES

1. Meyer, George; and Cicolani, Luigi: A Formal Structure for Advanced Automatic Flight-Control System. NASA TN D-7940, 1975.

2. Cicolani, L.; Sridhar, B.; and Meyer, G.: Configuration Management and Automatic Control of an Augmentor Wing Aircraft with Vectored Thrust. NASA TP-1222, 1978.

3. Pecsvaradi, Thomas: Four-Dimensional Guidance Algorithms for Aircraft in an Air Traffic Control Environment. NASA TN D-7829, 1975.

4. Kuznetsov, N. A.: Finding Control Algorithms for a Variable Optimality Criterion. Automation and Remote Control, vol. 27, no. 5, May 1966, pp. 735-744.

5. Willems, J. L.: The Computation of Finite Stability Regions by Means of Open Lyapunov Surfaces. International Journal of Control, vol. 10, no. 5, 1969, pp. 537-544.

6. Zachary, D. H.; Roberts, A. P.; and Newman, M. M.: Optimum Transient Response of a Saturating System Which has a Linear Region of Control. International Journal of Control, vol. 2, no. 4, 1965, pp. 353-363.

7. Benner, Margaret S.; McLaughlin, Milton D.; Sawyer, Richard H.; Van Gunst, Roger; and Ryan, John J.: A Flight Investigation with a STOL Airplane Flying Curved, Descending Instrument Approach Paths. NASA TN D-7669, 1974.

8. Weissenberger, S.: Optimal Command Generation for Tracking a Class of Discontinuous Trajectories. Transactions of the ASME, Journal of Dynamic Systems, Measurement Control, vol. 98, Series G, no. 2, June 1976, pp. 167-172.

9. Chen, Chi-tsong: Introduction to Linear System Theory. Holt, Reinhart and Winston, N.Y., 1970.

10. Scott, B. C.; Martin, P. W.; Hynes, C. S.; and Bryder, R. B.: Progress Toward Development of Civil Airworthiness Criteria for Powered Lift-Aircraft. NASA TM X-73,124, 1976.

11. Cleveland, W. B.; Vomaske, R. F.; Sinclair, S. R. M.: Augmentor Wing Jet STOL Research Aircraft Digital Simulation Model. NASA TM X-62149, 1972.

12. Cicolani, L. S.; and Meyer, G.: Digital Simulation of V/STOL Aircraft for Autopilot Research. In "Large-Scale Dynamic Systems." NASA SP-371, 1975, pp. 163-184.

13. Etkin, Bernard: Dynamics of Atmospheric Flight. Wiley, N.Y., 1972.

14. Anderson, Brian D. O.; and Moore, John B.: Linear Optimal Control. Prentice-Hall, Englewood Cliffs, N.J., 1971.

15. Walker, J. A.; and McClamrock, N. H.: Finite Regions of Attraction for the Problem of Lure. International Journal of Control, vol. 6, no. 4, Oct. 1967, pp. 331-336.

16. Weissenberger, Stein: Application of Results from the Absolute Stability Problem to the Computation of Finite Stability Domains. IEEE Transactions on Automatic Control (Correspondence), vol. AC-13, no. 1, Feb. 1968, pp. 124-125.

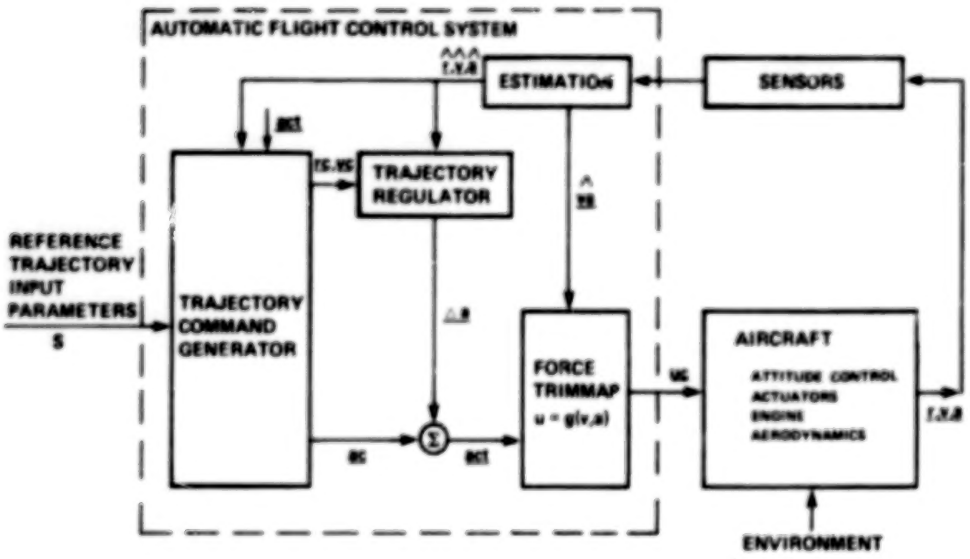

Figure 1.- Structure for an automatic flight-control system.

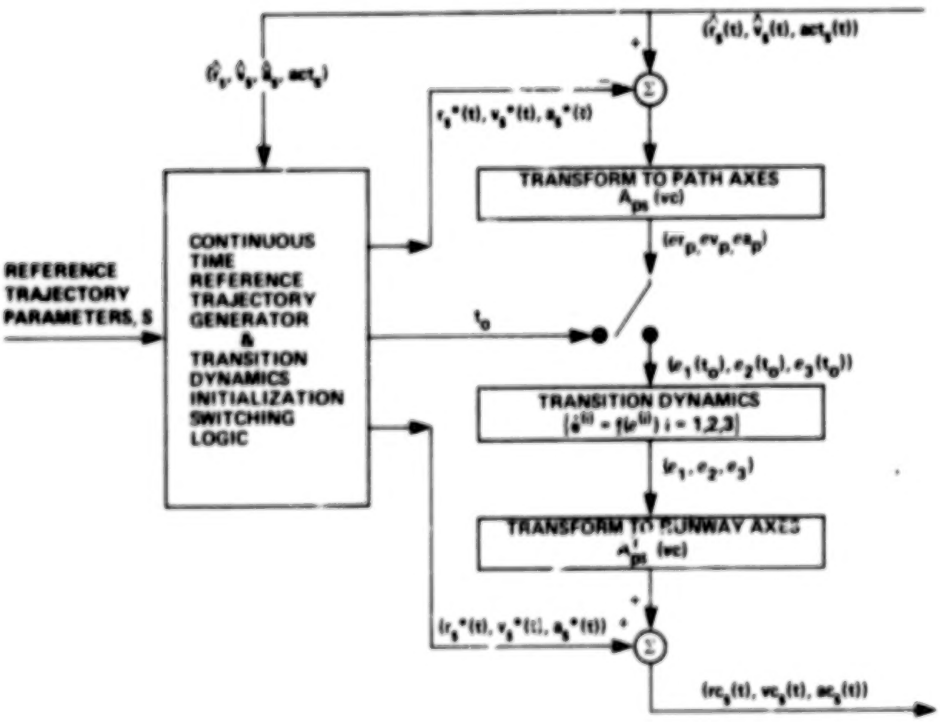

Figure 2.- Trajectory command generator structure.

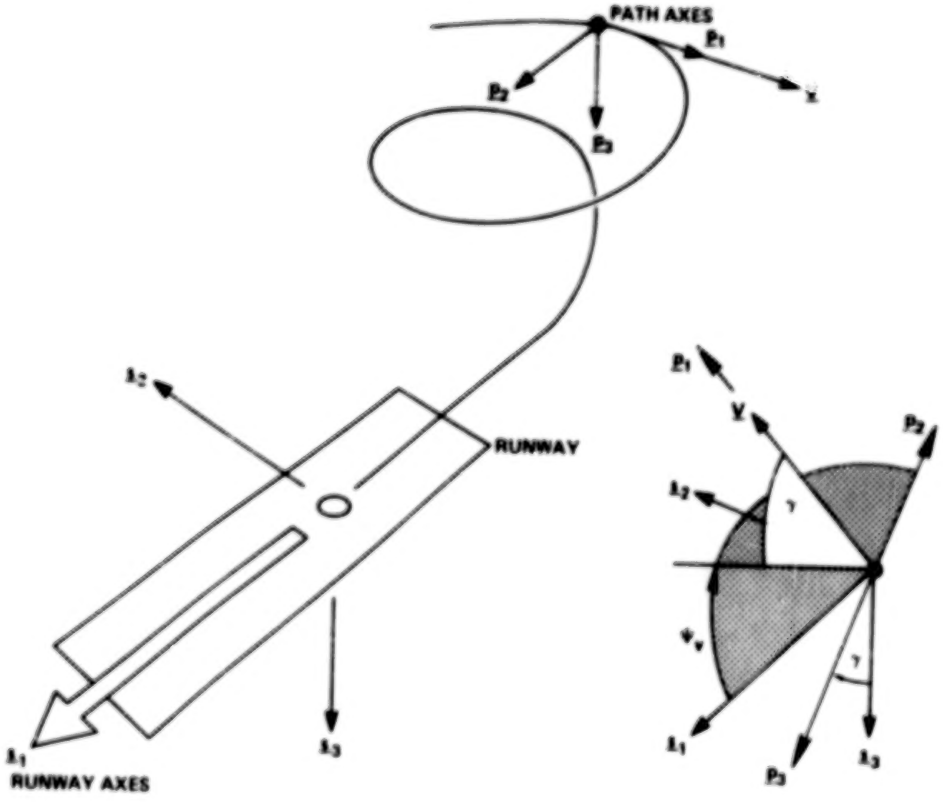

Figure 3.- Axis systems and transformation angles.

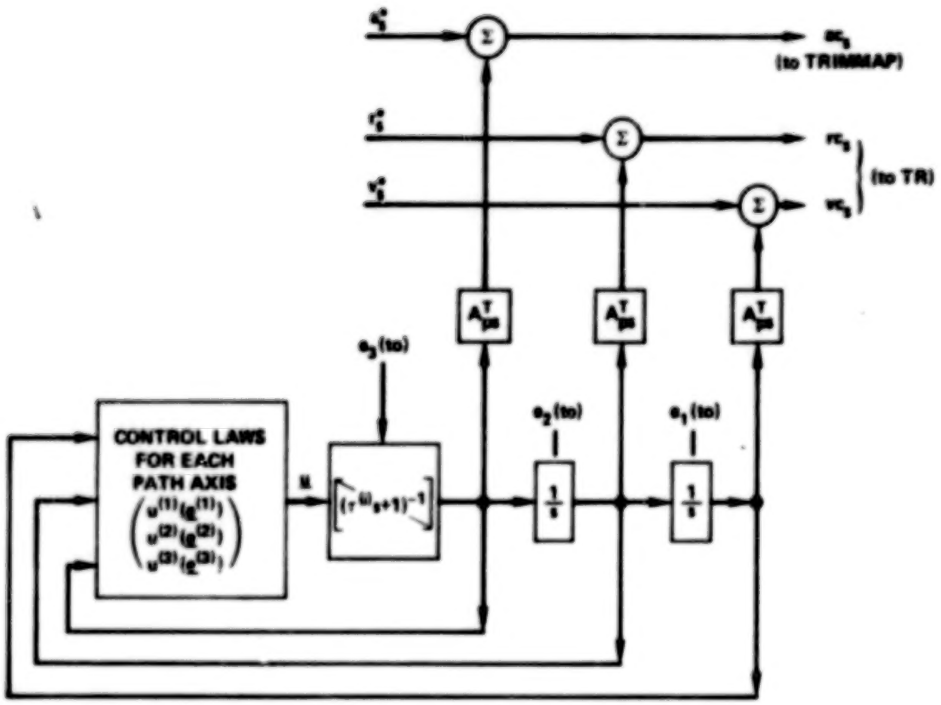

Figure 4.- Third-order transition dynamics structure.

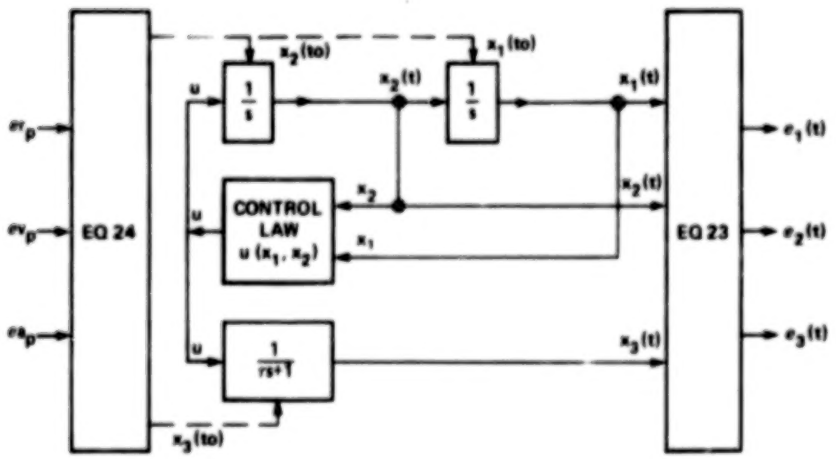

Figure 5.- Third-order transition dynamics structure using simplified control law construction.

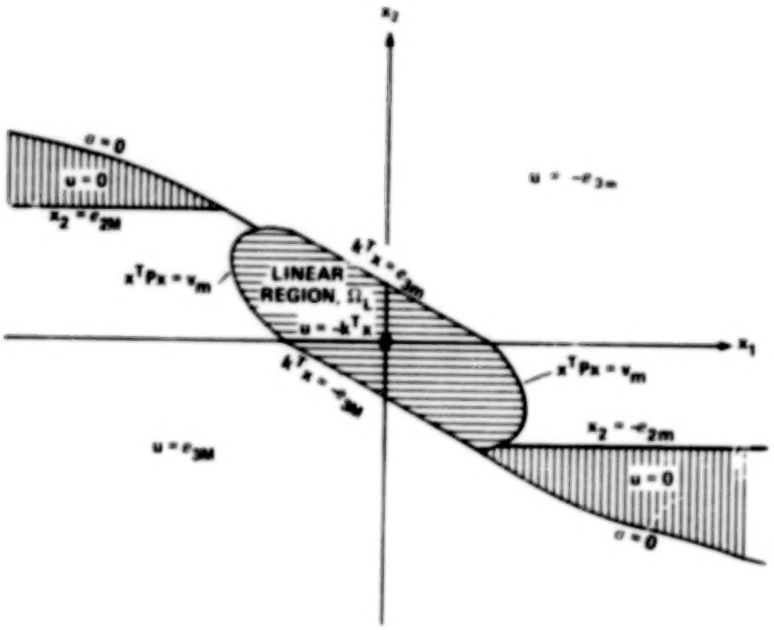

(a) Control law and switching boundaries in the x-plane.

Figure 6.- Transition dynamics.

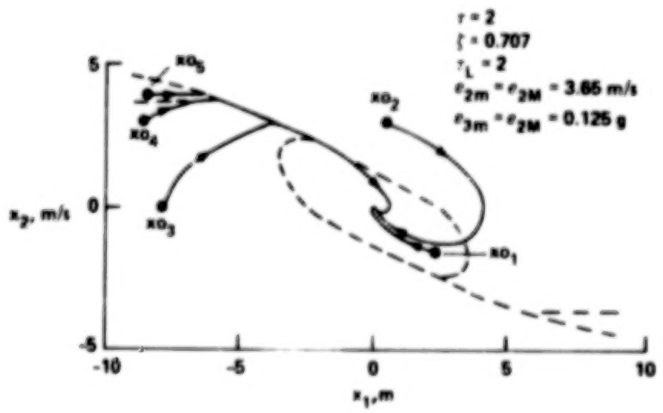

(b) x-plane trajectories.

Figure 6.- Continued.

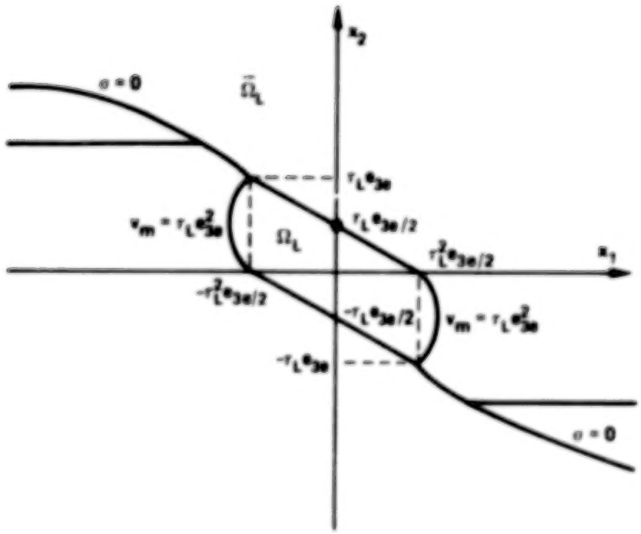

(c) Switching boundaries for $\rho = 0.707$, $e_{3m} = e_{3M} = e_{3e}$.

Figure 6.- Concluded.

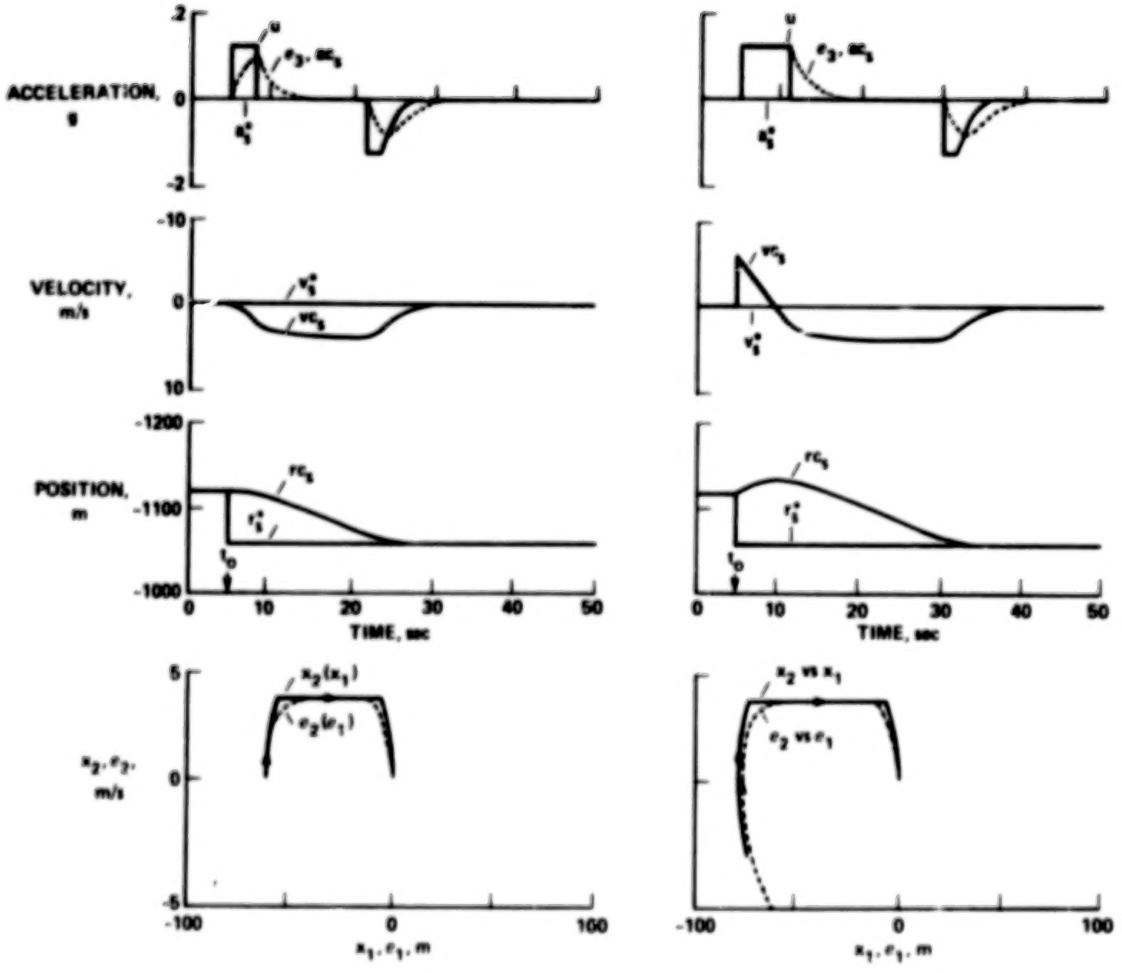

(a) Altitude step.

(b) Altitude step with initial altitude rate error.

Figure 7.- Transition maneuver examples, altitude step.

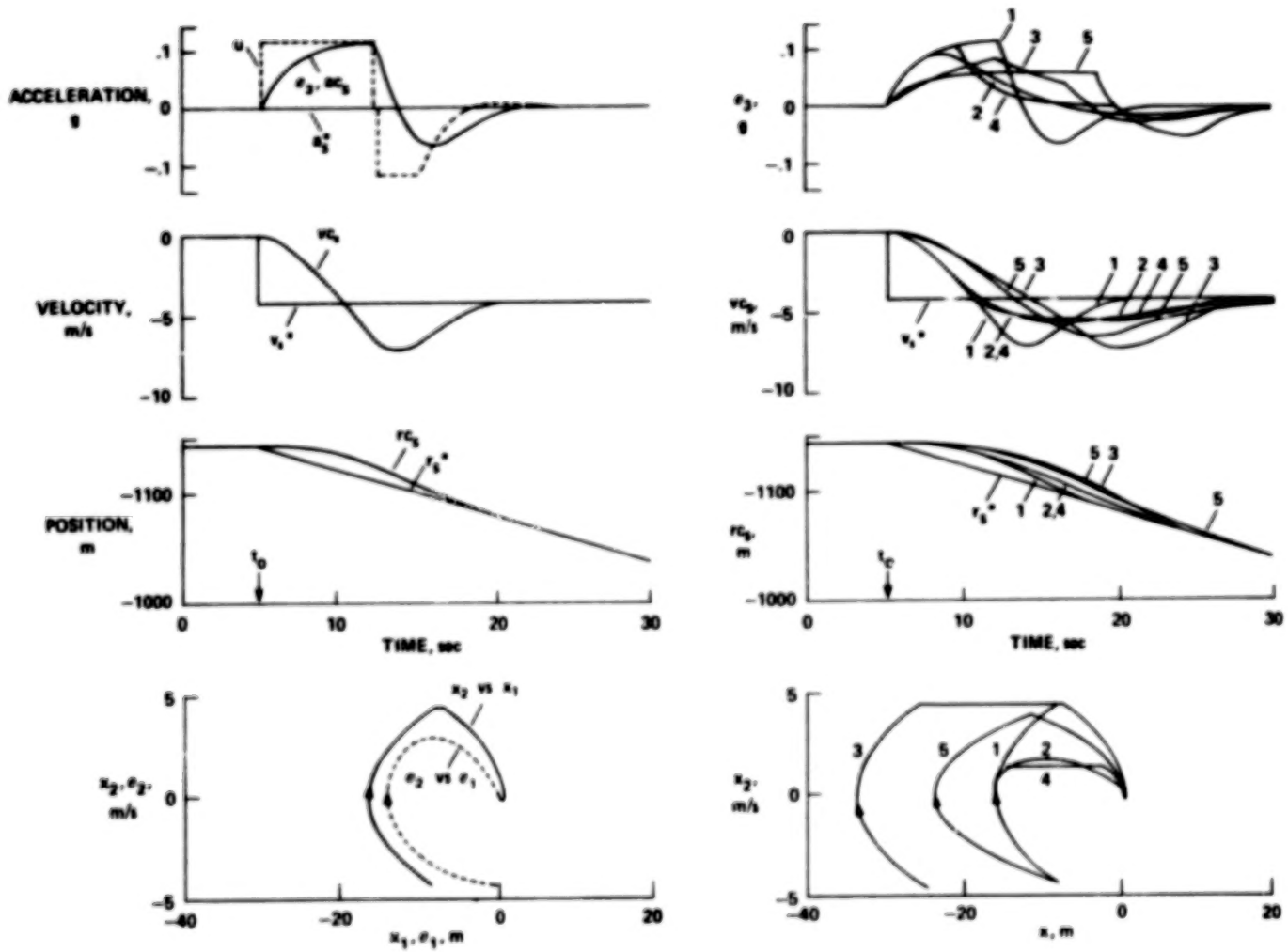

(a) Pitchover.

(b) Pitchover – effect of parameter values.

Figure 8.- Transition maneuver examples, pitchover.

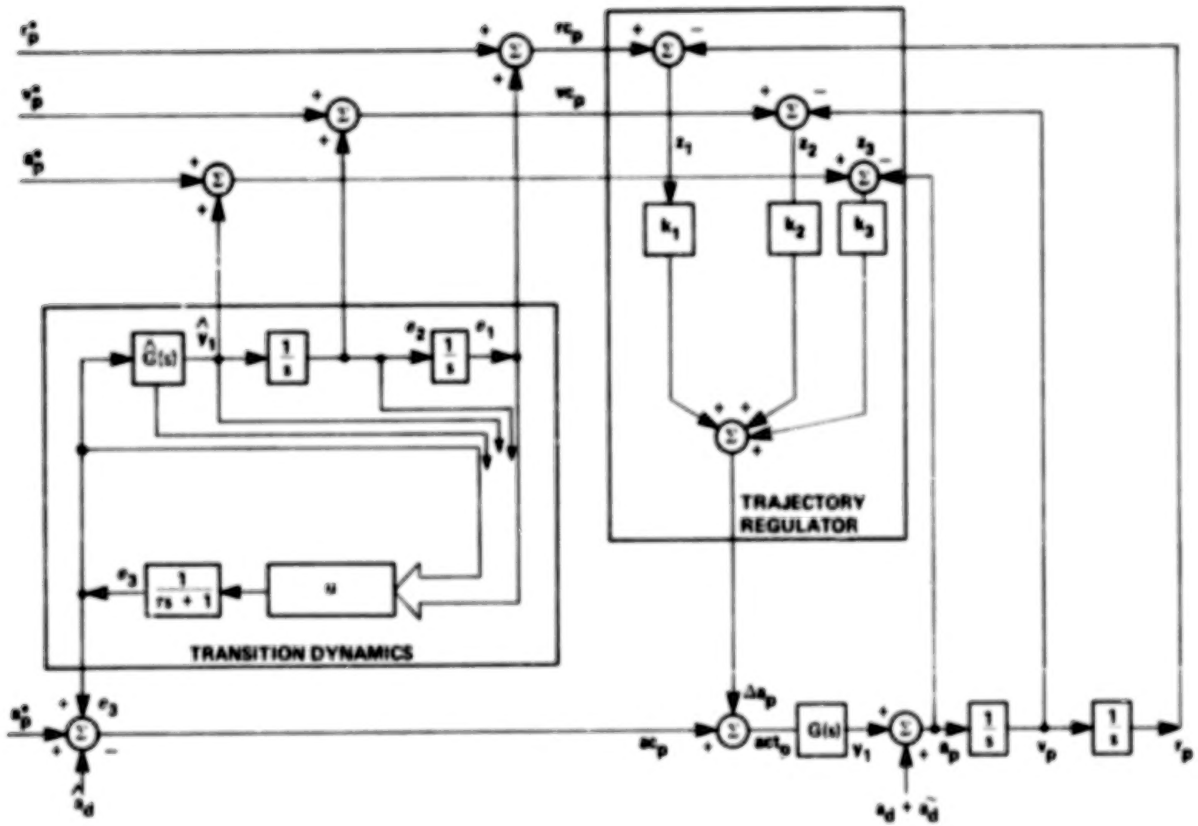

Figure 9.- System structure, single axis.

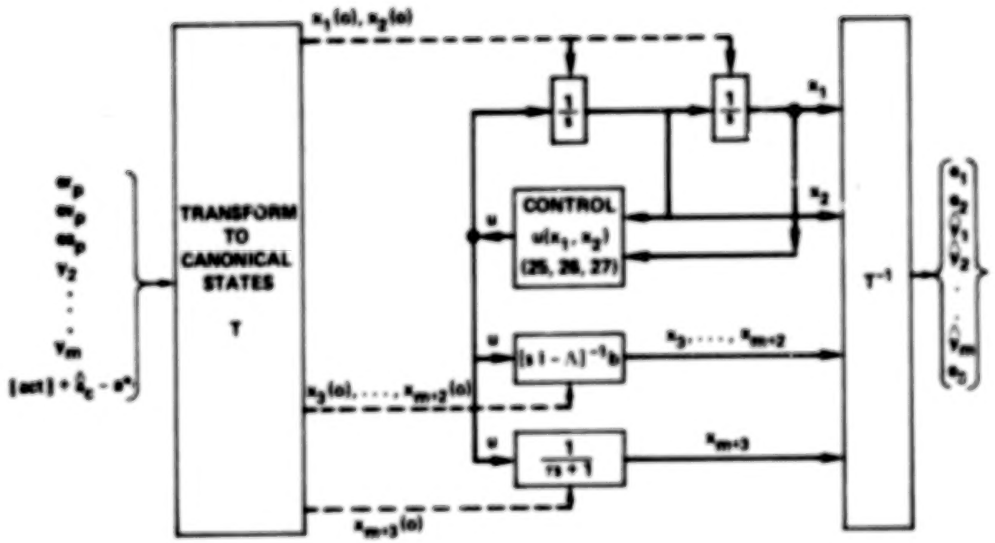

Figure 10.- Canonical transition dynamics structure with predictive modeling.

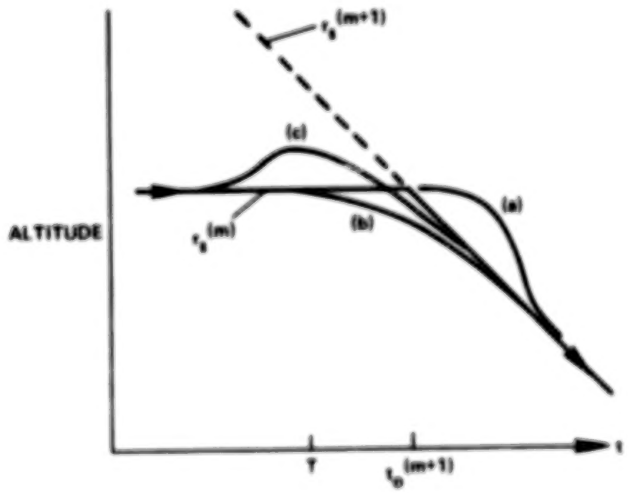

Figure 11.- Effect of initialization time on pitchover transition.

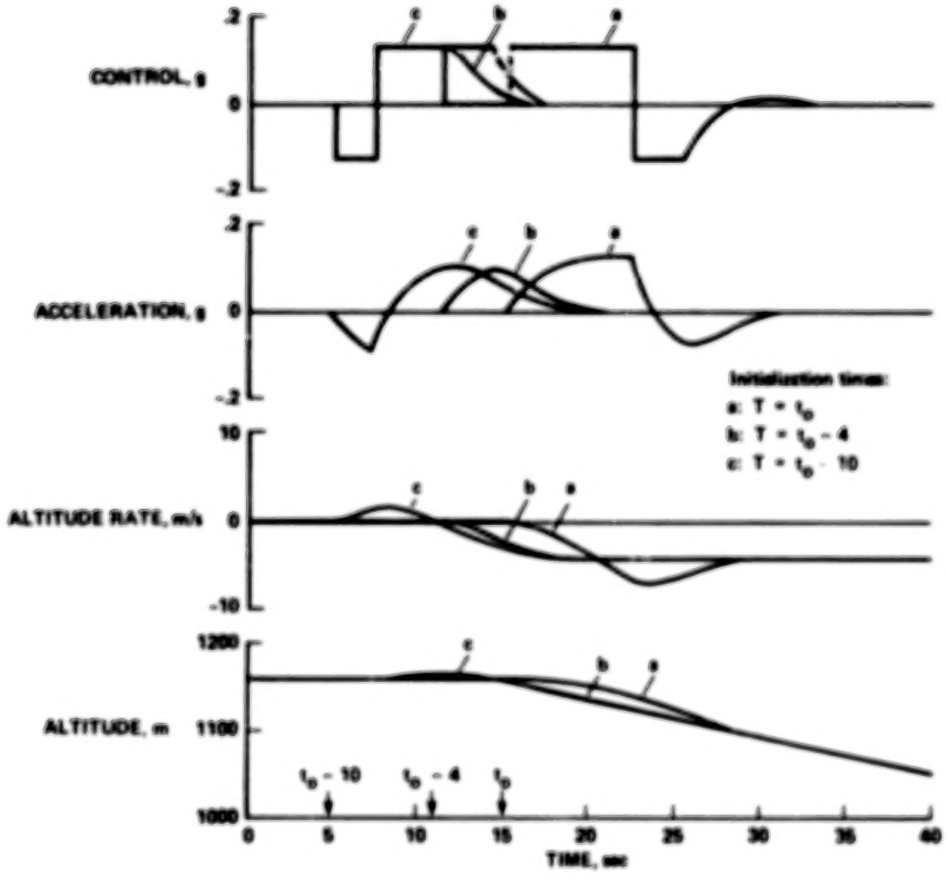

(a) Effects of initialization time.

Figure 12.- Effect of initialization time on pitchover maneuver.

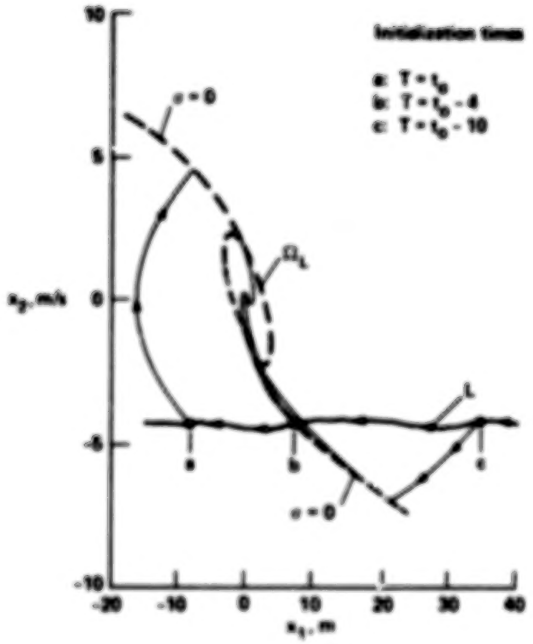

(b) x_1, x_2 plane trajectories — optimum nonlinear transition.

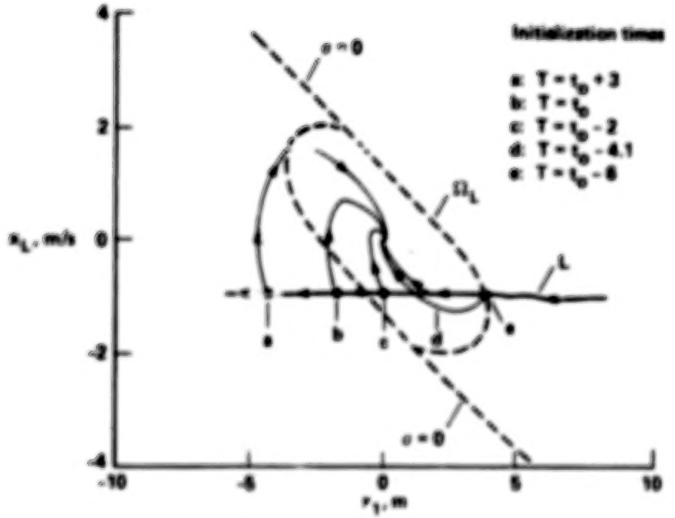

(c) x_1, x_2 plane trajectories — optimum linear transition.

Figure 12.- Concluded.

TABLE OF CONTENTS

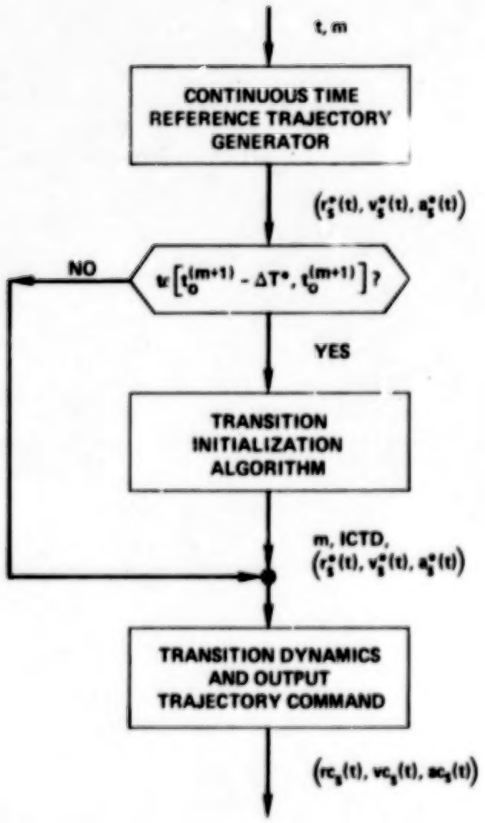

PARAMETERS:

$\Delta T^* = \min\left\{\Delta T, t_0^{(m+1)} - t_0^{(m)}\right\}$

ΔT = PRESELECTED TD INITIALIZATION PERIOD

m = LEG NUMBER

ICTD = TRANSITION DYNAMICS INITIALIZATION FLAG

Figure 13.- Command generator algorithm.

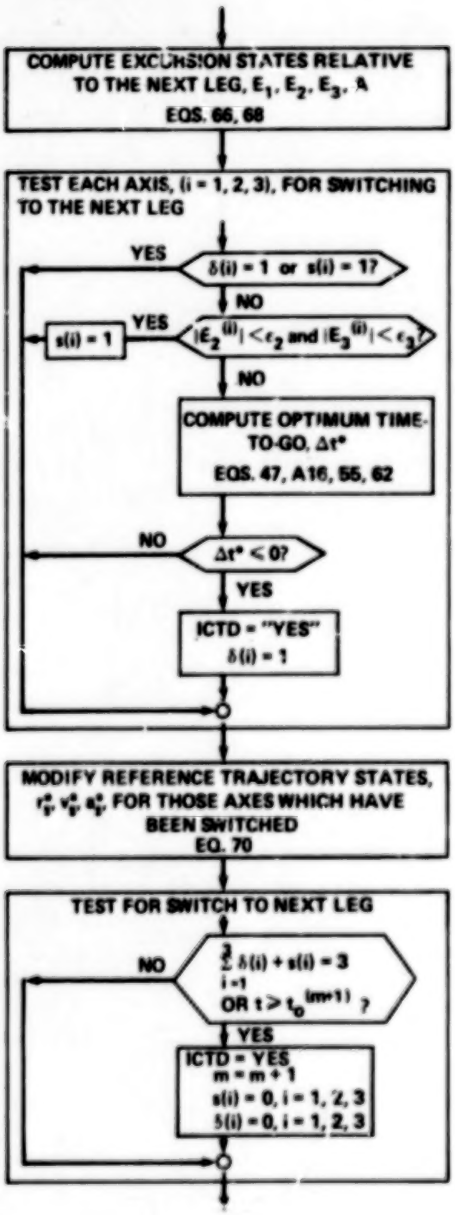

PARAMETERS

$\{\delta(i), i = 1, 2, 3\}$	SWITCHED-AXIS FLAG
$\{s(i), i = 1, 2, 3\}$	AMBIGUOUS AXIS FLAG
ϵ_2, ϵ_3	VELOCITY AND ACCELERATION THRESHOLDS
m	LEG NUMBER
ICTD	TD INITIALIZATION FLAG

(a) Computational flow diagram.

Figure 14.- Transition initialization algorithm.

EXCURSION STATES RELATIVE TO NEXT LEG

$$\Delta \equiv t - t_o^{(m+1)}$$

$$\begin{pmatrix} en_1 \\ en_2 \\ en_3 \end{pmatrix} = \begin{bmatrix} I & \Delta I & .5\Delta^2 I \\ \phi & I & \Delta I \\ \phi & \phi & \phi \end{bmatrix} \begin{pmatrix} en_1 \\ en_2 \\ en_3 \end{pmatrix}_{t_o^{(m+1)}} \qquad \text{EQ. (66)}$$

$$er_p = A_{ps}(\hat{r}_s - r_s^o)$$
$$ev_p = A_{ps}(\hat{v}_s - v_s^o)$$
$$g_p^o = A_{ps}\, g_s^o$$
$$ac_p = A_{ps}\, ac_s$$
$$act_p = A_{ps}\, act_s$$

$$\begin{pmatrix} E_1 \\ E_2 \\ E_3 \end{pmatrix} = -\begin{pmatrix} en_1 \\ en_2 \\ en_3 \end{pmatrix} + \begin{pmatrix} er_p \\ ev_p \\ |act_p| - g_p^o \end{pmatrix} \qquad \text{EQ. (68)}$$

$$A = -en_3 + ac_p$$

OPTIMUM TIME-TO-GO:

$$xn_1 = E_1^{(i)} + \gamma^{(i)} E_2^{(i)}$$
$$xn_2 = E_2^{(i)} + \gamma^{(i)} E_3^{(i)}$$
$$uLN = -k_1^{(i)}\, xn_1 - k_2^{(i)}\, xn_2^{(i)} \qquad \text{EQ. (47)}$$
$$VN = k_1^{(i)}\, k_2^{(i)}\, xn_1^2 + 2k_1^{(i)} xn_1\, xn_2 + k_2^{(i)}\, xn_2^2$$
$$\Omega \equiv \left\{ x : VN \le VM^{(i)},\ uLN \in [-a_{3m}^{(i)}, a_{3M}^{(i)}] \right\} \qquad \text{EQ. (A16)}$$

$$\Delta t^* = \begin{cases} -a & x \in \Omega,\ |A| \le \epsilon_3 \\ -b + \sqrt{\max\{0, b^2 - c\}} & x \in \Omega,\ |A| > \epsilon_3 \\ -a_1 & x \notin \Omega,\ |A| \le \epsilon_3 \\ -b_1 + \sqrt{\max\{0, b_1^2 - c_1\}} & x \notin \Omega,\ |A| > \epsilon_3 \end{cases} \qquad \begin{matrix} \text{EQ. (55)} \\ \text{EQ. (62)} \end{matrix}$$

$\{\gamma^{(i)}, k_1^{(i)}, k_2^{(i)}, VM^{(i)}, a_{3m}^{(i)}, a_{3M}^{(i)}\}$ - TRANSITION DYNAMICS PARAMETERS
$\{a, b, a_1, b_1\}$ - FUNCTIONS OF xn_1, xn_2. CF EQS. (55), (62)

REFERENCE TRAJECTORY MODIFICATION FOR SWITCHED AXES:

$$G = A_{ps}\,[\delta(i)]$$
$$r_s^o = r_s^o + G\, en_1$$
$$v_s^o = v_s^o + G\, en_2 \qquad \text{EQ. (70)}$$
$$g_s^o = g_s^o + G\, en_3$$

(b) Summary of equations for transition initialization algorithm.

Figure 14.- Concluded.

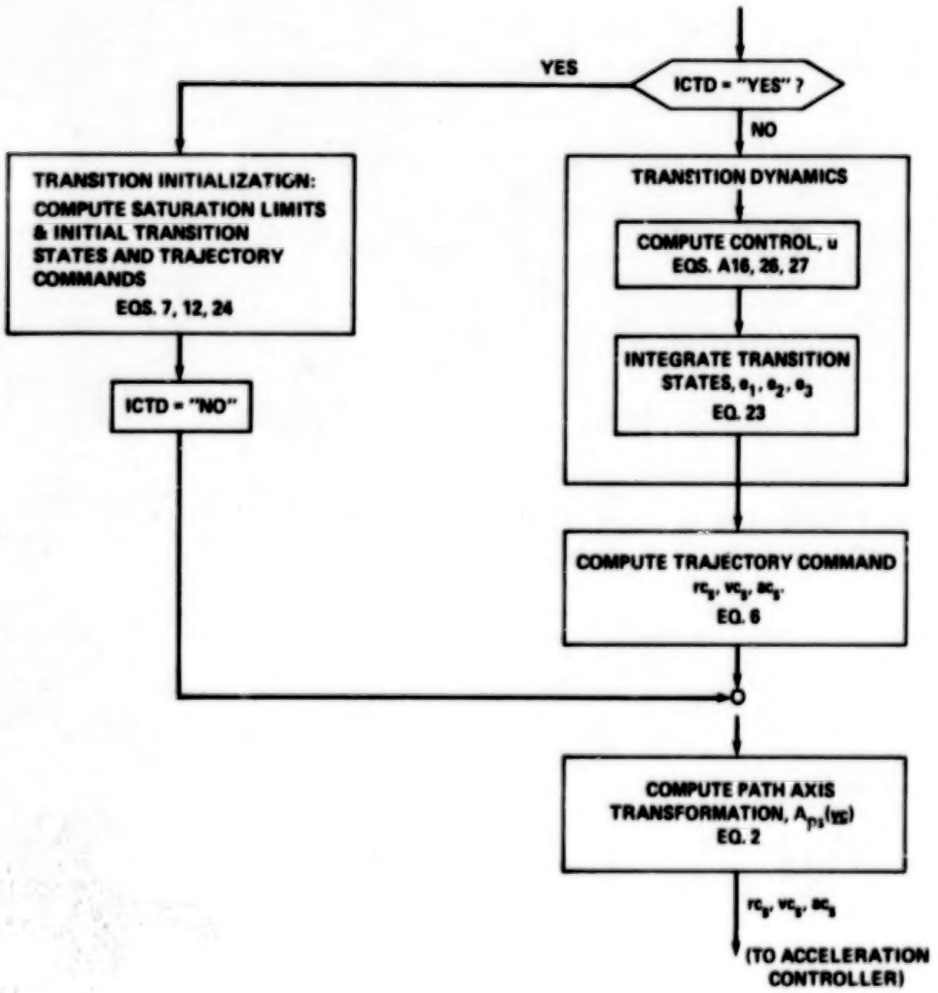

(a) Computational flow diagram.

Figure 15.- Transition dynamics algorithm for simulation test.

REQUIRED INPUT PARAMETERS FOR TD:

$$\left\{\left(\zeta^{(i)}, \tau_L{}^{(i)}, a_{2m}^{(i)}, a_{2M}^{(i)}, a_{3m}^{(i)}, a_{3M}^{(i)}, a_m^{(i)}, a_M^{(i)}\right), i = 1, 2, 3\right\}$$

EXPRESSIONS FOR AUXILIARY PARAMETERS

$$k_1{}^{(i)} = (\tau_L{}^{(i)}\zeta^{(i)})^{-2}$$

$$k_2{}^{(i)} = 2/\tau_L{}^{(i)} \qquad \text{EQ. (28)}$$

$$VM^{(i)} = \tau_L{}^{(i)}\zeta^{(i)}\left[6 + 32\zeta^{(i)}\left(\zeta^{(i)2} - .75\right)\right]$$

TRANSITION INITIALIZATION

$a_{2m}, a_{2M}, a_{3m}, a_{3M}, a_m, a_M \sim$ FUNCTIONS OF $\underline{r}^*, \underline{v}^*$, AS APECIFIED

$$e_1 = A_{ps} \cdot (\hat{r}_s - r_s^*)$$

$$e_2 = A_{ps} \cdot (\hat{v}_s - v_s^*)$$

$$act_p = A_{ps}\, act_s \qquad \text{EQ. (12)}$$

$$e_3 = [act_p] - A_{ps} \cdot a_s^*$$

$$x_1 = e_1 + [\tau^{(i)}\Delta]\, e_2 \qquad \text{EQ. (24)}$$

$$x_2 = e_2 + [\tau^{(i)}\Delta]\, e_3$$

$$rc_s = \hat{r}_s$$

$$vc_s = \hat{v}_s \qquad \text{EQ. (7)}$$

$$ac_s = a_s^* + A_{ps}^T e_3$$

where

$$[act_p] \equiv \left(\max\left\{-a_m^{(i)}, \min\left\{act_p^{(i)}, a_M^{(i)}\right\}\right\}, i = 1, 2, 3\right)^T$$

TD CONTROL FOR i^{th} AXIS, i = 1, 2, 3

$$V = k_1{}^{(i)} k_2{}^{(i)}\, x_1{}^{(i)2} + 2 k_1{}^{(i)} x_1{}^{(i)} x_2{}^{(i)} + k_2{}^{(i)} x_2{}^{(i)2}$$

$$u_L = -k_1{}^{(i)} x_1{}^{(i)} - k_2{}^{(i)} x_2{}^{(i)}$$

$$a_{3s} = \begin{cases} a_{3m}^{(i)} & x_2{}^{(i)} < 0 \\ a_{3M}^{(i)} & x_2{}^{(i)} > 0 \end{cases}$$

$$\sigma = .5\,|x_2{}^{(i)}|\, x_2{}^{(i)} + x_1{}^{(i)} a_{3s} \qquad \text{EQ. (26)}$$

$$\Omega \equiv \left\{x^{(i)} : V \le VM^{(i)}, u_L \in \left[-a_{2m}^{(i)}, a_{2M}^{(i)}\right]\right\} \qquad \text{EQ. (A16)}$$

$$u^{(i)} = \begin{cases} u_L & \text{IF } x \in \Omega \cap \left[\left\{u_L < 0, x_2{}^{(i)} > -a_{2m}^{(i)}\right\} \cup \left\{u_L > 0, x_2{}^{(i)} < a_{2M}^{(i)}\right\}\right] \\ 0 & \text{IF } x \in \Omega \cap \left[\left\{u_L < 0, x_2{}^{(i)} > -a_{2m}^{(i)}\right\} \cup \left\{u_L > 0, x_2{}^{(i)} < a_{2M}^{(i)}\right\}\right] \\ -a_{2m}^{(i)} & \text{IF } x \in \Omega \,\&\, x \in \left[\left\{\sigma > 0, x_2{}^{(i)} > -a_{2m}^{(i)}\right\} \cup \left\{\sigma = 0, x_2{}^{(i)} > 0\right\}\right] \\ 0 & \text{IF } x \in \Omega \,\&\, x \in \left[\left\{\sigma > 0, x_2{}^{(i)} < -a_{2m}^{(i)}\right\} \cup \left\{\sigma < 0, x_2{}^{(i)} > a_{2M}^{(i)}\right\}\right] \\ -a_{2M}^{(i)} & \text{IF } x \in \Omega \,\&\, x \in \left[\left\{\sigma < 0, x_2{}^{(i)} < a_{2m}^{(i)}\right\} \cup \left\{\sigma = 0, x_2{}^{(i)} < 0\right\}\right] \end{cases} \qquad \text{EQ. (27)}$$

(b) Summary of transition dynamics equations.

Figure 15.- Continued.

INTEGRATION OF TRANSITION STATES FOR i^{th} AXIS, $i = 1, 2, 3$

Δt = CONTROL CYCLE STEP SIZE

$$\begin{pmatrix} x_1^{(i)} \\ x_2^{(i)} \\ x_3^{(i)} \end{pmatrix} = \begin{bmatrix} 1 & \Delta t & 0 \\ 0 & 1 & 0 \\ 0 & 0 & e^{-\Delta t/\tau^{(i)}} \end{bmatrix} \begin{pmatrix} x_1^{(i)} \\ x_2^{(i)} \\ x_3^{(i)} \end{pmatrix} + \begin{pmatrix} .5\,\Delta t^2 \\ \Delta t \\ 1 - e^{-\Delta t/\tau^{(i)}} \end{pmatrix} u^{(i)}$$

$$\begin{pmatrix} e_1^{(i)} \\ e_2^{(i)} \end{pmatrix} = \begin{bmatrix} 1 & -\tau^{(i)} & -\tau^{(i)2} \\ 0 & 1 & -\tau^{(i)} \end{bmatrix} \begin{pmatrix} x_1^{(i)} \\ x_2^{(i)} \\ x_3^{(i)} \end{pmatrix} \qquad \text{EQ. (23)}$$

OUTPUT TRAJECTORY COMMANDS & PATH AXIS TRANSFORMATION

$$\begin{pmatrix} rc_s \\ vc_s \\ ac_s \end{pmatrix} = \begin{pmatrix} r_s^o \\ v_s^o \\ a_s^o \end{pmatrix} + \begin{pmatrix} A_{ps}^T e_1 \\ A_{ps}^T e_2 \\ A_{ps}^T e_3 \end{pmatrix}$$

$\gamma = \sin^{-1}(\overrightarrow{vc} \cdot \hat{s}_3 / |vc|)$

$\Psi_v = \tan^{-1}(\overrightarrow{vc} \cdot \hat{s}_1 / \overrightarrow{vc} \cdot \hat{s}_2)$

$$A_{ps} = \begin{bmatrix} \cos\gamma \cos\Psi_v & \cos\gamma \sin\Psi_v & -\sin\gamma \\ -\sin\Psi_v & \cos\Psi_v & 0 \\ \sin\gamma \cos\Psi_v & \sin\gamma \sin\Psi_v & \cos\gamma \end{bmatrix} \qquad \text{EQ. (2)}$$

(b) Concluded.

Figure 15.- Concluded.

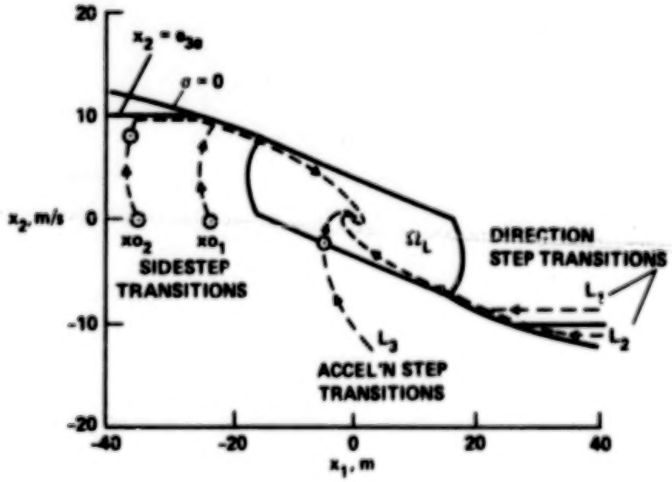

Figure 16.- Lateral axis – single state transitions.

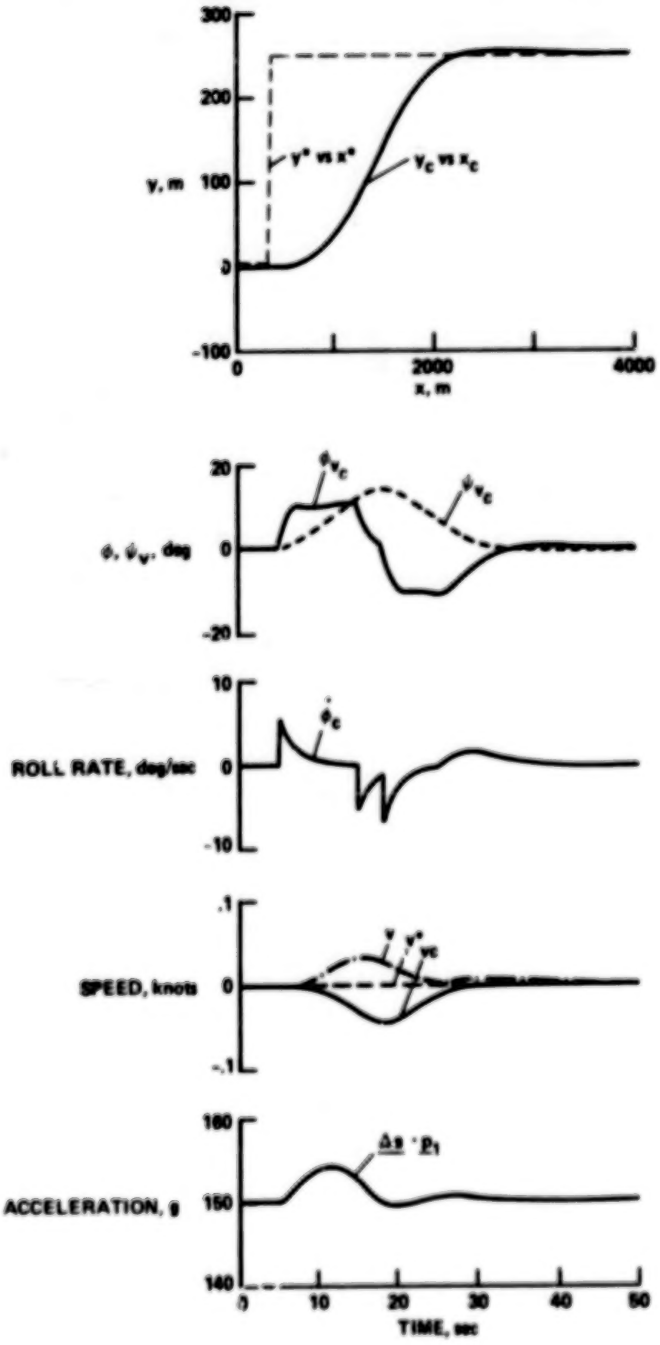

(a) Sidestep transition to a parallel path.

Figure 17.- Sidestep and direction step transition.

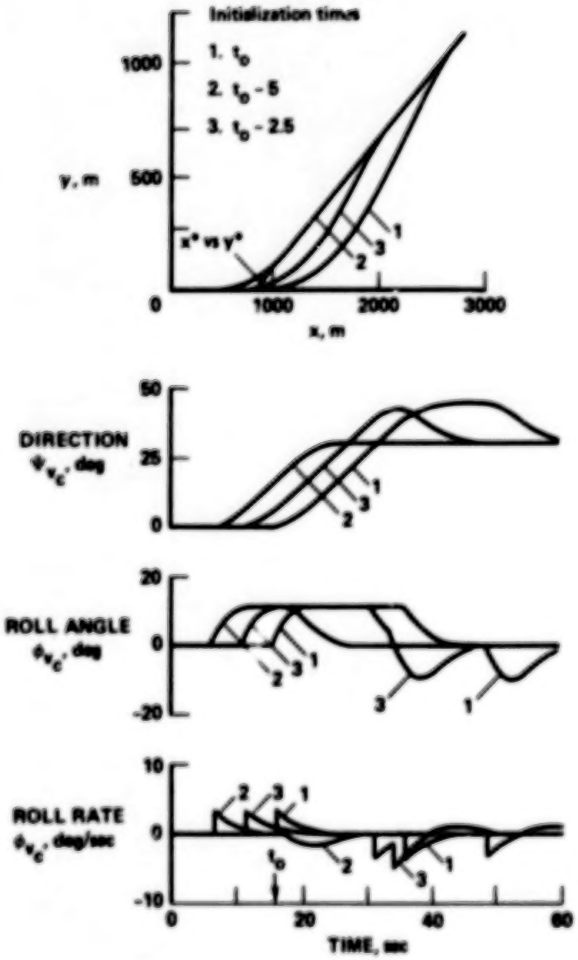

(b) Effects of transition initialization time.

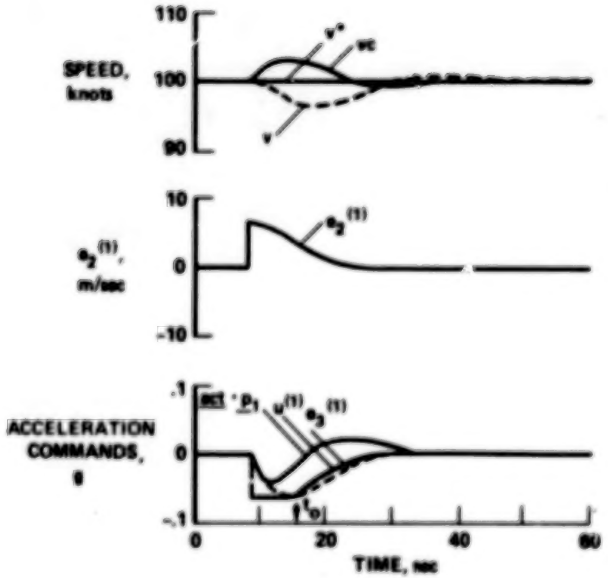

(c) Longitudinal axis activity.

Figure 17.- Concluded.

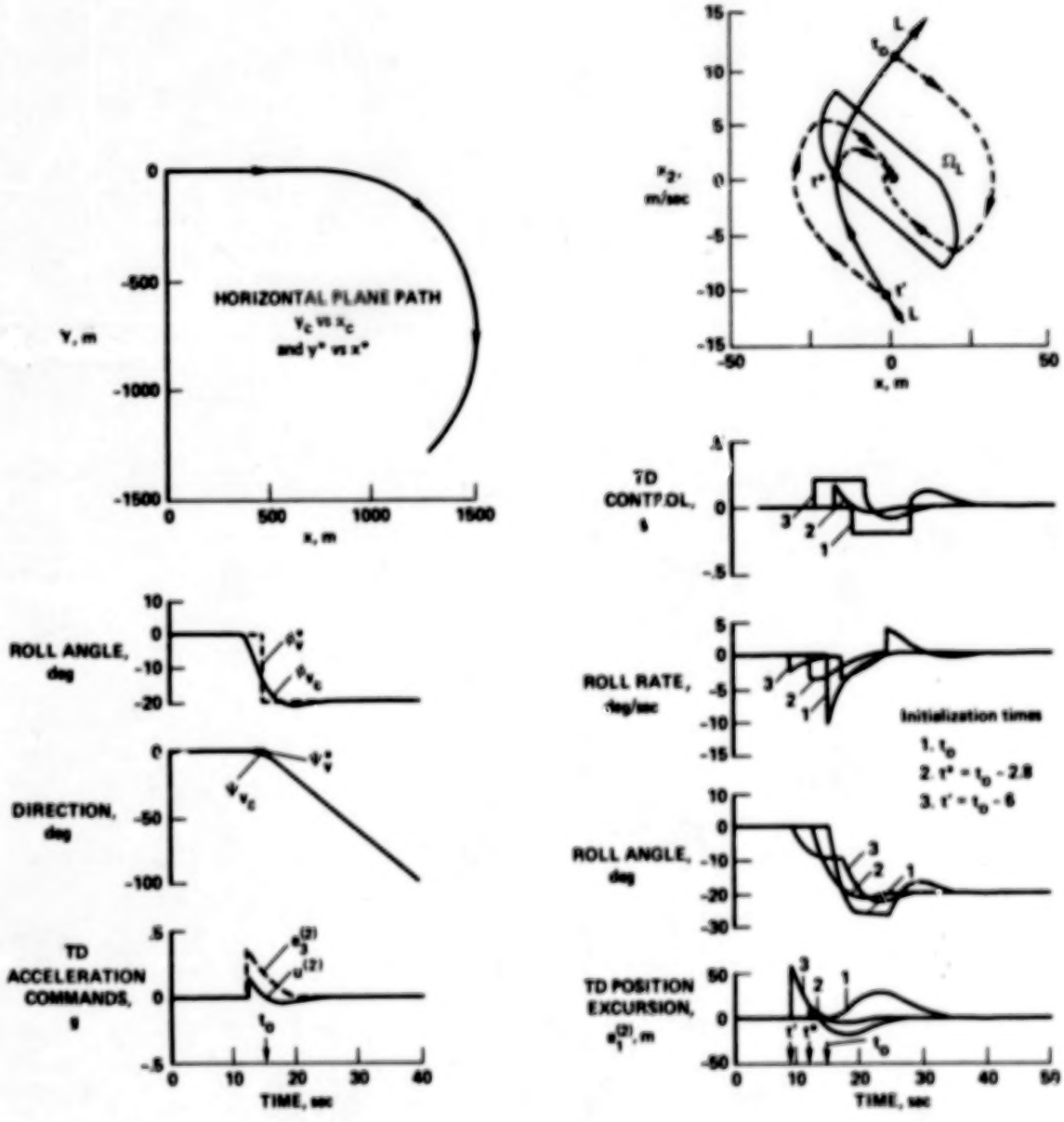

(a) Transition with optimum initialization.

(b) Effects of transition initialization time.

Figure 18.- Turn entry transition.

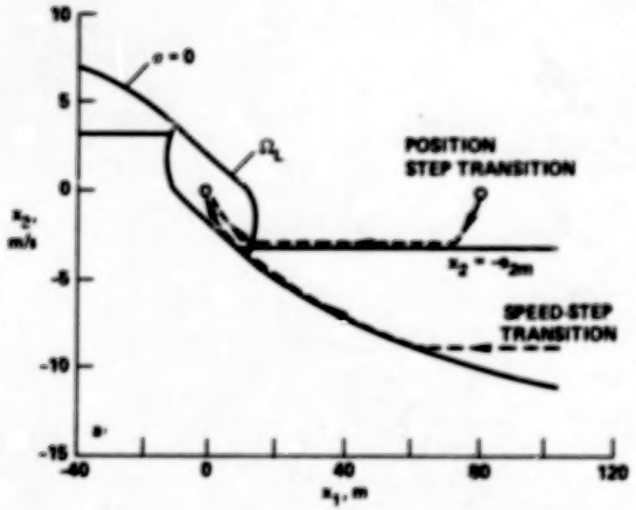

(a) x-plane control regions and transition trajectories.

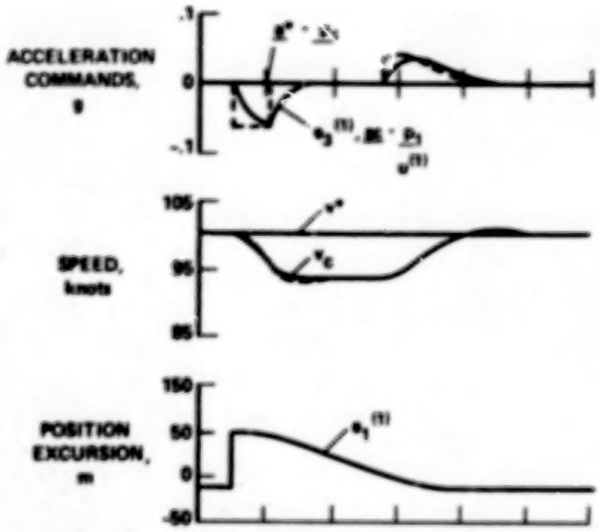

(b) Position step transition.

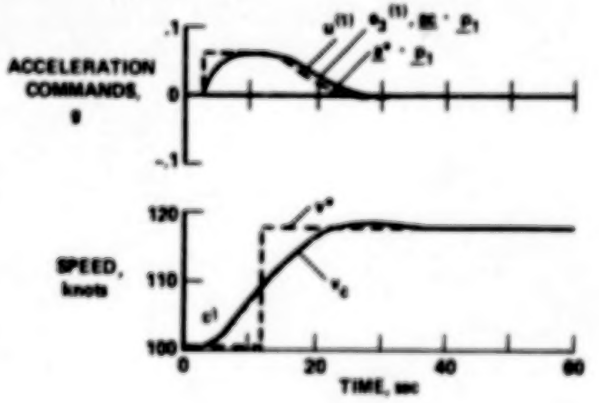

(c) Velocity step transition.

Figure 19.- Longitudinal axis transitions.

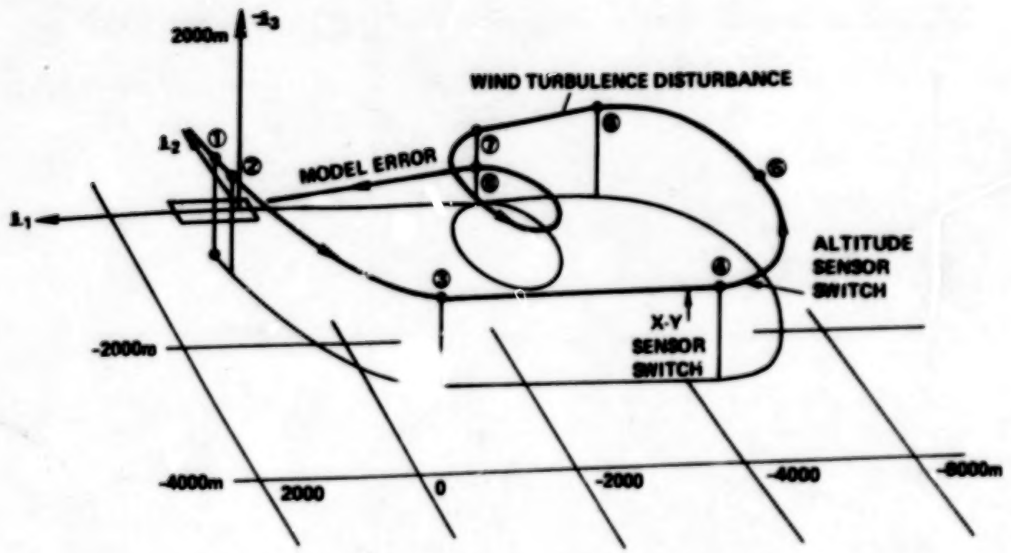

REFERENCE TRAJECTORY PARAMETERS

LEG	INITIAL TIME sec	INITIAL POSITION m			INITIAL VELOCITY			ACCELERATION	
		x_o	y_o	z_o	knots v	deg ψ_y	deg γ	g $\dot{V}$	m $\dot{h}_z$
1. LEVEL FLIGHT	0	629	-801	-1162	140	270	0	0	∞
2. DESCENDING TURN	11.6	629	-915	-1162	140	270	-3	0	-1524
3. DECELERATING LEVEL FLIGHT	45	-895	-2439	-1036	140	180	0	-.02	∞
4. TURN	98	-4300	-2439	-1036	120	180	0	0	-1219
5. DECELERATING TURN	127	-5518	-1220	-1336	120	90	0	-.035	-1219
6. GLIDE SLOPE	161	-4300	0	-1036	97	0	-5.9	-.021	∞
7. DECELERATING HELIX	194	-2808	0	-884	84	0	-7.5	-.01	-610
8. GLIDE SLOPE	294	-2808	0	-381	65	0	-7.5	0	∞

Figure 20.- STOL simulation test approach path.

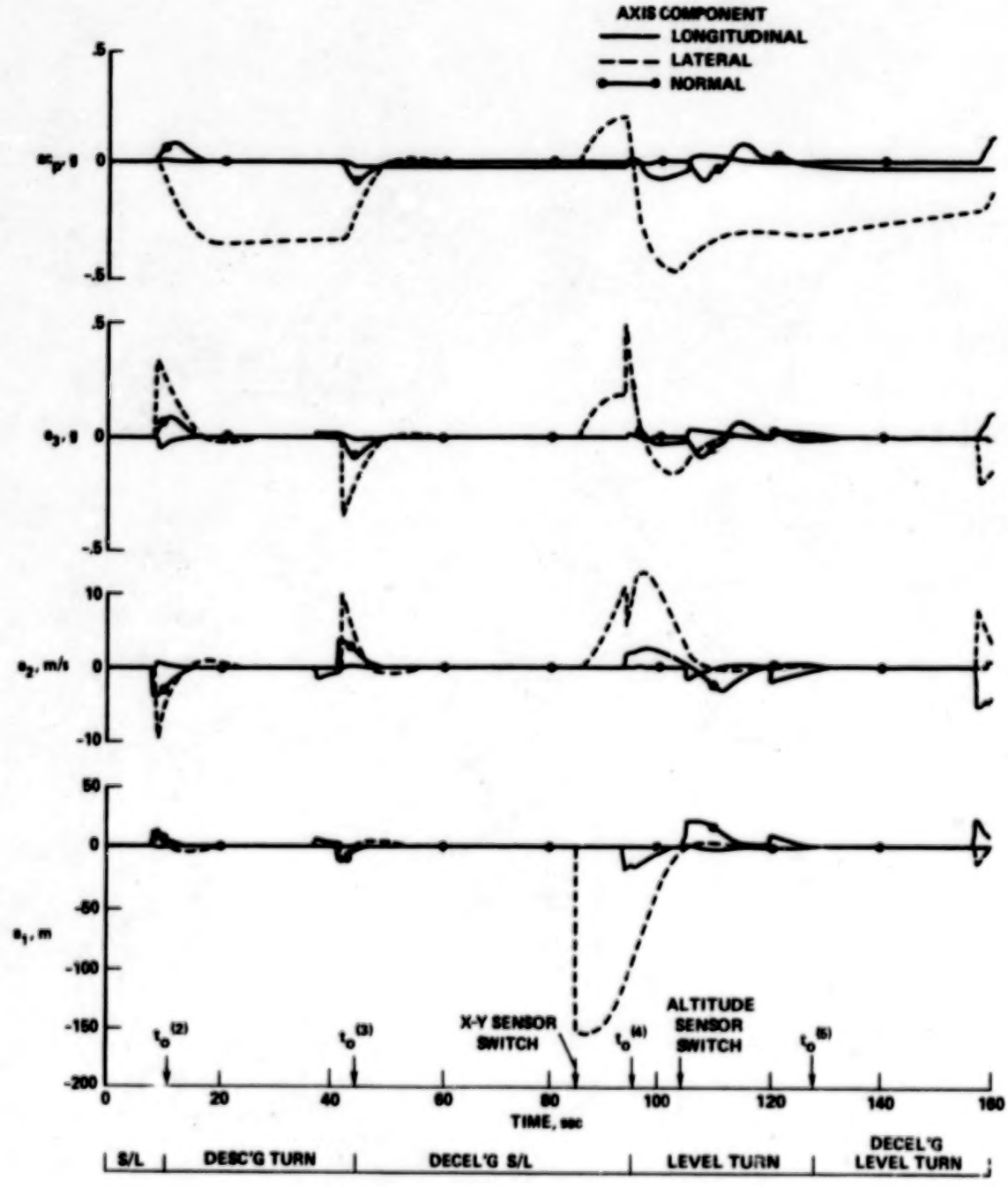

(a) Command generator variables.

Figure 21.- Simulation results — first half of test path.

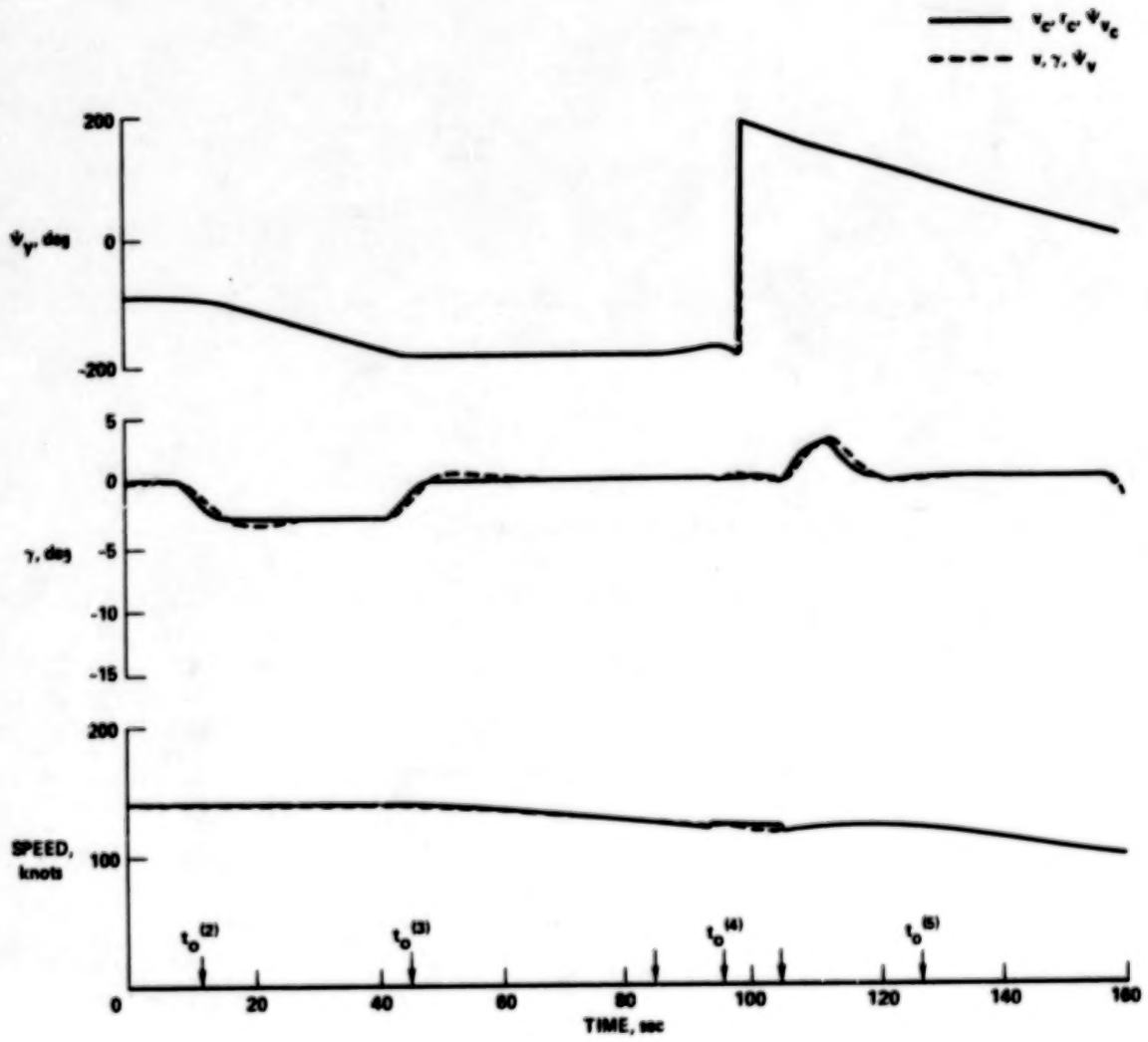

(b) Velocity commands and responses.

Figure 21.- Continued.

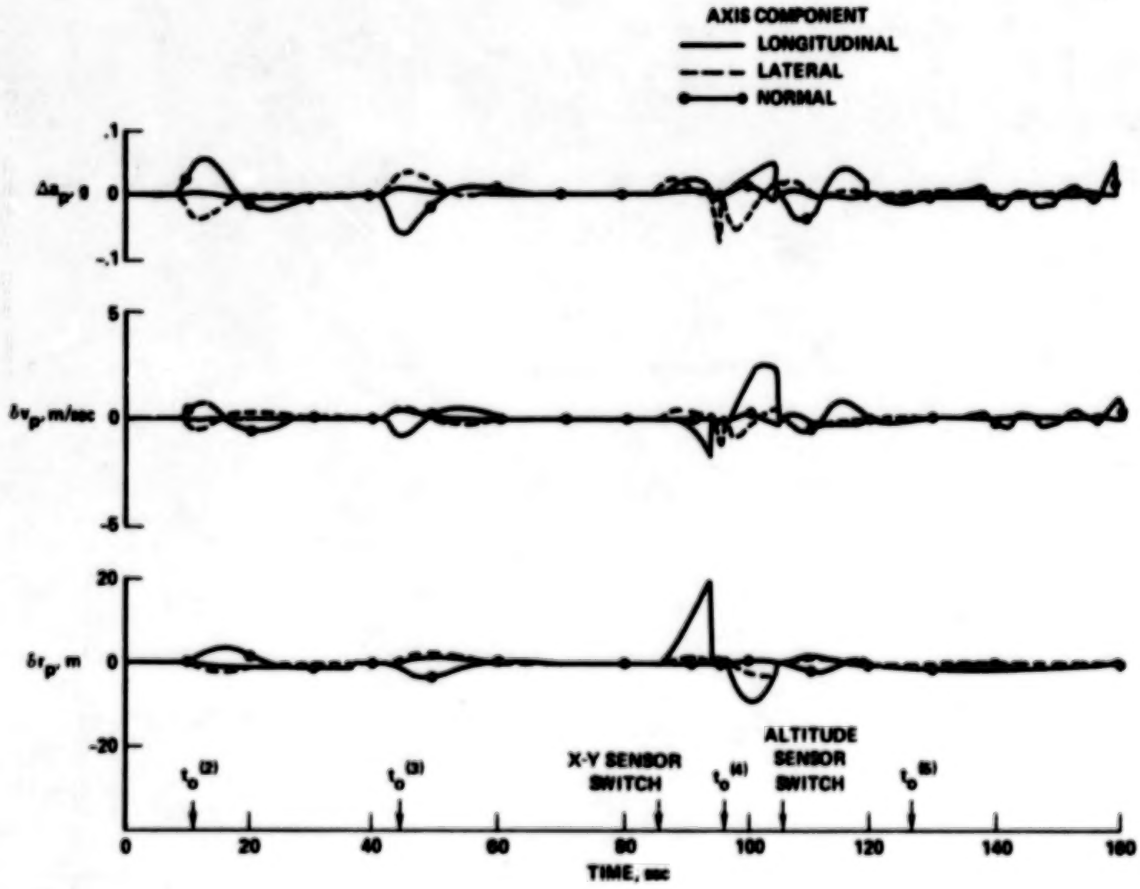

(c) Trajectory tracking variables.

Figure 21.- Continued.

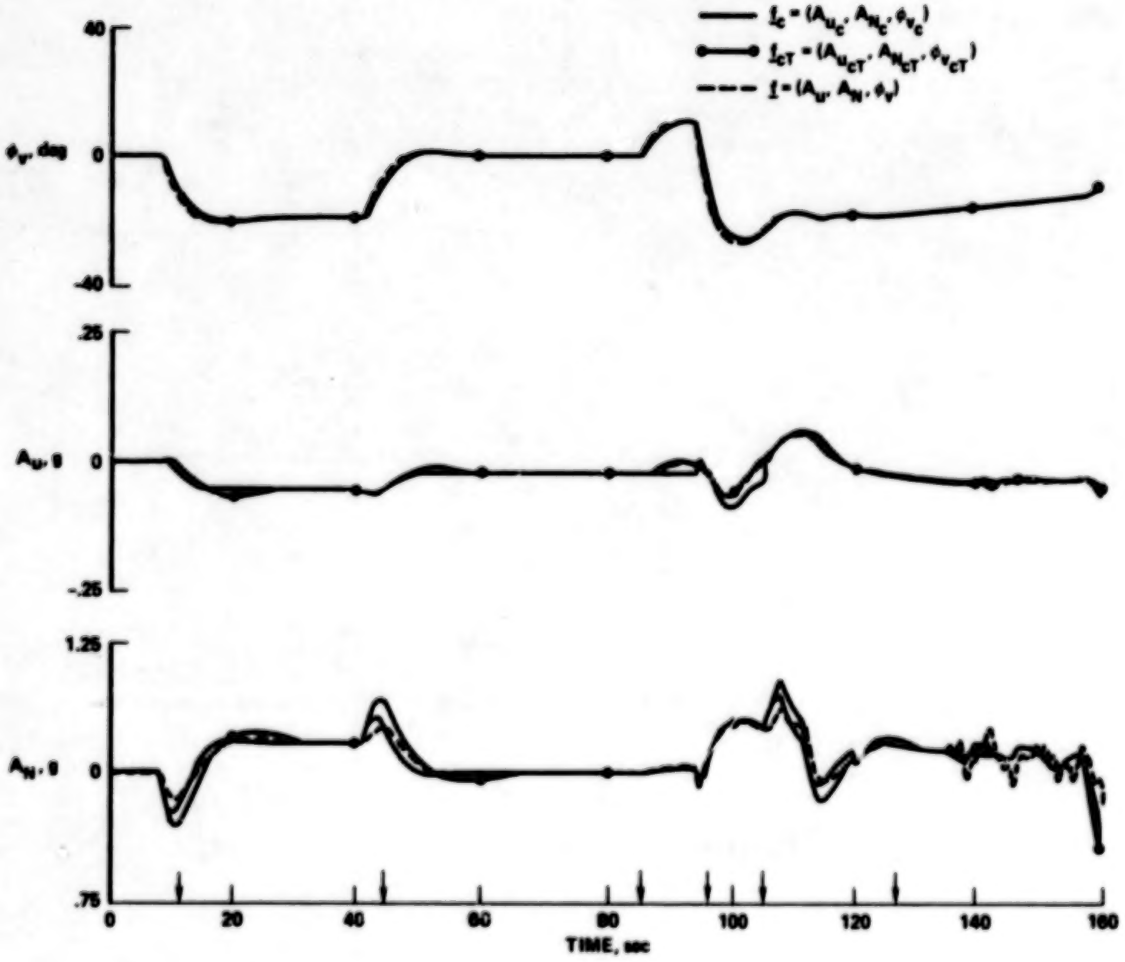

(d) Applied specific force commands and responses.

Figure 21.- Concluded.

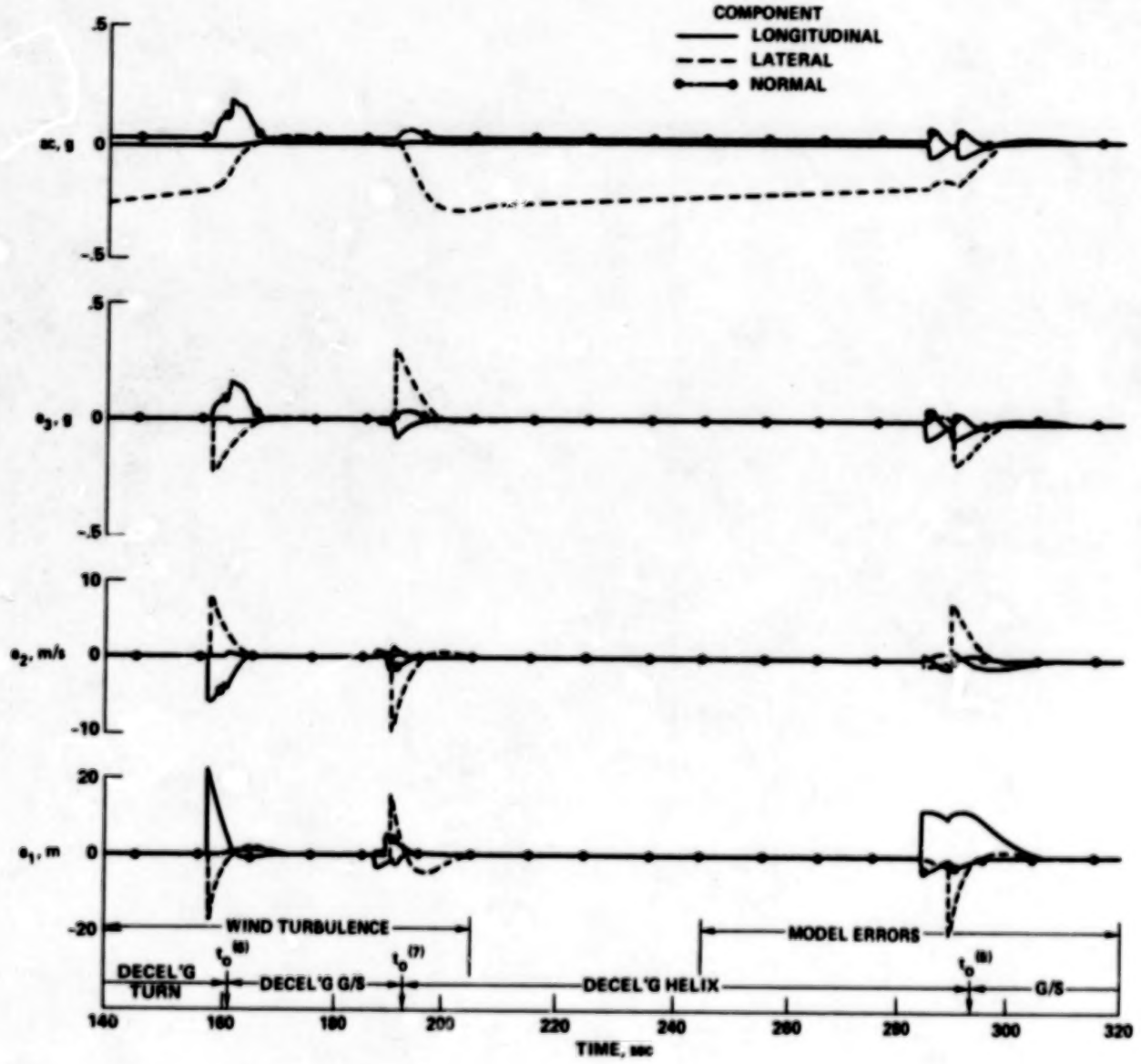

(a) Command generator variables.

Figure 22.- Simulation results – second half of test path.

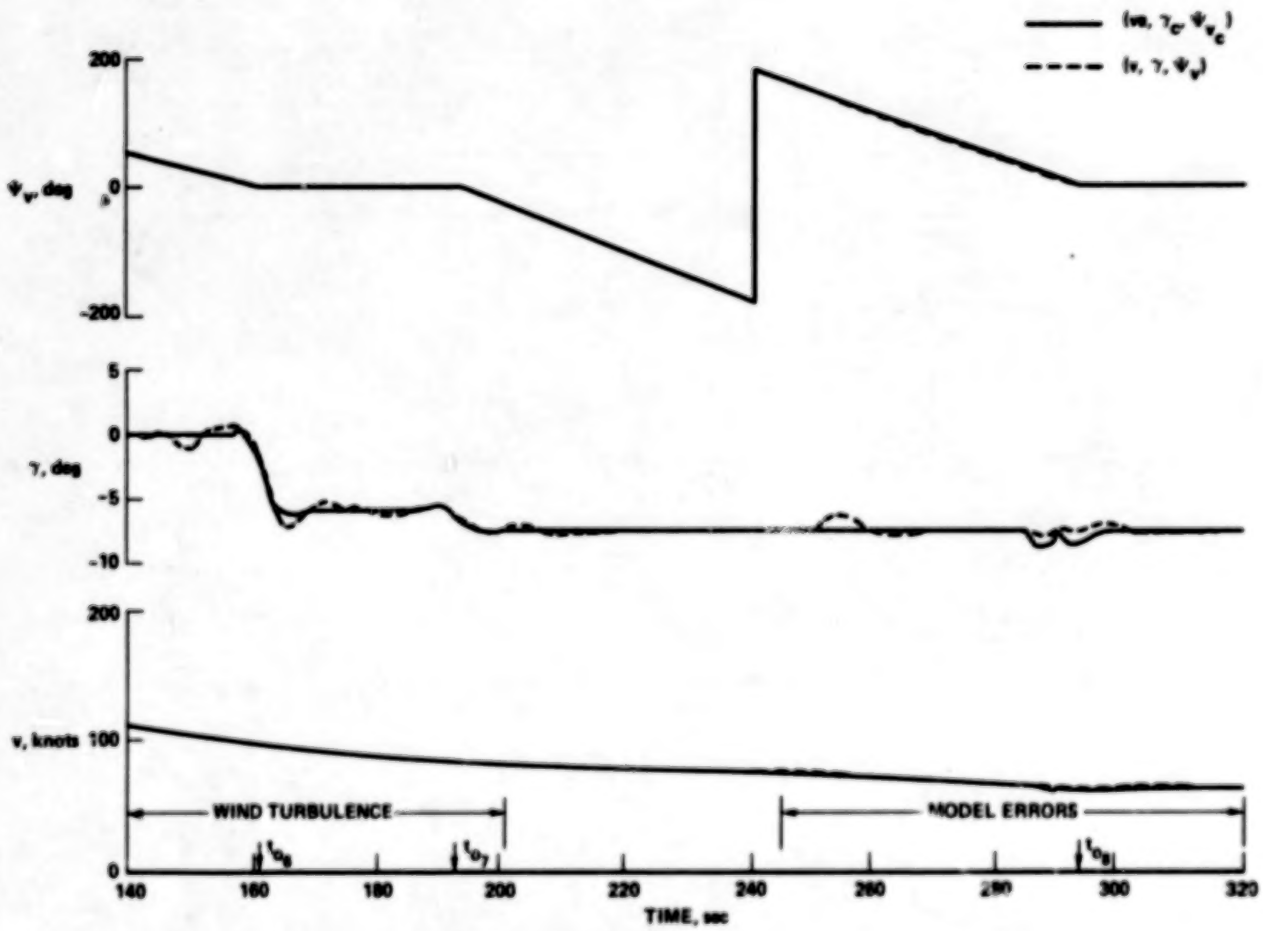

(b) Velocity commands and response.

Figure 22.- Continued.

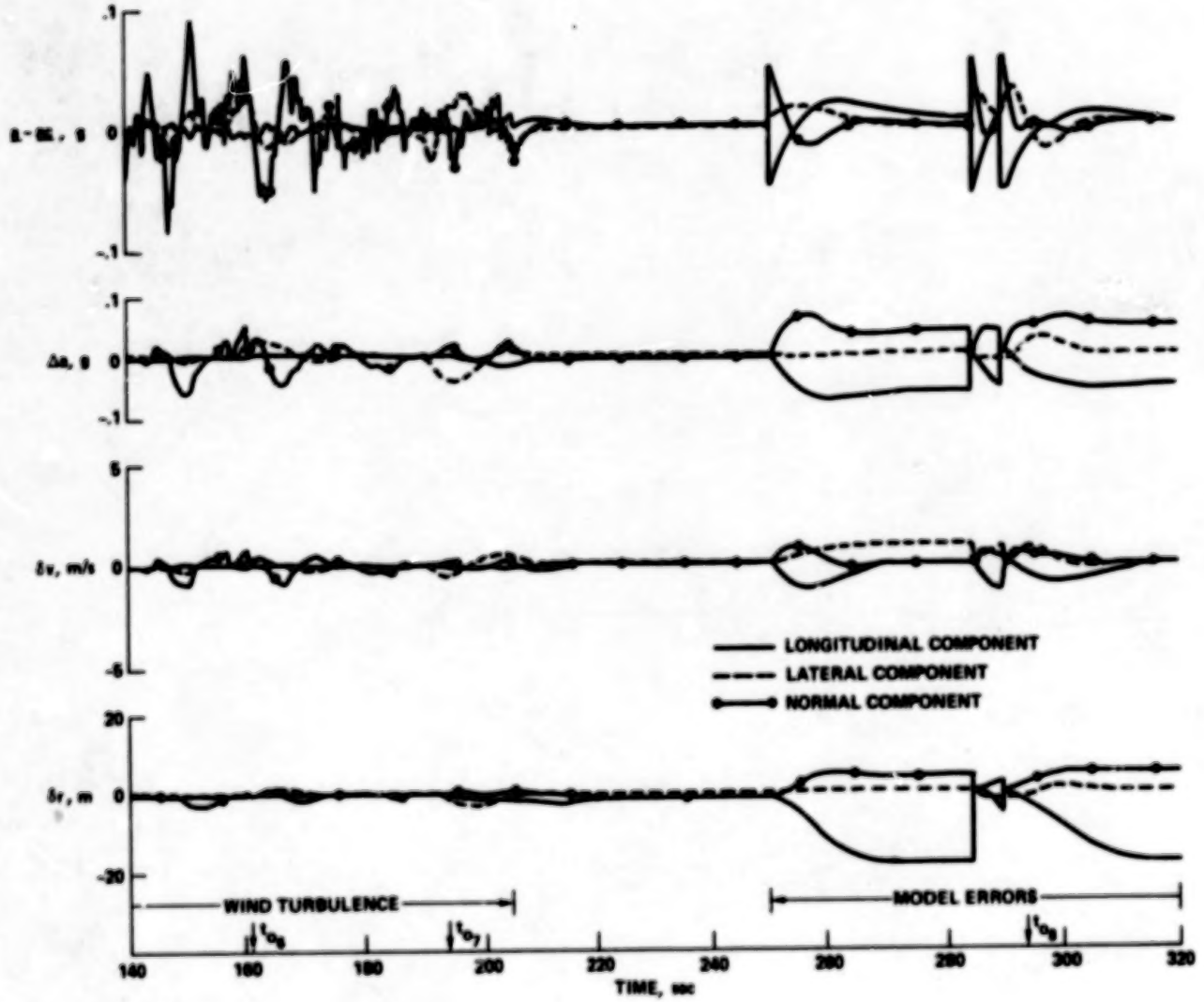

(c) Trajectory tracking variables.

Figure 22.- Continued.

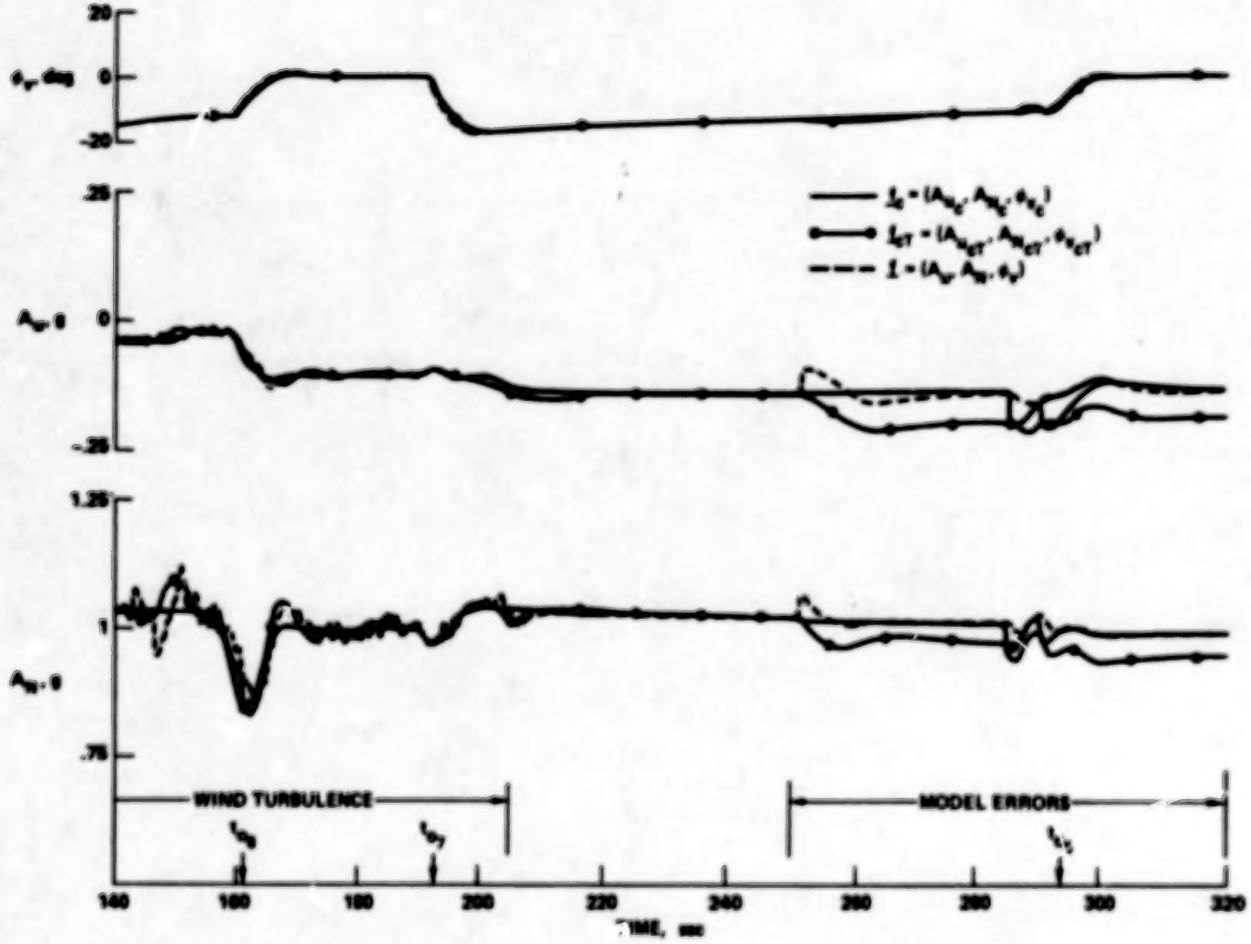

(d) Applied specific force commands and response.

Figure 22.- Concluded.

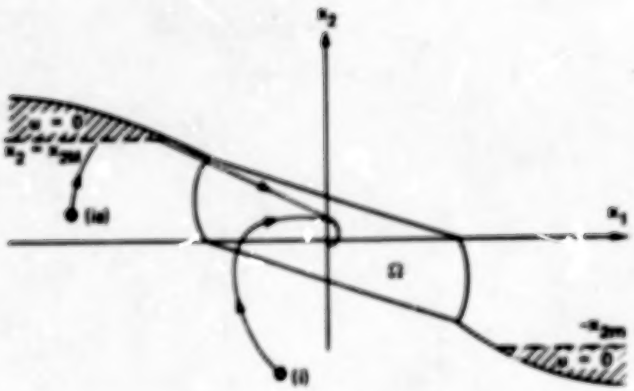

Figure 23.- Control law modifications to limit velocity.

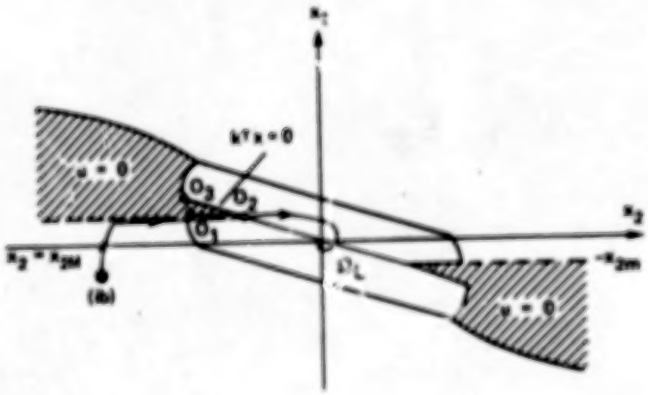

Figure 24.- Control law when velocity limit intersects Ω.

1. Report No. NASA TP-1221	2. Government Accession No.	3. Recipient's Catalog No.

4. Title and Subtitle

A NONLINEAR TRAJECTORY COMMAND GENERATOR FOR A DIGITAL FLIGHT CONTROL SYSTEM

5. Report Date
November 1978

6. Performing Organization Code

7. Author(s)

Luigi S. Cicolani and Stein Weissenberger*

8. Performing Organization Report No.
A-7074

9. Performing Organization Name and Address

NASA Ames Research Center
Moffett Field, California 94035

10. Work Unit No.
505-07-11

11. Contract or Grant No.

12. Sponsoring Agency Name and Address

National Aeronautics and Space Administration
Washington, D.C. 20546

13. Type of Report and Period Covered
Technical Paper

14. Sponsoring Agency Code

15. Supplementary Notes

*National Research Council Postdoctoral Research Associate

16. Abstract

A nonlinear Command Generator (CG) is required in an advanced digital autopilot concept for the control of VSTOL aircraft tracking complex four-dimensional reference trajectories. The reference trajectory is assumed piecewise flyable, consisting of a sequence of simple "legs" with discontinuities at the leg junction times. The CG generates smooth transitions from one leg to the next; these are optimized with respect to the time of initiating the transition and adaptive with respect to tracking errors at the time of initiating a transition. A variety of operational constraints on maneuvering as dictated by safety, aircraft limitations, and passenger comfort, including bounds on velocities, accelerations, and acceleration rates, are maintained. The transition is generated from a dynamic system that models the trajectory behavior of the aircraft and is regulated by a control algorithm synthesized with the help of Lyapunov stability theory and Jordan canonical transformations.

Operational application of the CG was examined in detail in a simulation of a flight-control system with the augmentor wing jet STOL research aircraft; the basic repertoire of single-axis maneuvers and operational constraints are discussed, and the system behavior is tested on a rigorous STOL approach path and as affected by various approximations in the CG synthesis and types of disturbances found in the operational environment. The simulation results indicate that a satisfactory nonlinear system with general maneuvering capabilities throughout the flight envelope was developed which satisfies the basic design objectives while maintaining a practicable degree of simplicity.

17. Key Words (Suggested by Author(s))	18. Distribution Statement
Automatic flight control Aircraft trajectory commands Constrained maneuvering Nonlinear control	Unlimited STAR Category - 08

19. Security Classif. (of this report)	20. Security Classif. (of this page)	21. No. of Pages	22. Price*
Unclassified	Unclassified	115	$5.50

*For sale by the National Technical Information Service, Springfield, Virginia 22161

NASA-Langley, 1978